ALMA MATER STUDIORUM — UNIVERSITÀ DI BOLOGNA

DOTTORATO DI RICERCA IN

Scienze Biotecnologiche e Farmaceutiche

Ciclo XXXI

Settore concorsuale di afferenza: 03/D1

Settore scientifico disciplinare: CHIM/08

TITOLO TESI

Development of multimethodological strategies for monitoring biorecognition phenomena of pharmaceutically relevant targets

Presentata da: Anna Tramarin

Coordinatore dottorato — Prof. Santi Mario Spampinato

Relatore — Prof.ssa Manuela Bartolini

Esame finale anno 2019

Development of multimethodological strategies for monitoring biorecognition phenomena of pharmaceutically relevant targets

Anna Tramarin

Contents

Abstract

In the continuous research for more targeted therapies, a full comprehension of molecular biorecognition phenomena, involving small molecules and biological targets, is pivotal to clarify pathophysiological mechanisms and rationally develop new and more effective drugs. The investigation of such interactions requires the development and application of advanced analytical approaches to profile the binding partners. Several analytical techniques have been applied over the years to elucidate different aspects of biomolecular phenomena, both in solution or involving target immobilization. The selection of the most suitable and informative approach depends on the issue to be addressed and, usually, the combination of several techniques may help better elucidating the phenomenon.

In the current dissertation, approaches based on mass spectrometry (MS), circular dichroism (CD) spectroscopy and surface plasmon resonance (SPR) biosensing have been used, both individually or in combination, to investigate two targets of pharmaceutical interest, namely human serum albumin (HSA) and human cholinesterases (ChEs). HSA, the most abundant plasma protein, plays a key role in a broad range of biological functions. Furthermore, HSA is used in clinical practice to treat different diseases, such as hypovolemia, hypoalbuminemia and sepsis and its integrity (or alteration of) also reflects the health status of the subject. Indeed, in circulatory system, it could undergo structural modifications which, from one side, may be studied as biomarker or prognostic features and, on the other hand, may trigger pathological paths. For this reason, the elucidation of the connection between HSA modifications, biological functions and the pathogenic role of altered HSA is crucial to be investigated. In this scenario, the binding capacity of pharmaceutical-grade HSA for intravenous infusion was studied implementing and employing a CD spectroscopy-based assay. The work focused on the investigation of the impairment of the binding capacity caused by commonly added stabilizers, i.e., N-acetyltryptophan and sodium octanoate, in the formulation. Results showed an altered binding capacity at site II caused by the presence of octanoate. The work also highlighted that, because of the high affinity binding of octanoate, its removal cannot be achieved by simple ultrafiltration or simple dialysis. Furthermore, SPR- and affinity chromatography-MS-based assays enabled an initial characterization of the interaction between an altered form of the protein, i.e. glycated HSA, and the receptor for advanced glycation end products (RAGE). The multimethodological approach provided further insights into such interaction, laying the groundwork for subsequent studies on the interaction between RAGE and circulating early and end glycation products formed under diabetic conditions.

Concerning ChEs, these enzymes have been widely studied as molecular targets in drug discovery for Alzheimer's disease. In particular, according to cholinergic hypothesis, the inhibition of ChEs

has represented and still represents the main strategy to temporally counteract cognitive impairment. In this context, both in solution functional assays and a tailored SPR-based assay were used for the identification of new potential inhibitors and for the affinity and kinetic studies on known ligands, respectively. The new developed SPR-based assay nicely complemented classic inhibition studies, providing further key elements for ranking new inhibitors, which can be classified not only on the basis of their potency but also on the basis of their kinetic parameters including residence time.

Overall, the tailored analytical strategies developed and applied in the projects reported in the current dissertation have contributed to elucidating biorecognition events and/or uncover alterations of such mechanisms which may result in pathological mechanisms. The final goal of elucidating some biorecognition events, indeed, is to provide pivotal information which can help the development of new and more effective drugs towards more targeted therapies.

Outline of the thesis

The current thesis includes the collection of studies carried out during the PhD program, aimed at investigating biorecognition events involving two pharmaceutically relevant targets, namely HSA and ChEs. The dissertation is divided in three main parts.

Part I briefly outlines the complex correlation between *in vitro* and *in vivo* activity. The opening **chapter I** focuses on the study of biorecognition phenomena. In particular, recent ligand–receptor theories, which better explain *in vivo* activity, are discussed. These novel approaches, which consider biological systems as *open-systems* characterized by a fluctuation of ligands, may give a better picture of the conditions encountered in the human body. In this context, *in vitro on-* and *off-* rate constants proved to correlate better than the affinity data with *in vivo* activities [1]. Therefore, the interest in robust methodologies able to provide kinetic information on drug binding events is growing. In this chapter, examples of analytical techniques employed over the years to structurally and functionally characterize bioactive molecules have been also discussed with particular focus on SPR, CD and MS techniques, which are the main analytical approaches used in the studies carried out during my PhD. **Chapter 2** reports the aims of the thesis.

Following the introductory part, the thesis reports the main studies carried out during the PhD program, most of which has been published in peer-reviewed journals. Each original article has been reprinted without modification with publishers' permission, when I am the first author, while it has been adapted, when my contribution to the work concerned only a part of the treated aspects. The readers, who would like to obtain further information about the studies, are invited to directly refer to published articles.

More in detail, the reports on the experimental work have been divided into two parts according to the two target macromolecules investigated, i.e. HSA and ChEs.

Part II collects HSA studies. **Chapter 3** provides a brief overview of this target with a particular focus on the biological functions relevant for the reported studies. The structural modifications that circulating HSA could undergo as a result of pathological conditions, such as high level of oxidative stress and inflammation (e.g. cysteinylation, glycation, oxidation) and the analytical strategies developed over the years to identify these modifications are discussed. The last part of this chapter also comments the connection between structural changes and pathological processes. **Chapter 4** contains the results from the study focused on the impairment of binding capacity of a pharmaceutical-grade HSA, which is triggered by stabilizers added when it is formulated for intravenous infusion, by means of a CD spectroscopy-based assay. Stabilizers clearance by two different purification methods, namely ultrafiltration and dialysis, is also discussed in the light of

the assessment of the availability of HSA binding sites obtained by the method proposed. **Chapter 5** reports the investigation of the binding between a form of glycated HSA, recently released on the market, and the extracellular region (VC1) of the human RAGE. The study has been carried out by SPR and affinity chromatography coupled to MS with a tailored multimethodological approach aiming at investigating such interaction and shedding light on complex interacting ligands.

Part III focuses on cholinesterase enzymes. **Chapter 6** provides a brief overview of AChE and BuChE enzymes (enzyme structure, biological function and their role as therapeutic targets for the treatment of neurodegenerative disorders, such as Alzheimer's disease) as well as of the marketed cholinesterase inhibitors, since most of the drugs released on the market for treating AD symptoms belongs to this class of compounds. Moreover, the new rational strategy, namely multi-target-directed ligands, developed for countering the multifactorial etiology of AD, is also presented. **Chapter 7** presents the development of a new SPR sensing surface to study binding affinity and kinetic parameters for the interaction of human AChE and known inhibitors. The suitability of the developed hAChE-based surface to obtain additional elements (k_{on}, k_{off}, residence time) which may aid the selection of favorite chemical scaffolds, is discussed. **Chapter 8** and **9** deal with the results achieved in the screening of two new classes of MTDL compounds, namely donepezil-lipoic acid hybrids and tacripyrimidines hybrids, by using the classic in solution Ellman's method [2]. These compounds have been designed to exert multiple functions including ChEs inhibition. In particular, the design of the former class aims at achieving anticholinesterase and antioxidant activities in a single molecule, while the second class of derivatives aims at achieving cholinesterase inhibition and calcium channels modulation. To assess whether the rational design was successful, the investigation of the inhibitory potency toward cholinesterase enzymes and the definition of SARs are key steps along the characterization of the biological profile of these new classes of derivatives as well as for the selection of the most promising hybrids. Results of such studies are discussed together with those achieved by other research groups on the other designed properties.

At the end of the third part, a brief conclusion is reported aimed at summing up all the findings and the future perspectives sketched out by the current dissertation.

PART I

In vitro studies to predict in vivo activity

Chapter 1

Analytical strategies for monitoring biorecognition phenomena

1.1 From *in vitro* studies to *in vivo* efficacy of drugs

Biorecognition phenomena between complementary chemical species underpin all physiological and pathological processes. The study of the different interactions which occur in biological systems, such as protein–protein, RNA–ribosome, DNA–protein, enzyme–substrate, antigen–antibody, enables the comprehension of the complex mechanisms underlining living systems [3].

Corpora non agunt nisi fixate. This iconic sentence, which transposes in a more contemporary expression means ‘‘a substance will not exert its physiological activity unless it is bound to the target’’, was coined at the end of the 20^{th} century by Paul Ehrlich and is a cornerstone of modern molecular medicine and pharmacology [4]. This concept points out the importance of studying the interactions in terms formation/disruption events since the biological effect modulated by a ligand to its target depends on the formation of the binary complexes. Similarly, a drug exerts a pharmacological effect as long as it is bound to its target, making the information on drug–target interaction important to help the prediction of *in vivo* drug action. As a result, during the early stages of drug discovery, many efforts are focused on the optimization of the selectivity and the affinity of drugs candidates toward their targets. Target affinity is usually assessed performing either a direct measurement of the binding or, indirectly, measuring the modulation of the target activity as a result of the binding (e.g. enzymatic activity assays).

Typically, these *in vitro* studies are carried out in *closed system*-based conditions (Fig. 1a) in which, throughout the experiment, the concentration of binding partners is treated as invariant [1]. In this scenario, assays can only partially mimic what happens in real systems, in which the interaction process is dynamic and the exposure time of the ligand to its target is limited in time and floating over time. In such static systems, drug–target binary complex is commonly quantified in terms of equilibrium dissociation constant (K_D). K_D is defined as the concentration of a substance necessary to bind 50% of macromolecular target population. This parameter is not up to the nature of interactants (ligand–receptor, ligand–enzyme, ligand–ion channel) and it is measured at the steady state, in which the concentration of both molecules is kept constant over the period of analysis. Similarly, for inhibitor–target studies, the inhibitory constant (K_i), measured in equilibrium

conditions, represents the concentration of inhibitor capable to inhibit of 50% the biological activity of an enzyme.

Besides these parameters act as guides during drug discovery route to predict the *in vivo* behavior of drugs, they can only provide a clue of the *in vivo* effectiveness. Indeed, the *closed system*-based conditions can only partially reflect the dynamic process to which drugs are subjected in the human body, where their concentration fluctuates over time both locally and globally [1]. *In vivo*, compounds undergo different interactions besides the primary target, such as binding to serum proteins. Similarly, several steps such as absorption, distribution metabolism and excretion (ADME) rule the drug fate, thus influencing the concentration of compound that reaches the primary target-harboring tissue and, as a consequence, the rate of the interaction. In this scenario, the human body is better described as an *open system* (Fig. 1a) in which the local concentration of the ligand as well as the time window in which it is available for the interaction with the target change over time.

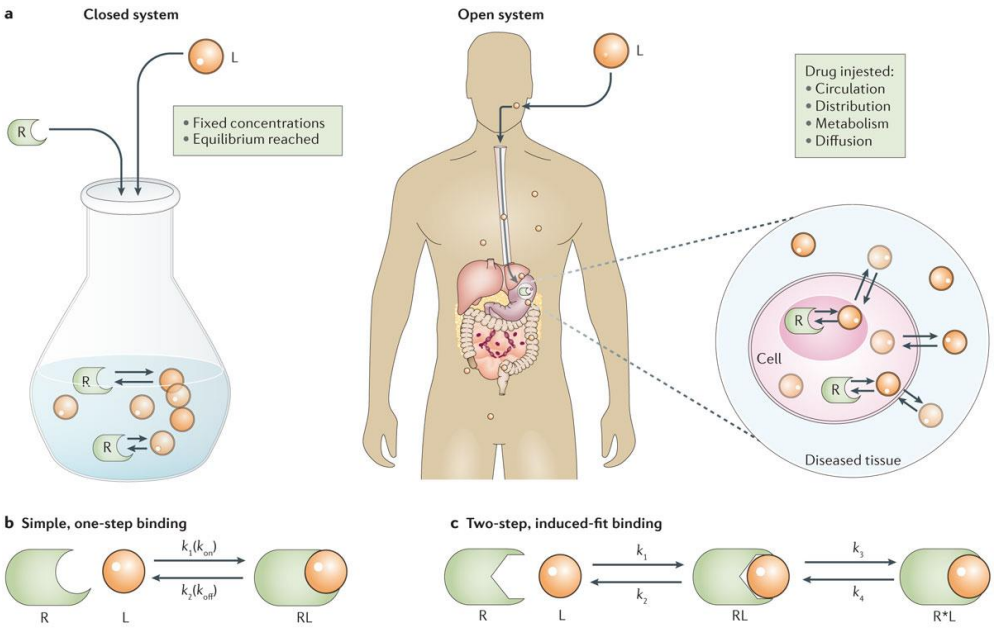

Figure 1| **Kinetic aspects of ligand–target binary interactions. (a)** Representative picture of a closed and an open system. The former is characterized by constant concentrations of reactants enabling the formation of a real equilibrium between free and bound drug. The latter, more representative of the real conditions in the human body, is characterized by a fluctuation of the ligand as a result of multiple factors including absorption, distribution, metabolism and excretion. **(b)** Schematic simple 1:1 interaction for the receptor (R) and its ligand (L) characterized by a one-step mechanism with the corresponding formation/disruption kinetic constants. **(c)** Schematic 1:1 ligand–receptor interaction characterized by a two-step mechanism with the corresponding formation/disruption kinetic constants. In this case, the binding between the two interactants induces the isomerization of the receptor. The k_3 and k_4 constants represent further association and dissociation rate parameters respectively, which account for the reversible conformational transition of the complex. Reprinted with permission from [5].

From this perspective, the time-dependent variation of the ligand concentration is an important parameter that should be considered for better mimicking *in vivo* biomolecular interactions. In this context, the possibility of assessing the steady state affinity constant on the basis of individual kinetic rate constants ($K_D = k_{off}/k_{on}$) can provide further insights into the affinity–activity relationship. Kinetic rate constants, namely association (k_{on}) and dissociation (k_{off}) rate constants, seems to better correlate with *in vivo* activities [5]. Therefore, in addition to affinity and inhibitory potency, kinetic binding data are increasingly recognized as key parameters to be considered in the optimization of a lead compound [6,7]. As examples of hit compounds selected on the basis of their target binding kinetic properties, the fast *off*-rate dopamine D_2 antagonist JNJ-37822681 (treatment of schizophrenia and bipolar disorder) [8] and inhibitors of the colony-stimulating factor 1 receptor (target in oncology and rheumatoid arthritis) [9] can be mentioned. The importance of considering kinetic parameters is exemplified by the experimental proof that chemical entities with the same affinity but different *on*- and *off*-rates may display different biological activities. This is exemplified by some muscarinic M3 antagonists, used in therapy as bronchodilators, which display similar affinities but different kinetic rates and duration of action: atropium (K_D = 0.2 nM; k_{on} = 1.5 x 10^9 $M^{-1}min^{-1}$; k_{off} = 0.27 min^{-1}) and ipratropium (K_D = 0.2 nM; k_{on} = 0.5 x 10^9 $M^{-1}min^{-1}$; k_{off} = 0.07 min^{-1}) [10]. Notably, quantification of k_{off} for ligand–target complexes grants easy access to *residence time* ($\tau = 1/k_{off}$), which corresponds to the reciprocal of the dissociation rate constant and represents the time that a drug 'resides' in the target. Indeed, τ parameter results a more critical tool when structure–kinetic relationship (SKR) studies are performed [11]. Therefore, we are witnessing growing interest in robust methodology able to provide kinetic information on drug binding events already at early steps in the drug discovery process. Among these methodologies, surface plasmon resonance (SPR) based assays, radioligand binding/competition assays, biolayer interferometry and kinetic probe competition assays (kPCA) based on the time-resolved fluorescence energy transfer (TR-FRET) are worth to be mentioned [10,12,13].

The access to kinetic parameters (and to residence time) acquires even more importance when interactions involve more than a single reaction step such as in the case of target isomerization induced by the binding. Taking the example of the most common 1:1 interaction between a ligand and its target (Fig. 1b-c), in pharmacology two situations are usually observed. In the simplest case (Fig.1b) the interaction is characterized by association and dissociation both in one single step (Fig. 1b). Herein, *on*- and *off*- rates (in the figure labeled k_1 and k_2, respectively) directly refer to formation and disruption events. In the second case (Fig. 1c), the interactions between the two binders (RL complex) envisages a rearrangement into a conformation, in the figure named R*L, characterized by a greater stability and higher affinity [14]. The additional isomerization reaction

implies that these two interactants cannot directly decouple. In this case, also known as two-state reaction, the k_{off} is made from all microscopic rate constants involved in the reaction, also accounting for forward and reverse isomerization steps (in the figure k_3 and k_4, respectively) (Eq. 1).

$$k_{off} = \frac{k_2 k_4}{(k_2 + k_3 + k_4)} \quad (1)$$

In medicinal chemistry, efforts to obtain the majority of details regarding a selective interaction increase the success rate of better performing drug candidates. Of course, the *in vivo* duration of drug action as well as its pharmacodynamic efficacy depend on multiple variables in addition to molecular drug–target interactions. However, the combination of primary measurements of potency and drug–target affinity (IC_{50} or K_D values) with metrics such as residence time and kinetic data, provides additional information during SAR studies, enhancing the connection of *in vitro* measurements and *in vivo* effect. In this scenario, the development and application of advanced analytical strategies enabling monitoring, directly or indirectly, biomolecular interactions are key aspects to elucidate specific features which underpin biomolecular phenomena and to favor the rational development of new and more efficient drugs.

1.2 Analytical methods for rationalizing binding events

The employment of analytical techniques and the development of experimental methods to rationalize binding events constitute a connection bridge between pharmacological hypothesis and the comprehension of specific network of communication, eventually resulting in the discovery of new drugs with better therapeutic properties. The investigation of biological systems to clarify the role of biological targets and their behavior upon interaction with ligands requires the development and application of advanced analytical approaches to profile the binding partners. Indeed, an in-depth characterization of structural and functional features of biological targets is pivotal to define the relationship between the tridimensional conformation of a macromolecule and its function. In drug discovery, the characterization of the ligand-target interaction may highlight the key amino acids involved in the binding and help the rational design of new ligands. Moreover, investigation of biorecognition phenomena using a set of different binders may facilitate the definition of the chemical space to be further investigated along the lead optimization phase. In this context, the determination of thermodynamic and kinetic data using *in vitro* systems mimicking physiological setting enables to better predict the ligand behavior at the target *in vivo*.

Over the years, different analytical techniques have been employed to characterize ligand–target interactions, both in solution or upon target immobilization. Each of these may enable the investigation of different aspects of biomolecular phenomena. The selection of the most suited

approach depends on the specific aspect to be investigated and requires an in-depth knowledge of the specific features of each method. Moreover, the use of orthogonal analytical techniques within a multimethodological approach ensures complementary information which may facilitate the understanding of the phenomenon.

Among the multitude of techniques, for their wide use in drug discovery we can quote X-ray crystallography [15,16], nuclear magnetic resonance (NMR) [17,18], mass spectrometry (MS) [19–25] circular dichroism spectroscopy (CD) [26–29], equilibrium dialysis [30,31], ultrafiltration [32] and ultracentrifugation [33,34], fluorescence spectroscopy [35,36], affinity separation approaches such as high-performance affinity chromatography (HPALC) [37–40] and affinity capillary electrophoresis (ACE) [41–44], quartz crystal microbalance (QCM) [45,46], microscale thermophoresis (MST) [47–49], isothermal titration calorimetry (ITC) [50–52] and biosensors based on different technologies such as surface acoustic wave (SAW) [53,54] or surface plasmon resonance (SPR) [55–60]. In structural field, in recent years cryo-electronic microscopy (cryo-EM) [61,62] has become a valid label-free method to obtain details of macromolecule structures. This in solution technique is based on the rapid cooling of biomolecules to cryogenic temperatures. The formation of amorphous solids by means of a vitrification process enables the retention of native structures. Biomolecules are then screened by electron diffraction patterns (particles distribution, orientation and concentration) obtaining highly-informative 3D models.

MS is a powerful technique employed at different stages of the drug discovery path. For instance, it is used to qualitatively and quantitatively identify known and unknown chemical entities, to investigate the purity of synthesized compounds and to elucidate structural and functional properties of biomolecules [19,21]. Besides providing specific sequence and exact mass of molecules, MS is a robust and reliable tool for studies on macromolecular systems. Non-covalent biomolecular assemblies, from small molecule–protein/nucleic acid interactions to macromolecular complexes, can be investigated as well as affinity values (K_D), stoichiometry and target specificity of the binding can be assessed. Moreover, MS enables the localization of the binding site by epitope mapping approaches or allows to evaluate structural modifications of macromolecules. In some cases, e.g. using ion mobility, MS can also provide details regarding binding-induced conformational changes [20,21]. The versatility of the technique, the possibility of identifying and separately quantifying several compounds in a single scan as well as the high automation granted by the modern MS platforms confer to MS a great potential for rapid, sensitive and high throughput analyses.

Toward the characterization process, CD spectroscopy is undoubtedly the technique of choice when conformational details of free or bound molecules are required (Fig. 2), granting the determination

of the absolute configuration of chiral chemical entities or achiral molecules in a chiral environment [63]. Intrinsic chirality of compounds, or the asymmetric arrangement of atoms upon binding can be used to obtain details on the interaction, also when crystal structures or data from *in silico* studies are lacking. Secondary structure studies (Fig. 2) are usually employed as ‘‘quality control’’ for elucidating batch-to-batch the correct protein folding. Besides this application, secondary structure analysis is also employed to investigate biological processes, such as the relationship between protein conformational changes and pathological conditions. Indeed, changes in the secondary structure of proteins or peptides may influence their functionality and, in some cases, play a role in the pathogenesis of different disorders such as neurodegenerative diseases like Alzheimer’s and Parkinson’s diseases or amyotrophic lateral sclerosis. In AD, for instance, analyses carried out in aqueous solution confirmed that amyloid beta protein shifts from mainly α-helix conformation to β-sheet conformation, responsible for amyloid plaques aggregation and disease progression [64–66].

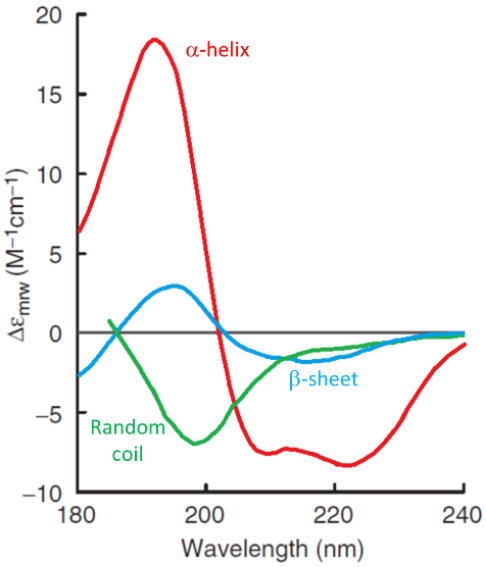

Figure 2| **Typical CD spectra of proteins secondary structures.** Typical α-helical (red), random coil (green), β-sheet (light blue) secondary structures. Reprinted with permission from [67].

CD technique also enables the assessment of thermodynamic parameters [26]. In particular, the induced CD (ICD) phenomenon, which arises when the interaction between a guest and its host perturbs the symmetry of the system (as a consequence of conformational changes), can be exploited to this purpose. ICD can be a valid tool to investigate ligand–target binding events, providing the assessment of the binding mode(s) as well as the determination of the binding parameters. Since ICD signal arises as a consequence of the complex formation, ICD monitoring allows to extrapolate specific information on the absolute configuration of chiral molecules along with how the two interactants involved in the binding are mutually oriented. Furthermore, ICD

studies can provide affinity constants, accounting for possible simultaneous competitors. Moreover, the technique ensures monitoring the formation of the ligand–target complex without interfering with the in solution equilibrium process.

Among analytical techniques enabling kinetic evaluation, SPR- or SAW-based biosensors as well as QCM are extensively used. Indeed, these techniques share the potential to monitor formation and disruption events in real-time, extrapolating kinetic parameters (k_{on}, k_{off}) besides thermodynamic data (K_D). Despite each method possesses its own specific physical transducer, they all feature anchorage of the ligand (usually the macromolecule) on a surface and flowing of the analytes (such as drugs) on the immobilized ligand. In detail, SPR detects shifts in the refractive index of the sensing medium near the surface layer (Fig. 3), SAW monitors changes in acoustic waves characteristics, i.e. frequency and amplitude, and QCM recognizes changes in frequency and dissipation of a quartz crystal resonator. Among these, SPR has assumed a central role over the last decades for monitoring biomolecular interactions.

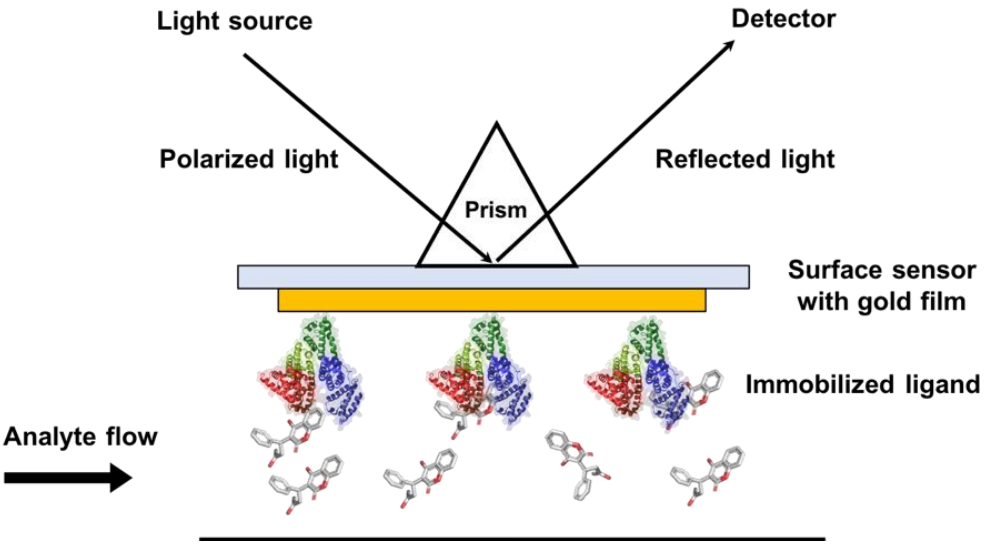

Figure 3 | SPR biosensing. At a specific angle of incident, a portion of the light energy couples with the electron of the metal surface layer. The defined SPR angle at which resonance takes place is dependent on the refractive index of the material near the metal surface. After biomolecular interaction, shift in the reflected light can be detected and the magnitude is directly related to the amount of ligand–analyte complex.

SPR biosensing allows retrieving information about the complex formation without the need of any labeling, providing qualitative information (yes/no binding) as well as quantitative thermodynamic and kinetic data. SPR phenomenon (Fig. 3) takes place when a beam of incident light hits a metal surface (typically a gold surface), located at the interface between two materials characterized by diverse refractive indices. At a specific angle of incidence, a portion of the light energy couples with the electrons of the metal surface layer. The defined SPR angle at which resonance takes place

depends on the refractive index of the material near the metal surface. Since changes in the refractive index are directly related to the mass of the sensing medium near the surface, changes in the reflected light, resulting from the biomolecular interactions, can be detected and the formation/disruption events easily assessed. Moreover, dissociation rate constant of a drug–target complex grants easy access to residence time (τ), which is a useful tool in combination with functional data for a better prediction of the *in vivo* activity of a drug toward a specific target. SPR biosensing approaches are also developed to achieve preliminary information on the ADME behavior for new chemical entities. In this context, different experimental set-ups have been developed over the years to investigate the binding to two of the major abundant proteins in plasma, namely human serum albumin (HSA) and α1-acid glycoprotein (AGP) [59]. The versatility of the methodology grants the investigation of either simple protein/protein or protein/small molecule (< 200 Da) binding as well as monitoring interactants in physiological environments (i.e. human plasma/serum). The low amount of sample required for screening makes SPR a suitable choice when a low amount of one/both interactants is available. Furthermore, the highly automated and integrated instrumentation minimizes operator procedures, thus improving the throughput and facilitating the screening of series of compounds during drug selection phase.

Recently, the integration of *in silico* approaches with structural and functional studies has reduced time-consuming steps/studies in drug discovery programs [68,69]. Computational methods can be used at different stages: from target recruitment, to hit-to-lead process up to optimization of compounds. The possibility of calculating free energy of reactions or simulating molecular dynamics of macromolecules assists the prioritization process. In the fragment-based lead discovery and design, the virtual screening favors and speeds up the rational design of new therapeutic molecules and pharmacological probes, easing the efforts of synthetic chemists [70].

Chapter 2

Scope of the thesis

Biorecognition phenomena between complementary chemical species underpin all physiological and pathological processes. The investigation of such phenomena requires the development and application of advanced analytical approaches to profile the binding partners. Within the variety of analytical methods developed and employed over the years to elucidate different aspects of biomolecular phenomena, a case-by-case selection must be done on the basis of the specific system under study and the information to be retrieved. Moreover, it is worth taking into consideration that the combination of different techniques may promote a better comprehension of a studied biomolecular system [71]. Keeping in mind these considerations, the main purpose of the here presented work was the development and application of tailored methodologies to investigate biorecognition phenomena involving two pharmaceutically relevant targets, namely human serum albumin (HSA) and human cholinesterases (ChEs).

HSA is the most abundant protein in plasma, playing a significant role in several biological functions. In particular, the ability of binding many endogenous and exogenous compounds has been widely studied since it strongly influences the bioavailability and pharmacokinetics of drugs [59]. Furthermore, HSA is used in clinical practice to treat different diseases, such as hypovolemia, hypoalbuminemia and sepsis and its integrity (or alteration of) also reflects the health status of the subject. Indeed, HSA could undergo several structural modifications in bloodstream. For instance, oxidation and glycation (promoted by high levels of oxidative stress and inflammation) not only may affect its biological functions but also might lead to activation of pathological events. For this reason, the comprehension of the connection between HSA modifications, biological functions and pathogenic role of altered HSA is crucial to be studied.

In this context, impairment of binding capacity upon structural modification as well as the possible role of such forms as mediators of pathological events is worth to be investigated. Concerning the former aspect, since quality of HSA administered as biological drug might have health implications, the impairment of the binding capacity of a pharmaceutical-grade HSA, clinically administered by infusion, will be investigated. A CD spectroscopy-based assay will be employed in the attempt of elucidating the effect of stabilizers, which are required for HSA pasteurization, on HSA binding capacity, also offering a useful analytical method to monitor their clearance. On the other hand, concerning the pathological implications of HSA alteration, HSA glycation will be considered with

particular focus of its interaction with RAGE, due to the important pathological path in which this receptor seems to be involved.

Concerning the second selected target, inhibition of cholinesterase enzymes, namely acetylcholinesterase (AChE) and butyrylcholinesterase (BuChE), has been one of the most investigated strategies pursued in the field of drug discovery for Alzheimer's disease (AD). Notwithstanding a number of alternative and potentially more effective strategies are under investigation, inhibition of cholinesterases is still a valid therapeutic way to enhance, although temporally, patient's quality of life. According to the so-called multi-target-directed ligand (MTDL) strategy, anticholinesterase activity is combined with other activities at other identified key targets for AD in order to achieve a single compound with multiple actions. Thus, in the context of drug discovery for AD, analytical strategies based on in solution assays will be employed to investigate new MTDLs designed to act as ChE inhibitors.

In parallel, strategies involving target immobilization will be developed to complement classic in solution assay. In particular, a SPR-based assay will be developed to help the prioritization of favorite chemical scaffolds by complementing inhibitory data with affinity and kinetic parameters. Combination of functional and binding data should reduce the attrition rate in the early phase of drug discovery.

References

[1] R.A. Copeland, D.L. Pompliano, T.D. Meek, Drug-target residence time and its implications for lead optimization, Nat. Rev. Drug Discov. 5 (2006) 730.

[2] G.L. Ellman, K.D. Courtney, V. Andres, R.M. Featherstone, A new and rapid colorimetric determination of acetylcholinesterase activity, Biochem. Pharmacol. 7 (1961) 88–95.

[3] P.J. Tonge, Drug–target kinetics in drug discovery, ACS Chem. Neurosci. 9 (2018) 29–39.

[4] P. Ehrlich, Chemotherapeutics: scientific principles, methods and results, Lancet. 182 (1913) 445–451.

[5] R.A. Copeland, The drug–target residence time model: a 10-year retrospective, Nat. Rev. Drug Discov. 15 (2016) 87–95.

[6] J.F. Morrison, C.T. Walsh, The behavior and significance of slow-binding enzyme inhibitors, Adv. Enzymol. Relat. Areas Mol. Biol. 61 (1988) 201–301.

[7] L.T. Gooljarsingh, C. Fernandes, K. Yan, H. Zhang, M. Grooms, K. Johanson, R.H. Sinnamon, R.B. Kirkpatrick, J. Kerrigan, T. Lewis, M. Arnone, A.J. King, Z. Lai, R.A. Copeland, P.J. Tummino, A biochemical rationale for the anticancer effects of Hsp90 inhibitors: slow, tight binding inhibition by geldanamycin and its analogues, Proc. Natl. Acad. Sci. U. S. A. 103 (2006) 7625–30.

[8] X. Langlois, A. Megens, H. Lavreysen, J. Atack, M. Cik, P. te Riele, L. Peeters, R. Wouters, J. Vermeire, H. Hendrickx, G. Macdonald, M. De Bruyn, Pharmacology of JNJ-37822681, a specific and fast-dissociating D2 antagonist for the treatment of schizophrenia, J. Pharmacol. Exp. Ther. 342 (2012) 91–105.

[9] J.C.M. Uitdehaag, C.M. Sünnen, A.M. van Doornmalen, N. de Rouw, A. Oubrie, R. Azevedo, M. Ziebell, E. Nickbarg, W.-J. Karstens, S. Ruygrok, Multidimensional profiling of CSF1R screening hits and inhibitors, J. Biomol. Screen. 16 (2011) 1007–1017.

[10] W. Keighley, The need for high throughput kinetics early in the drug, Drug Discov. World. (2011) 39–45.

[11] R.A. Copeland, Evaluation of enzyme inhibitors in drug discovery. A guide for medicinal chemists and pharmacologists, Methods Biochem. Anal. 46 (2005) 1–265.

[12] F. Schiele, P. Ayaz, A. Fernández-Montalván, A universal homogeneous assay for high-throughput determination of binding kinetics, Anal. Biochem. 468 (2015) 42–9.

[13] P.J. Tummino, R.A. Copeland, Residence time of receptor-ligand complexes and its effect on biological function, Biochemistry. 47 (2008) 5481–92.

[14] E. Fabini, B. Zambelli, L. Mazzei, S. Ciurli, C. Bertucci, Surface plasmon resonance and isothermal titration calorimetry to monitor the Ni(II)-dependent binding of Helicobacter pylori NikR to DNA, Anal. Bioanal. Chem. 408 (2016) 7971–7980.

[15] H. Zheng, K.B. Handing, M.D. Zimmerman, I.G. Shabalin, S.C. Almo, W. Minor, X-ray crystallography over the past decade for novel drug discovery - where are we heading next?, Expert Opin. Drug Discov. 10 (2015) 975–89.

[16] A.L. Carvalho, J. Trincão, M.J. Romão, X-Ray crystallography in drug discovery, in: Methods Mol. Biol., 2010: pp. 31–56.

[17] M. Pellecchia, I. Bertini, D. Cowburn, C. Dalvit, E. Giralt, W. Jahnke, T.L. James, S.W. Homans, H. Kessler, C. Luchinat, B. Meyer, H. Oschkinat, J. Peng, H. Schwalbe, G. Siegal, Perspectives on NMR in drug discovery: a technique comes of age, Nat. Rev. Drug Discov. 7 (2008) 738–45.

[18] A.D. Gossert, W. Jahnke, NMR in drug discovery: a practical guide to identification and validation of ligands interacting with biological macromolecules, Prog. Nucl. Magn. Reson. Spectrosc. 97 (2016) 82–125.

[19] L. Pedro, R. Quinn, Native mass spectrometry in fragment-based drug discovery, Molecules. 21 (2016) 984.

[20] K.J. Pacholarz, R.A. Garlish, R.J. Taylor, P.E. Barran, Mass spectrometry based tools to investigate protein–ligand interactions for drug discovery, Chem. Soc. Rev. 41 (2012) 4335.

[21] F. Riccardi Sirtori, A. Altomare, M. Carini, G. Aldini, L. Regazzoni, MS methods to study macromolecule-ligand interaction: applications in drug discovery, Methods. 144 (2018) 152–174.

[22] M. Carini, L. Regazzoni, G. Aldini, Mass spectrometric strategies and their applications for molecular mass determination of recombinant therapeutic proteins, Curr. Pharm. Biotechnol. 12 (2011) 1548–57.

[23] E. Calleri, C. Temporini, G. Caccialanza, G. Massolini, Target-Based Drug Discovery: the emerging success of

frontal affinity chromatography coupled to mass spectrometry, ChemMedChem. 4 (2009) 905–916.

[24] E. Calleri, S. Ceruti, G. Cristalli, C. Martini, C. Temporini, C. Parravicini, R. Volpini, S. Daniele, G. Caccialanza, D. Lecca, C. Lambertucci, M.L. Trincavelli, G. Marucci, I.W. Wainer, G. Ranghino, P. Fantucci, M.P. Abbracchio, G. Massolini, Frontal Affinity chromatography−mass spectrometry useful for characterization of new ligands for GPR17 receptor, J. Med. Chem. 53 (2010) 3489–3501.

[25] V. D'Atri, A. Goyon, B. Bobaly, A. Beck, S. Fekete, D. Guillarme, Protocols for the analytical characterization of therapeutic monoclonal antibodies. III – Denaturing chromatographic techniques hyphenated to mass spectrometry, J. Chromatogr. B. 1096 (2018) 95–106.

[26] D. Tedesco, C. Bertucci, Induced circular dichroism as a tool to investigate the binding of drugs to carrier proteins: classic approaches and new trends, J. Pharm. Biomed. Anal. 113 (2015) 34–42.

[27] C. Bertucci, M. Pistolozzi, A. De Simone, Circular dichroism in drug discovery and development: an abridged review, Anal. Bioanal. Chem. 398 (2010) 155–166.

[28] S.S. Wesolowski, D.E. Pivonka, A rapid alternative to X-ray crystallography for chiral determination: case studies of vibrational circular dichroism (VCD) to advance drug discovery projects, Bioorg. Med. Chem. Lett. 23 (2013) 4019–25.

[29] B.A. Wallace, R.W. Janes, B.A. Wallace, Circular dichroism and synchrotron radiation circular dichroism spectroscopy: tools for drug discovery, Biochem. Soc. Trans. 31 (2003) 631–3.

[30] N.J. Waters, R. Jones, G. Williams, B. Sohal, Validation of a rapid equilibrium dialysis approach for the measurement of plasma protein binding, J. Pharm. Sci. 97 (2008) 4586–4595.

[31] M.J. Banker, T.H. Clark, J.A. Williams, Development and validation of a 96-well equilibrium dialysis apparatus for measuring plasma protein binding, J. Pharm. Sci. 92 (2003) 967–74.

[32] F. Zhang, J. Xue, J. Shao, L. Jia, Compilation of 222 drugs' plasma protein binding data and guidance for study designs, Drug Discov. Today. 17 (2012) 475–485.

[33] J.L. Cole, Methods in enzymology: analytical ultracentrifugation. Preface, in: Methods Enzymol., 2015: pp. xix–xx.

[34] J. Liu, J.D. Andya, S.J. Shire, A critical review of analytical ultracentrifugation and field flow fractionation methods for measuring protein aggregation, AAPS J. 8 (2006) E580-9.

[35] T. Hesterkamp, J. Barker, A. Davenport, M. Whittaker, Fragment based drug discovery using fluorescence correlation: spectroscopy techniques: challenges and solutions, Curr. Top. Med. Chem. 7 (2007) 1582–91.

[36] T.J. Burke, K.R. Loniello, J.A. Beebe, K.M. Ervin, Development and application of fluorescence polarization assays in drug discovery, Comb. Chem. High Throughput Screen. 6 (2003) 183–94.

[37] D.S. Hage, High-performance affinity chromatography: a powerful tool for studying serum protein binding, J. Chromatogr. B. Analyt. Technol. Biomed. Life Sci. 768 (2002) 3–30.

[38] K. Vuignier, D. Guillarme, J.-L. Veuthey, P.-A. Carrupt, J. Schappler, High performance affinity chromatography (HPAC) as a high-throughput screening tool in drug discovery to study drug-plasma protein interactions, J. Pharm. Biomed. Anal. 74 (2013) 205–12.

[39] T.A. Noctor, M.J. Diaz-Perez, I.W. Wainer, Use of a human serum albumin-based stationary phase for high-performance liquid chromatography as a tool for the rapid determination of drug-plasma protein binding, J. Pharm. Sci. 82 (1993) 675–6.

[40] C. Temporini, G. Brusotti, G. Pochetti, G. Massolini, E. Calleri, Affinity-based separation methods for the study of biological interactions: the case of peroxisome proliferator-activated receptors in drug discovery, Methods. 146 (2018) 12–25.

[41] A. Espada, M. Molina-Martin, Capillary electrophoresis and small molecule drug discovery: a perfect match?, 17 (2012) 396–404.

[42] M. Quaglia, E. De Lorenzi, Capillary electrophoresis in drug discovery, in: Methods Mol. Biol., 2010: pp. 189–202.

[43] C. Bertucci, M. Bartolini, R. Gotti, V. Andrisano, Drug affinity to immobilized target bio-polymers by high-performance liquid chromatography and capillary electrophoresis, J. Chromatogr. B. Analyt. Technol. Biomed. Life Sci. 797 (2003) 111–29.

[44] M. Cheng, Z. Chen, Recent advances in screening of enzymes inhibitors based on capillary electrophoresis, J. Pharm. Anal. 8 (2018) 226–233.

[45] L. Tian, W. Wei, Y. Mao, Kinetic studies of the interaction between antitumor antibiotics and DNA using quartz crystal microbalance, Clin. Biochem. 37 (2004) 120–7.

[46] C.J. Fee, Label-free, real-time interaction and adsorption analysis 2: quartz crystal microbalance, Methods Mol. Biol. 996 (2013) 313–22.

[47] P. Linke, K. Amaning, M. Maschberger, F. Vallee, V. Steier, P. Baaske, S. Duhr, D. Breitsprecher, A. Rak, An automated microscale thermophoresis screening approach for fragment-based lead discovery, J. Biomol. Screen. 21 (2016) 414–421.

[48] A.M. Mueller, D. Breitsprecher, S. Duhr, P. Baaske, T. Schubert, G. Längst, MicroScale thermophoresis: a rapid and precise method to quantify protein–nucleic acid interactions in solution, in: Methods Mol. Biol., 2017: pp. 151–164.

[49] M. Asmari, R. Ratih, H.A. Alhazmi, S. El Deeb, Thermophoresis for characterizing biomolecular interaction, Methods. 146 (2018) 107–119.

[50] W.H. Ward, G.A. Holdgate, Isothermal titration calorimetry in drug discovery, Prog. Med. Chem. 38 (2001) 309–76.

[51] V. Linkuvienė, G. Krainer, W.-Y. Chen, D. Matulis, Isothermal titration calorimetry for drug design: precision of the enthalpy and binding constant measurements and comparison of the instruments, Anal. Biochem. 515 (2016) 61–64.

[52] A. Velazquez-Campoy, S.A. Leavitt, E. Freire, Characterization of protein-protein interactions by isothermal titration calorimetry, in: Methods Mol. Biol., 2015: pp. 183–204.

[53] K. Länge, G. Blaess, A. Voigt, R. Götzen, M. Rapp, Integration of a surface acoustic wave biosensor in a microfluidic polymer chip, Biosens. Bioelectron. 22 (2006) 227–32.

[54] M. Meininger, T. Schmitz, T. Wagner, A. Ewald, U. Gbureck, J. Groll, C. Moseke, Real-time measurement of protein adsorption on electrophoretically deposited hydroxyapatite coatings and magnetron sputtered metallic films using the surface acoustic wave technique, Mater. Sci. Eng. C. 61 (2016) 351–354.

[55] U.H. Danielson, Integrating surface plasmon resonance biosensor-based interaction kinetic analyses into the lead discovery and optimization process, Future Med. Chem. 1 (2009) 1399–1414.

[56] M.A. Cooper, Optical biosensors in drug discovery, Nat. Rev. Drug Discov. 1 (2002) 515–528.

[57] P. Singh, SPR biosensors: historical perspectives and current challenges, Sensors Actuators B Chem. 229 (2016) 110–130.

[58] R. Karlsson, P.S. Katsamba, H. Nordin, E. Pol, D.G. Myszka, Analyzing a kinetic titration series using affinity biosensors, Anal. Biochem. 349 (2006) 136–147.

[59] E. Fabini, U.H. Danielson, Monitoring drug–serum protein interactions for early ADME prediction through Surface Plasmon Resonance technology, J. Pharm. Biomed. Anal. 144 (2017) 188–194.

[60] R.L. Rich, Y.S. Day, T.A. Morton, D.G. Myszka, High-resolution and high-throughput protocols for measuring drug/human serum albumin interactions using BIACORE, Anal. Biochem. 296 (2001) 197–207.

[61] F. Merino, S. Raunser, Electron cryo-microscopy as a tool for structure-based drug development, Angew. Chemie Int. Ed. 56 (2017) 2846–2860.

[62] D. Quentin, S. Raunser, Electron cryomicroscopy as a powerful tool in biomedical research, J. Mol. Med. 96 (2018) 483–493.

[63] S.M. Kelly, N.C. Price, The use of circular dichroism in the investigation of protein structure and function, Curr. Protein Pept. Sci. 1 (2000) 349–84.

[64] M. Bartolini, C. Bertucci, M.L. Bolognesi, A. Cavalli, C. Melchiorre, V. Andrisano, Insight into the kinetic of amyloid beta (1-42) peptide self-aggregation: elucidation of inhibitors' mechanism of action, Chembiochem. 8 (2007) 2152–61.

[65] M. Bartolini, C. Bertucci, V. Cavrini, V. Andrisano, beta-Amyloid aggregation induced by human acetylcholinesterase: inhibition studies, Biochem. Pharmacol. 65 (2003) 407–16.

[66] C.A. Ross, M.A. Poirier, Protein aggregation and neurodegenerative disease, Nat. Med. 10 (2004) S10–S17.

[67] F.S. Ruggeri, J. Habchi, A. Cerreta, G. Dietler, AFM-based single molecule techniques: unraveling the amyloid pathogenic species, Curr. Pharm. Des. 22 (2016) 3950–70.

[68] J. Piñero, L.I. Furlong, F. Sanz, In silico models in drug development: where we are, Curr. Opin. Pharmacol. 42

(2018) 111–121.

[69] P. V Desai, The integration of computational chemistry during drug discovery to drive decisions: are we there yet?, Future Med. Chem. 8 (2016) 1717–1720.

[70] L. Ferreira, R. dos Santos, G. Oliva, A. Andricopulo, Molecular docking and structure-based drug design strategies, Molecules. 20 (2015) 13384–13421.

[71] M.R. Siddiqui, Z.A. Alothman, N. Rahman, Analytical techniques in pharmaceutical analysis: a review, Arab. J. Chem. 10 (2017) S1409–S1421.

PART II

Human serum albumin

Chapter 3

Introduction

3.1 General remarks

Human serum albumin (HSA) is the most abundant plasma protein in humans, representing more than 50% of the total protein content in bloodstream. Its high concentration (~ 600 μM) and net negative charge modulate fluid distribution between compartments, accounting for ~70% to colloid osmotic pressure [1]. Beside oncotic properties, HSA exerts a broad range of biological functions including antioxidant activity, inflammatory and immunological modulation, stabilization of hemostatic and endothelial functions and the carrier role for a vast variety of ligands [2]. Recent surveys have highlighted that almost half of all developing new drugs are withdrawn before marketing, because of absorption, distribution, metabolism, excretion, toxicity (ADMET) issues [3]. Since, ADMET profile and the therapeutic activity of drugs depend on the circulating free fraction, binding to serum proteins, including binding to HSA, is a crucial parameter in the drug discovery process [4]. Moreover, because of the ability of HSA to bind a variety of structurally different endogenous and exogenous compounds, competition of new drug candidates for the same binding site of marketed drugs is also a key aspect to be evaluated during drug development.

Due to its biological functions, pharmaceutical-grade HSA for infusion is widely used in clinical practice to treat different diseases, such as hypovolemia, hypoalbuminemia, shock, acute respiratory distress syndrome, burns, hemorrhage and hemodialysis [5,6]. Moreover, it is usually part of the therapy for the treatment of acute liver failure and chronic liver diseases, which are characterized by a strong impairment of albumin metabolism [7,8]. HSA is proposed as biomarker for several diseases [9], namely rheumatoid arthritis, cancer, obesity related to post-menopause, ischemia or altered glycemic values-based diseases. Indeed, HSA could undergo structural modifications in the bloodstream, including cysteinylation, oxidation, glycation and truncation both at the N- and C-terminal. For instance, pathological conditions characterized by high levels of oxidative stress and inflammation, e.g. cirrhosis and diabetes mellitus, are known to induce structural changes, which, in some cases, affect HSA non-oncotic functions [10]. Some of these altered forms of HSA seem playing a role in the progression and/or complication of some important diseases, making the elucidation of the relationship between HSA modifications, biological functions and pathogenic role of altered HSA, crucial to be understood [2,11]. For instance, some chronic complications of diabetes have been related to the increased levels of protein glycation which occurs as a consequence of the higher levels of glucose in the blood of these patients. In this context,

monitoring variations in glycation has been proposed as possible biomarker in patients suffering from diabetes [12–14]. In this scenario, analytical methods to investigate structural features and functional properties, which are strictly connected with protein integrity, e.g. binding capacity, are of relevance in clinical research and in the early stages of drug discovery.

The huge amount of biological functions exerted by HSA in many physiological and pathological setting makes albumin one of the most investigated proteins. Nevertheless, its role in the modulation of many processes has not been completely clarified. For this reason, HSA still remains an intriguing object of research.

3.2 Albumin structure

HSA biosynthesis starts in the hepatocytes with the production of pre-pro-albumin. This form is subsequently modified into pro-albumin and cleaved of the N-terminal oligopeptide in endoplasmic reticulum and in Golgi apparatus, respectively. HSA is released with a daily rate of 10–15 g/day into the bloodstream, where it remains with a relatively long half-life time (~20 days) [1]. The mature plasma protein is composed by 585 residues and has a molecular weight of 66438 Da. Protein high solubility is granted by the presence of several ionizable amino acid residues, e.g. lysines, arginines and glutamic acids, with a net negative charge. Furthermore HSA structure is characterized by the presence of a single tryptophan residue (Trp214) which ensures fluorescence studies [9]. The protein is composed by 17 cysteines-based disulfide bonds, which increase protein stability and flexibility. Cysteine at position 34 is the only cysteine residue not involved in disulfide bridges, constituting the larger reservoir of thiols in plasma [15]. This residue acts as radical scavenging in circulatory system and can bind different endogenous ligands, e.g. nitric oxide (NO) and metal ions. Moreover, free Cys34 may interact with different circulating molecules and, in a limited extent, with other circulating HSA molecules, forming protein dimers [16].

HSA secondary structure displays the typical features of α-helix-rich proteins (~68 % α helices content) [17]. HSA consists of three homologous domains (I, II, III), which are divided into two sub-domains, labeled A and B which contain 6 and 4-helices, respectively. In solution, the six subdomains, namely IA (residues 1–112), IB (residues 113–195), IIA (residues 196–303), IIB (residues 304–383), IIIA (residues 384–499) and IIIB (residues 500–585) assemble asymmetrically, in the so-called heart-sharp conformation [18,19] (Fig. 4). Nevertheless, the huge flexibility of this macromolecule makes HSA conformation easily changeable [19].

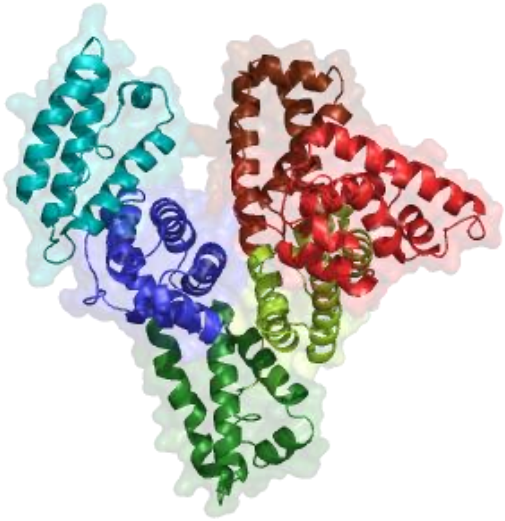

Figure 4| Three-dimensional structure of albumin. Heart-sharp conformation of HSA caused by subdomains disposition: IA (red), IB (brown), IIA (light green), IIB (dark green), IIIA (blue), IIIB (cyan).

3.3 Structural modifications of circulating HSA

HSA undergoes several changes which may affect protein structure and conformation. Among them, the most common and investigated are cysteinylation, truncation at the N- and C- terminal, oxidation and glycation.

Oxidation of HSA, which is promoted by reactive oxygen species (ROS), chemical products derived from lipid peroxidation, ascorbic acid and hydroxyl radicals formed via Fenton reaction, can affect protein integrity and functionality [20]. Oxidation of Cys34 represents the major alteration of circulating HSA and despite this process occurs in physiological conditions, it is enhanced by increased oxidative stress and age. In about 20–30 % of the circulating protein, this residue is involved in mixed disulfide bonds with another cysteine residue or glutathione residue. These modifications, i.e., cysteinylation or glutathionylation, lead to the formation of a reversibly oxidized form of HSA which is also known as non-mercaptoalbumin 1 (HNA1). Almost 5 % of the total content of HSA in plasma undergoes irreversible oxidation into sulfinic or sulfonic acid, forming the so-called non-mercaptoalbumin 2 (HNA2). Cys34 acts as antioxidant compound towards NO and other radicals as well as it displays binding capacity for different ligands (metal ions, NO, drugs). For this reason, its alterations may cause an impairment of HSA redox potential and functionality [9,21]. Moreover, oxidation of Cys34 by other cysteines promotes *N*-homocysteinylation of Lys525, which has been related to the onset of pathological states such as thrombogenesis or production of antibodies against the modified albumin form [22–24]. Less frequently, oxidative modifications may involve lysine, arginine or methionine residues. Oxidation of these amino acids, such as arginine at position 410, has been shown to possibly increase the rate of HSA clearance [25,26].

The truncations at the N- and C- terminal are other common modifications. Since the N-terminal domain of HSA is able to bind circulating free metal ions, the removal of asparagine–alanine residues impairs HSA scavenging activity towards circulating metal ions [15,27]. On the other hand, the truncation at C- terminal decreases protein half-life time, from 20 days to less than 80 h [28].

Circulating glycated HSA is the result of physiological non-enzymatic glycation of the native protein by reducing sugars. This modification, which accounts for almost 10 % of the total HSA content in healthy people, increases 2 or 3 times in case of diabetes mellitus. Indeed, despite this process is physiological and increases in aging, it results much faster under diabetic conditions defined by chronic hyperglycemia. Moreover, because of HSA long half-life and high concentration, as compared to other proteins, glycated HSA is proposed as a possible biomarker for diabetes control [29]. Initially chemically reversible Schiff bases and Amadori adducts are formed. The formation of the early glycation adducts involves several lysines, such as Lys525 (as prevalent site of glycation), Lys199, Lys281, Lys489, and arginine residues (e.g. Arg410) [20,30]. Overtime, these products slowly undergo further rearrangements, e.g. oxidation, degradation and dehydration, resulting in the irreversible formation of the so-called advanced glycation end products (AGEs) [31]. Glycation process modifies the structure of the protein. Moreover, since this process may involve aminoacid residues located in or near HSA binding sites, it also may compromise HSA binding capacity for endogenous and exogenous compounds [32].

Besides these common modifications, it is worth mentioning also dimerization, nitration and nitrosylation [2].

3.4 HSA biological functions

Albumin displays important biologic functions, which can be divided into oncotic and non-oncotic. Indeed, HSA plays an important role as fluid modulator through body compartments and regulates ~70–80 % of the oncotic pressure in plasma. This function is granted for two-thirds by the osmotic effect, which is related to its molecular weight, while for one-third by Gibbs-Donnan effect. Indeed, in physiological conditions the net negative charge of HSA recalls positively charged ions (e.g. sodium and water) inside intravascular compartments. As a result of its osmotic effect, HSA is widely used in clinical practice as plasma expander, e.g. in case of hypovolemic shock [33].

HSA also owns different non-oncotic properties which, in most of the cases, are strictly connected to its peculiar structure (Fig. 5) [9,10].

HSA remarkable binding capacity reflects its organization in multidomains. Under physiological conditions, the protein binds a huge variety of endogenous ligands, such as fatty acids, ions,

hormones as well as exogenous compounds, i.e. drugs and their metabolites [10]. Moreover, HSA is also responsible for bilirubin binding, favoring its clearance [1]. Over the years, albumin binding sites have been widely investigated. According to the classification proposed by Sudlow, HSA has two major binding sites for drugs (sites I and II) located in sub-domains IIA and IIIA, respectively.

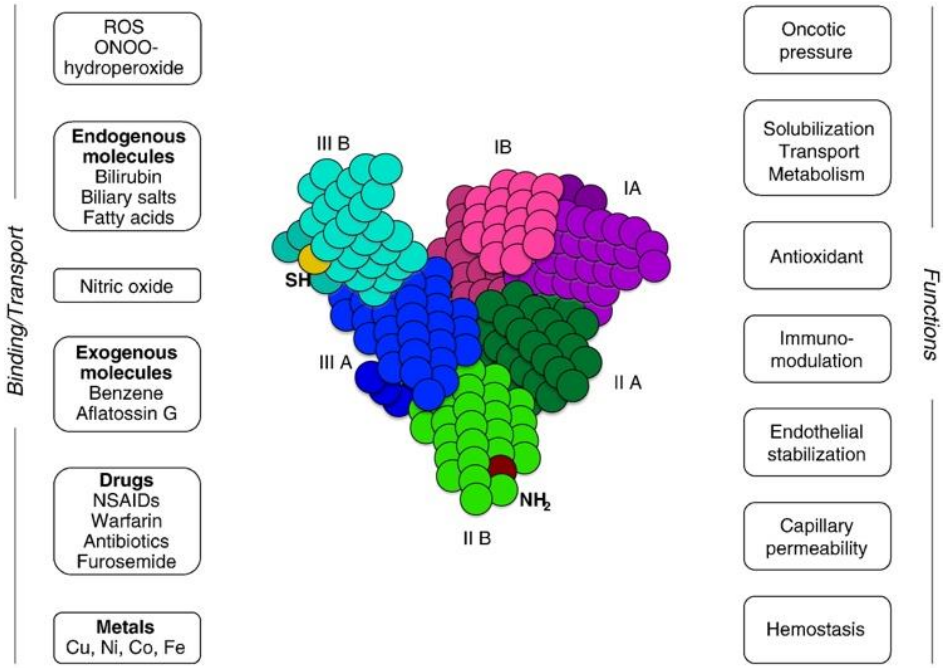

Figure 5| HSA biological functions and binding properties. On the right column, HSA oncotic and non-oncotic biological functions are listed while the left panel lists the most common classes of endogenous and exogenous ligands. Reprinted with permission from [34].

Site I, which is larger and more flexible than site II, enables the binding of heterocyclic compounds, e.g. warfarin or phenylbutazone [35]. Site II, smaller and less adaptable, is called indole-benzodiazepine binding site and hosts aromatic or indole-compounds, like diazepam or L-tryptophan. Recently, a third binding site (site III), allosterically coupled with the other two, has been identified in sub-domain IB [36]. Site III is considered a promiscuous pocket, on the basis of its different ligand recognition capacity: among its binders, biliverdin, bilirubin and several anticancer agents are included. HSA binding capacity promotes drugs solubility, thus enabling their transport to the sites of action. Moreover, the great capacity of the main binding sites to discriminate stereoisomers makes binding of drugs highly influenced by stereochemistry [37].

Another important function of HSA is its antioxidant activity. Cys34 represents the major reservoir of thiols in plasma (~ 80%), acting as scavenger for ROS. The pronounced antioxidant capacity displayed by this residue is related to the low pK_a of the corresponding thiol group (about 5.0), in contrast to the pK_a of the other aminothiols (cysteine and glutathione residues). As consequence, at

physiological pH, Cys34 predominantly exists as thiolate anion, which grants the peculiar nucleophilic reactivity against metals and oxygen/nitrogen reactive species [38]. HSA scavenger activity is also assisted by aminoacidic residues (methionines) and the ability of the N-terminal portion to chelate iron and copper ions, inhibiting their involvement in the formation of hydroxyl radicals via Fenton reaction [15].

HSA is also considered an important modulator of prostaglandins bioavailability, resulting in the activation of inflammatory response promoted by immune system [39]. Moreover, the ability of Cys34 to bind NO seems to prevent its rapid inactivation prolonging its antiplatelet effect and the antithrombotic activity [40]. Finally, HSA is involved in immune response to both Gram-positive and Gram-negative bacteria due to protein interaction with some components located on the bacteria surface. This event promotes the interaction with the Toll-like receptor 4, thus modulating albumin anti-inflammatory activity [41].

The relationship between HSA structure and physiological properties requires the development of different analytical strategies capable of correlating structural and functional features. The following section briefly resumes the principal analytical techniques employed over the years in the structural characterization of HSA as well as binding capacity and antioxidant activity as main non-oncotic properties.

3.5 Analytical strategies for HSA characterization

Structural and functional integrity of HSA have been widely investigated over the years. In particular, because of its important physiological role, many efforts have been made to develop tailored strategies capable to identify and quantitate altered HSA structures. Among analytical methods used to highlighting HSA structural integrity, methods focused on the qualitative and quantitative investigation of the most frequent and abundant HSA alterations are particularly relevant. Among chromatographic techniques, ion exchange chromatography (IEC), size exclusion chromatography (SEC) and reverse-phase chromatography (RP-LC), all coupled with UV or MS detection, represent the most commonly used approaches. For instance, IEC strategy is suitable to investigate HSA isoforms arising from altered Cys34 oxidative state [43,44]. On the other hand, SEC is useful to highlight the formation of dimers and aggregates thanks to its ability to resolve different compounds as function of their hydrodynamic volume. For example, a SEC-based method has been applied to evaluate the formation of dimeric products in the presence of high levels of oxidative stress or as function of temperature [44]. Hyphenation of RP-LC with MS grants analyses of HSA modifications by both top-down and bottom-up approaches [46] which allowed the study of HSA truncation, cysteinylation and glycation [2]. For instance, many studies have been carried out

using RP-LC-MS in order to obtain information concerning HSA glycation extent or preferential glycation sites involved in the process [46,47]. Besides chromatographic methods, HSA alterations can be investigated using capillary zone electrophoresis (CZE), in which analytes are separated on the basis of their charge, shape and size [48]. Moreover, this technique allows performing analyses in physiological-like environment (i.e. aqueous solutions).

HSA conformational changes are usually investigated by means of spectroscopic techniques, namely circular dichroism (CD) and fluorescence spectroscopies [2]. CD method has been widely used to evaluate HSA secondary structure along with functional features resulting from several different conditions: high temperature, pro-oxidant compounds, addition of stabilizers in the pharmaceutical-grade HSA or sugar concentration during *in-vitro* glycation process [49]. Instead, HSA fluorescence, which is granted by the presence of a single tryptophan residue (Trp214), has been used to assess stability and isomers conformation as well as to investigate conformational changes involving domain II, where Trp214 is located [50].

Many efforts in the development of analytical strategies have been also made to assess HSA binding capacity and antioxidant activity. Over the years, drug binding to HSA has been measured by several techniques. Among them, it is worth mentioning equilibrium dialysis, ultrafiltration (UF), high performance affinity chromatography (HPAC), Hummel-Dreyer method, affinity capillary electrophoresis (ACE), capillary electrophoresis-frontal analysis (CE-FA), ultrafast affinity extraction, spectroscopic approaches and surface plasmon resonance (SPR) [2]. In particular, HPAC enables the quantitative determination of drug–HSA binding on the basis of retention time. Indeed, drugs with stronger affinities towards immobilized HSA will show higher retention times compared with drugs characterized by lower affinities. Frontal affinity chromatography (FAC) and/or zonal elution chromatography enable the determination of association constants, granting precision, low-time consuming and reduced sample handling [51,52]. The main drawback of the technique is the huge amount of analyte consumption for analyses, representing a limitation when low quantities are extracted from biological samples. Conversely, SPR-based technology enables affinity and kinetic estimation of binding events using small quantities of materials. The interaction is monitored in real-time and the high automation grants time saving [53,54]. Indeed, different compounds can be screened using the same HSA sensing surface granting a fast screening process. Moreover, altered HSA isoforms as well as albumins from different species can be immobilized onto SPR platforms. In the first case, SPR approach may favor the correlation between structural modifications and HSA binding properties. In the latter, it may underline the species-dependent binding, pointing out the caution necessary before the extrapolation of data for clinical studies [55,56]. Besides conformational analysis, CD

spectroscopy has been widely employed to investigate ligand–HSA interactions. The achievement of affinity binding constants relies on the onset of induced circular dichroism (ICD): a typical CD signal peculiar of the complex. Similarly, well-characterized ICD markers can be exploited for competition studies at the main binding sites of HSA, disclosing the binding site as well as the binding mode of compounds [37,57]. HSA binding capacity as function of structural modifications (e.g. glycation) has been recently questioned by several research groups [58,59]. Moreover, a CD spectroscopy-based assay to investigate the impairment of HSA binding properties resulting from stabilizers addition, namely sodium octanoate and N-acetyltryptophan, is presented in the chapter 4.
In addition to HSA binding capacity, HSA antioxidant activity is one of the mostly studied non-oncotic functions. HSA antioxidant capacity is strictly connected to protein structure, mostly depending on the presence of a free thiol group at the Cys34 residue and on the N-terminal binding capacity towards free ions. As a consequence, structural changes triggered by pro-oxidant microenvironment can deeply affect this function [48]. Analytical approaches used to assess antioxidant properties of HSA include Ellman's assay, albumin cobalt binding assay (ACB), oxygen radical absorbance capacity assay (ORAC) and 3,3',5,5'-tetramethylbenzidine (TMB)-based assay [2]. ACB assay tests the binding capacity of the N-terminal portion of the protein towards cobalt ions (Co) by means of a colorimetric reaction. This approach is employed in clinical practice to investigate the level of ischemia modified albumin (IMA) in circulating albumin pool, which reflects, in turn, a decrease in HSA antioxidant activity. IMA levels have also been proposed as biomarkers for acute coronary syndrome. Newly, ACB-based method has been employed to test antioxidant capacity of pharmaceutical-grade HSA [60]. Another colorimetric reaction, based on the interaction between free thiol groups and a chromogenic agent, is Ellman's assay. This method is indirectly used to test HSA scavenger activity on the basis of the availability of Cys34 residues to form a colorimetric complex with 5,5'-dithiobis-2-nitrobenzoic acid (DTNB) [61]. For instance, this approach enables the evaluation of antioxidant activity as function of structural changes triggered by *in vitro* glycation and oxidation processes. Moreover it can be used to compare circulating HSA scavenger activity between healthy control subjects and diabetic patients [62,63]. Finally, ORAC and TMB assays can evaluate HSA antioxidant capacity towards peroxyl radicals and hydroxyl radicals respectively of pharmaceutical formulations and altered proteins [60].

3.6 Clinical implications of modified circulating HSA

Circulating HSA could undergo structural modifications in the bloodstream, such as oxidation, cysteinylation and glycation, which may affect its physiological functions. Moreover, a significant decrease in physiological albumin amount has been related to an increasing hazard of morbidity and

mortality in renal and liver diseases, rheumatoid arthritis, ischemia, cancer and hypoalbuminemia [9]. In this scenario, modifications of HSA structure may reflect pathological conditions of human body, resulting in a possible use of HSA as prognostic biomarker in diseases, such as kidney, liver failure and aging (Fig. 6) [2].

Oxidative stress increases with aging, thus promoting HSA oxidation and, as consequence, a decrease of the native isoform. Impairment in the overall redox state directly contributes to elderly-related complications, such as an increasing risk of cardiovascular pathologies [65]. Oxidative stress and oxidized HSA have also been related to renal diseases. For example, a significant oxidation of HSA is encountered in primary nephrotic syndrome [66].

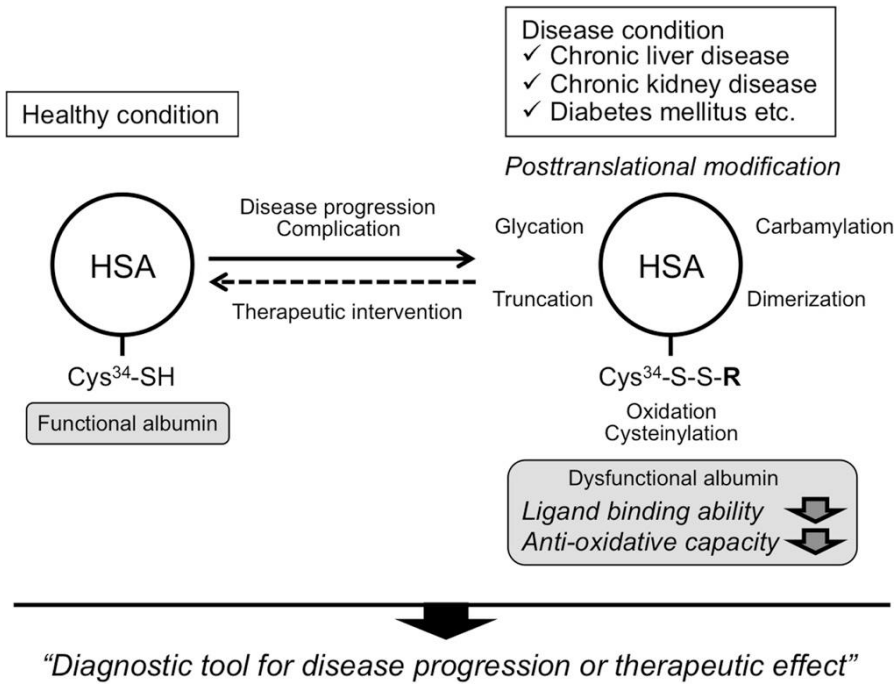

Figure 6| Clinical implication of the equilibrium between physiological and modified HSA. HSA alterations as prognostic biomarkers in several diseases. Reprinted with permission from [64].

Circulating levels of HNAs (1 and 2) are considered important biomarkers of the oxidative stress status of patients which are submitted to hemodialysis. Moreover, the total fraction of HNA (HNA1+ HNA2) is strongly tied to the decrease of creatinine clearance. In the end-stage renal disease, an increased level of cysteinylated HSA has been observed. These high levels, in turn, promote oxidative stress. Moreover, alteration of the native HSA affects its vasculoprotective properties, promoting cardiovascular complications in hemodialysis patients [64]. Impaired HSA functions have been reported during end-stages of renal failure, e.g. binding capacity at site II of the protein. Moreover, the alterations of the N-terminal portion of the protein, which also occur under

these conditions, contribute to increase the levels of IMA which, in turn, enhances the incidence percentage of coronary heart disease [12].

Oxidative stress also plays a key role in the pathogenesis of liver diseases, such as cirrhosis [34]. This pathology alters not only the content of albumin as a consequence of a reduced production in the liver, but also HSA structural quality. Indeed, increased levels of HNA1 and HNA2 along with the carbonylated HSA have been detected in cirrhotic patients. In particular, these modified isoforms increase in case of decompensated cirrhosis and in patients which suffer of acute-on-chronic-liver failure [67]. In case of decompensated cirrhosis and severe alcoholic hepatitis, an increase of HSA dimers, C- and N-terminal truncations and cysteinylation have been also reported. The quantification of all these altered isoforms favors the estimation of the residual native HSA in plasma, which has been shown to be a better predictor of patient survival after 1-year instead of albumin content (currently considered in clinical practice) [68]. Cirrhosis also increases IMA ratio which, in turn, enhances the severity of cirrhosis itself and leads to many complications. In this scenario, the carrier function for fatty acids and site-II ligands as well as the antioxidant activity have been shown to be considerably impaired.

Finally, circulating glycated HSA increases in diabetic conditions and serum levels of glycated HSA have been proposed as a better short-term indicator of diabetes than glycated hemoglobin. Concerning its involvement in pathological processes, recent evidence suggests that advanced glycation end products (AGEs) may play a role in the onset of diabetic complications including retinopathy, nephropathy and cardiomyopathy. Similarly, RAGE activation by AGEs seems to be involved in the ethiopathogenesis of some chronic diabetes complications. This observation has recently increased the interest and the efforts towards the investigation of such interaction [69,70]. In this context, a multimethodological strategy to investigate the binding of glycated HSA with RAGE is presented in chapter 5.

References

[1] T. Peters, All about albumin, First ed., Academic Press, London, 1996.

[2] M. Naldi, M. Baldassarre, M. Domenicali, M. Bartolini, P. Caraceni, Structural and functional integrity of human serum albumin: analytical approaches and clinical relevance in patients with liver cirrhosis, J. Pharm. Biomed. Anal. 144 (2016) 138–153.

[3] J. Hodgson, ADMET—turning chemicals into drugs, Nat. Biotechnol. 19 (2001) 722–726.

[4] C. Bertucci, E. Domenici, Reversible and covalent binding of drugs to human serum albumin: methodological approaches and physiological relevance, Curr. Med. Chem. 9 (2002) 1463–1481.

[5] G.R. Haynes, R.J. Navickis, M.M. Wilkes, Albumin administration-what is the evidence of clinical benefit? A systematic review of randomized controlled trials, Eur. J. Anaesthesiol. 20 (2003) 771–93.

[6] A. Liberati, L. Moja, I. Moschetti, G.F. Gensini, R. Gusinu, Human albumin solution for resuscitation and volume expansion in critically ill patients, Intern. Emerg. Med. 1 (2006) 243–5.

[7] P. Caraceni, O. Riggio, P. Angeli, C. Alessandria, S. Neri, F.G. Foschi, F. Levantesi, A. Airoldi, S. Boccia, G. Svegliati-Baroni, S. Fagiuoli, R.G. Romanelli, R. Cozzolongo, V. Di Marco, V. Sangiovanni, F. Morisco, P. Toniutto, A. Tortora, R. De Marco, M. Angelico, I. Cacciola, G. Elia, A. Federico, S. Massironi, R. Guarisco, A. Galioto, G. Ballardini, M. Rendina, S. Nardelli, S. Piano, C. Elia, L. Prestianni, F.M. Cappa, L. Cesarini, L. Simone, C. Pasquale, M. Cavallin, A. Andrealli, F. Fidone, M. Ruggeri, A. Roncadori, M. Baldassarre, M. Tufoni, G. Zaccherini, M. Bernardi, Long-term albumin administration in decompensated cirrhosis (ANSWER): an open-label randomised trial, Lancet. 391 (2018) 2417–2429.

[8] S. Harm, C. Schildböck, J. Hartmann, Removal of stabilizers from human serum albumin by adsorbents and dialysis used in blood purification, PLoS One. 13 (2018) 1–18.

[9] G. Fanali, A. Di Masi, V. Trezza, M. Marino, M. Fasano, P. Ascenzi, Human serum albumin: from bench to bedside, Mol. Aspects Med. 33 (2012) 209–290.

[10] M. Fasano, S. Curry, E. Terreno, M. Galliano, G. Fanali, P. Narciso, S. Notari, P. Ascenzi, The extraordinary ligand binding properties of human serum albumin, IUBMB Life. 57 (2005) 787–796.

[11] J. V Valencia, S.C. Weldon, D. Quinn, G.H. Kiers, J. DeGroot, J.M. TeKoppele, T.E. Hughes, Advanced glycation end product ligands for the receptor for advanced glycation end products: biochemical characterization and formation kinetics, Anal. Biochem. 324 (2004) 68–78.

[12] E. Sbarouni, P. Georgiadou, V. Voudris, Ischemia modified albumin changes – review and clinical implications, Clin. Chem. Lab. Med. 49 (2011) 177–84.

[13] D. Gupta, C.G. Lis, Pretreatment serum albumin as a predictor of cancer survival: a systematic review of the epidemiological literature, Nutr. J. 9 (2010) 69.

[14] M. Koga, S. Kasayama, Clinical impact of glycated albumin as another glycemic control marker, Endocr. J. 57 (2010) 751–62.

[15] M. Taverna, A.-L. Marie, J.-P. Mira, B. Guidet, Specific antioxidant properties of human serum albumin, Ann. Intensive Care. 3 (2013) 4.

[16] M.M. Castellanos, C.M. Colina, Molecular dynamics simulations of human serum albumin and role of disulfide bonds, J. Phys. Chem. B. 117 (2013) 11895–11905.

[17] N.J. Greenfield, Using circular dichroism spectra to estimate protein secondary structure, Nat. Protoc. 1 (2006) 2876–90.

[18] K. Taguchi, V.T. Giam Chuang, T. Maruyama, M. Otagiri, Pharmaceutical aspects of the recombinant human serum albumin dimer: structural characteristics, biological properties and medical applications, J. Pharm. Sci. 101 (2012) 3033–3046.

[19] M. Dockal, D.C. Carter, F. Rüker, Conformational transitions of the three recombinant domains of human serum albumin depending on pH., J. Biol. Chem. 275 (2000) 3042–50.

[20] F. Monacelli, D. Storace, C. D'Arrigo, R. Sanguineti, R. Borghi, D. Pacini, A.L. Furfaro, M.A. Pronzato, P. Odetti, N. Traverso, Structural alterations of human serum albumin caused by glycative and oxidative stressors revealed by circular dichroism analysis, Int. J. Mol. Sci. 14 (2013) 10694–709.

[21] K. Oettl, G. Marsche, Redox state of human serum albumin in terms of cysteine-34 in health and disease, in:

Methods Enzymol., 2010: pp. 181–195.

[22] C. Bertucci, B. Nanni, P. Salvadori, Reversible binding of ethacrynic acid to human serum albumin: difference circular dichroism study, Chirality. 11 (1999) 33–38.

[23] A.J. Stewart, C.A. Blindauer, S. Berezenko, D. Sleep, D. Tooth, P.J. Sadler, Role of Tyr84 in controlling the reactivity of Cys34 of human albumin, FEBS J. 272 (2005) 353–362.

[24] J. Perła-Kaján, T. Twardowski, H. Jakubowski, Mechanisms of homocysteine toxicity in humans, Amino Acids. 32 (2007) 561–572.

[25] Y. Iwao, M. Anraku, K. Yamasaki, U. Kragh-Hansen, K. Kawai, T. Maruyama, M. Otagiri, Oxidation of Arg-410 promotes the elimination of human serum albumin, Biochim. Biophys. Acta - Proteins Proteomics. 1764 (2006) 743–749.

[26] A. Temple, T.-Y. Yen, S. Gronert, Identification of specific protein carbonylation sites in model oxidations of human serum albumin, J. Am. Soc. Mass Spectrom. 17 (2006) 1172–1180.

[27] M. Naldi, F.A. Giannone, M. Baldassarre, M. Domenicali, P. Caraceni, M. Bernardi, C. Bertucci, A fast and validated mass spectrometry method for the evaluation of human serum albumin structural modifications in the clinical field, Eur. J. Mass Spectrom. 19 (2013) 491–496.

[28] D. Bar-Or, L.T. Rael, R. Bar-Or, D.S. Slone, M.L. Craun, The formation and rapid clearance of a truncated albumin species in a critically ill patient, Clin. Chim. Acta. 365 (2006) 346–349.

[29] P.A.C. Freitas, L.R. Ehlert, J.L. Camargo, P.A.C. Freitas, L.R. Ehlert, J.L. Camargo, Glycated albumin: a potential biomarker in diabetes, Arch. Endocrinol. Metab. 61 (2017) 296–304.

[30] J. Anguizola, R. Matsuda, O.S. Barnaby, K.S. Hoy, C. Wa, E. DeBolt, M. Koke, D.S. Hage, Review: Glycation of human serum albumin, Clin. Chim. Acta. 425 (2013) 64–76.

[31] C. Wa, R.L. Cerny, W.A. Clarke, D.S. Hage, Characterization of glycation adducts on human serum albumin by matrix-assisted laser desorption/ionization time-of-flight mass spectrometry, Clin. Chim. Acta. 385 (2007) 48–60.

[32] K. Oettl, R.E. Stauber, Physiological and pathological changes in the redox state of human serum albumin critically influence its binding properties., Br. J. Pharmacol. 151 (2007) 580–90.

[33] T.W. Evans, Review article: Albumin as a drug-biological effects of albumin unrelated to oncotic pressure, Aliment. Pharmacol. Ther. 16 (2002) 6–11.

[34] P. Caraceni, M. Domenicali, A. Tovoli, L. Napoli, C.S. Ricci, M. Tufoni, M. Bernardi, Clinical indications for the albumin use: still a controversial issue, Eur. J. Intern. Med. 24 (2013) 721–728.

[35] U. Kragh-Hansen, Molecular aspects of ligand binding to serum albumin, Pharmacol. Rev. 33 (1981) 17–53.

[36] F. Zsila, Subdomain IB is the third major drug binding region of human serum albumin: toward the three-sites model, Mol. Pharm. 10 (2013) 1668–1682.

[37] C. Bertucci, M. Pistolozzi, Species-dependent stereoselective drug binding to albumin: a circular dichroism study, Chirality. 20 (2008) 552–558.

[38] L. Turell, R. Radi, B. Alvarez, The thiol pool in human plasma: the central contribution of albumin to redox processes, Free Radic. Biol. Med. 65 (2013) 244–253.

[39] A.J.O. Brien, J.N. Fullerton, K.A. Massey, G. Auld, G. Sewell, S. James, J. Newson, E. Karra, A. Winstanley, W. Alazawi, R. Garcia-Marquez, J. Cordoba, A. Nicolaou, D.W. Gilroy, Prostaglandin E2 mediates immunosuppression in acutely decompensated cirrhosis, Nat. Publ. Gr. 20 (2014) 518–523.

[40] R. Spinella, R. Sawhney, R. Jalan, Albumin in chronic liver disease: structure, functions and therapeutic implications, Hepatol. Int. 10 (2016) 124–132.

[41] V. Arroyo, R. García-Martinez, X. Salvatella, Human serum albumin, systemic inflammation, and cirrhosis, J. Hepatol. 61 (2014) 396–407.

[42] L. Turell, H. Botti, S. Carballal, R. Radi, B. Alvarez, Sulfenic acid-A key intermediate in albumin thiol oxidation, J. Chromatogr. B. 877 (2009) 3384–3392.

[43] T. Hayashi, S. Era, K. Kawai, H. Imai, K. Nakamura, E. Onda, M. Yoh, Observation for redox state of human serum and aqueous humor albumin from patients with senile cataract, Pathophysiology. 6 (2000) 237–243.

[44] N. Sharma, V. Sivalingam, S. Maurya, A. Prasad, P. Khandelwal, S.C. Yadav, B.K. Patel, New insights into in vitro amyloidogenic properties of human serum albumin suggest considerations for therapeutic precautions,

FEBS Lett. 589 (2015) 4033–4038.

[45] M. Colzani, G. Aldini, M. Carini, Mass spectrometric approaches for the identification and quantification of reactive carbonyl species protein adducts, J. Proteomics. 92 (2013) 28–50.

[46] A. Lapolla, D. Fedele, R. Reitano, N.C. Aricò, R. Seraglia, P. Traldi, E. Marotta, R. Tonani, Enzymatic digestion and mass spectrometry in the study of advanced glycation end products/peptides, J. Am. Soc. Mass Spectrom. 15 (2004) 496–509.

[47] R. Kisugi, T. Kouzuma, T. Yamamoto, S. Akizuki, H. Miyamoto, Y. Someya, J. Yokoyama, I. Abe, N. Hirai, A. Ohnishi, Structural and glycation site changes of albumin in diabetic patient with very high glycated albumin., Clin. Chim. Acta. 382 (2007) 59–64.

[48] A.-L. Marie, C. Przybylski, F. Gonnet, R. Daniel, R. Urbain, G. Chevreux, S. Jorieux, M. Taverna, Capillary zone electrophoresis and capillary electrophoresis-mass spectrometry for analyzing qualitative and quantitative variations in therapeutic albumin, Anal. Chim. Acta. 800 (2013) 103–110.

[49] C. Bertucci, B. Nanni, A. Raffaelli, P. Salvadori, Chemical modification of human albumin at cys 34 by ethacrynic acid : structural characterisation and binding properties, J. Pharm. Biomed. Anal. 18 (1998) 127–136.

[50] H. Zoellner, J.Y. Hou, T. Hochgrebe, A. Poljak, M.W. Duncan, J. Golding, T. Henderson, G. Lynch, Fluorometric and mass spectrometric analysis of nonenzymatic glycosylated albumin, Biochem. Biophys. Res. Commun. 284 (2001) 83–89.

[51] H.S. Kim, I.W. Wainer, Rapid analysis of the interactions between drugs and human serum albumin (HSA) using high-performance affinity chromatography (HPAC), J. Chromatogr. B Anal. Technol. Biomed. Life Sci. 870 (2008) 22–26.

[52] D.S. Hage, High-performance affinity chromatography: a powerful tool for studying serum protein binding, J. Chromatogr. B Anal. Technol. Biomed. Life Sci. 768 (2002) 3–30.

[53] E. Fabini, U.H. Danielson, Monitoring drug–serum protein interactions for early ADME prediction through Surface Plasmon Resonance technology, J. Pharm. Biomed. Anal. 144 (2017) 188–194.

[54] Å. Frostell-Karlsson, A. Remaeus, H. Roos, K. Andersson, P. Borg, M. Hämäläinen, R. Karlsson, Biosensor analysis of the interaction between immobilized human serum albumin and drug compounds for prediction of human serum albumin binding levels, J. Med. Chem. 43 (2000) 1986–1992.

[55] E. Fabini, G.M.L. Fiori, D. Tedesco, N.P. Lopes, C. Bertucci, Surface plasmon resonance and circular dichroism characterization of cucurbitacins binding to serum albumins for early pharmacokinetic profiling, J. Pharm. Biomed. Anal. 122 (2016) 166–172.

[56] C. Fortugno, T. van der Gronde, G. Varchi, A. Guerrini, C. Bertucci, Species-dependent binding of new synthesized bicalutamide analogues to albumin by optical biosensor analysis, J. Pharm. Biomed. Anal. 111 (2015) 324–332.

[57] D. Tedesco, C. Bertucci, Induced circular dichroism as a tool to investigate the binding of drugs to carrier proteins: classic approaches and new trends, J. Pharm. Biomed. Anal. 113 (2015) 34–42.

[58] E. Rahnama, M. Mahmoodian-Moghaddam, S. Khorsand-Ahmadi, M.R. Saberi, J. Chamani, Binding site identification of metformin to human serum albumin and glycated human serum albumin by spectroscopic and molecular modeling techniques: a comparison study, J. Biomol. Struct. Dyn. 33 (2015) 513–533.

[59] A. Singha Roy, P. Ghosh, S. Dasgupta, Glycation of human serum albumin affects its binding affinity towards (−)-epigallocatechin gallate, J. Incl. Phenom. Macrocycl. Chem. 85 (2016) 193–202.

[60] J.-L. Plantier, V. Duretz, V. Devos, R. Urbain, S. Jorieux, Comparison of antioxidant properties of different therapeutic albumin preparations, Biologicals. 44 (2016) 226–233.

[61] G.L. Ellman, Tissue sulfhydryl groups, Arch. Biochem. Biophys. 82 (1959) 70–77.

[62] P. Faure, N. Wiernsperger, C. Polge, A. Favier, S. Halimi, Impairment of the antioxidant properties of serum albumin in patients with diabetes: protective effects of metformin, Clin. Sci. 114 (2008) 251–256.

[63] N. Sakata, A. Moh, S. Takebayashi, Contribution of superoxide to reduced antioxidant activity of glycoxidative serum albumin, Heart Vessels. 17 (2002) 22–29.

[64] H. Watanabe, T. Imafuku, M. Otagiri, T. Maruyama, Clinical implications associated with the post-translational modification–induced functional impairment of albumin in oxidative stress–related diseases, J. Pharm. Sci. 106 (2017) 2195–2203.

[65] R. Bhayadia, B.M.W. Schmidt, A. Melk, M. Hömme, Senescence-induced oxidative stress causes endothelial

dysfunction, Journals Gerontol. Ser. A Biol. Sci. Med. Sci. 71 (2016) 161–169.

[66] L. Musante, M. Bruschi, G. Candiano, A. Petretto, N. Dimasi, P. Del Boccio, A. Urbani, G. Rialdi, G.M. Ghiggeri, Characterization of oxidation end product of plasma albumin 'in vivo,' Biochem. Biophys. Res. Commun. 349 (2006) 668–673.

[67] K. Oettl, V. Stadlbauer, F. Petter, J. Greilberger, C. Putz-Bankuti, S. Hallström, C. Lackner, R.E. Stauber, Oxidative damage of albumin in advanced liver disease, Biochim. Biophys. Acta - Mol. Basis Dis. 1782 (2008) 469–473.

[68] M. Domenicali, M. Baldassarre, F.A. Giannone, M. Naldi, M. Mastroroberto, M. Biselli, M. Laggetta, D. Patrono, C. Bertucci, M. Bernardi, P. Caraceni, Posttranscriptional changes of serum albumin: clinical and prognostic significance in hospitalized patients with cirrhosis, Hepatology. 60 (2014) 1851–1860.

[69] G. Degani, A.A. Altomare, M. Colzani, C. Martino, A. Mazzolari, G. Fritz, G. Vistoli, L. Popolo, G. Aldini, A capture method based on the VC1 domain reveals new binding properties of the human receptor for advanced glycation end products (RAGE), Redox Biol. 11 (2017) 275–285.

[70] R. Ramasamy, S.F. Yan, A.M. Schmidt, Receptor for AGE (RAGE): signaling mechanisms in the pathogenesis of diabetes and its complications, Ann. N. Y. Acad. Sci. 1243 (2011) 88–102.

Chapter 4

New insights into the altered binding capacity of pharmaceutical-grade human serum albumin: site-specific binding studies by induced CD spectroscopy

***Anna Tramarin**, Daniele Tedesco, Marina Naldi, Maurizio Baldassarre, Carlo Bertucci, Manuela Bartolini. Journal of Pharmaceutical and Biomedical Analysis (2018), 162(5): 171-178. Doi 10.1016/j.jpba.2018.09.022.* [1].

Abstract

The ADMET profile of drugs is strongly affected by human serum albumin (HSA), due to its leading role as carrier of poorly soluble compounds in plasma; a critical assessment of the binding capacity of HSA and the evaluation of binding competition between drugs are therefore pivotal for a reliable pharmacokinetic and pharmacodynamic characterization. In clinical practice, a potential source of impairment in the binding properties of HSA is the use of octanoate and *N*-acetyltryptophan as stabilizers during the production of pharmaceutical-grade HSA for infusion (*i*-HSA), which is currently administered in the treatment of a growing range of pathological conditions. The peculiar sensitivity of circular dichroism (CD) spectroscopy towards the stereochemical features of high-affinity binding events is herein exploited to achieve a site-specific assessment of the effect of stabilizers on the binding properties of *i*-HSA. The binding affinity and capacity of fatty-acid-free HSA towards site-selective induced circular dichroism (ICD) markers for the three high-affinity binding sites of HSA was compared to that of *i*-HSA submitted to ultrafiltration and dialysis to remove both stabilizers. Results showed a considerable impairment of the binding capacity of *i*-HSA at site II and a relatively lower influence on the binding properties of site I. Ultrafiltration proved to be ineffective in depleting octanoate, while the proposed dialysis protocol, which involves a pH-induced reversible unfolding of the protein, resulted in a total clearance of both stabilizers, confirmed by the full restoration of the binding properties of HSA at all binding sites. The outcomes of this study proved that CD spectroscopy is a suitable technique to evaluate the binding properties of *i*-HSA, ensuring an assessment of the availability of the binding sites and the possibility of monitoring the clearance of stabilizers. Eventually, the proposed method for their depletion might constitute a connection bridge between albumin *in vitro* studies and its clinical applications.

4.1 Introduction

Human serum albumin (HSA) is the major plasma protein in humans, constituting more than 50% of the total protein content in plasma [2]. Due to its high concentration (~ 40 g/L) and its net negative charge, HSA contributes to ~ 70 % of the total osmotic pressure, regulating the distribution of plasma fluids between compartments. Besides its oncotic properties, HSA owns other important biological functions, defined as non-oncotic, related to its unique binding capacity for a huge variety of endogenous and exogenous compounds and to its antioxidant activity (both direct and mediated by the transport of free radical scavengers), as well as to its role in the inflammatory and immunological modulation, stabilization of hemostatic and endothelial functions and control of extracellular pH [3,4]. The structure of HSA consists of three homologous domains, each formed by two sub-domains (IA-B, IIA-B and IIIA-B) [2,5]. At least three main binding sites for drugs (labeled I-III) and seven binding sites for long-chain fatty acids have been identified and thoroughly investigated over the years, unveiling the complex network of interactions that regulates the properties of HSA as a carrier protein [6–9]. The binding to HSA modulates the solubility of drugs in plasma and influences their ADMET profile and therapeutic activity; therefore, the characterization of drug–HSA binding is pivotal for a full pharmacokinetic and pharmacodynamic evaluation [10].

The beneficial effects of the administration of HSA by intravenous infusion have been highlighted in several clinical settings, such as hypovolemia, hypoalbuminemia, burns, hemorrhage and hemodialysis, as well as liver diseases characterized by an altered albumin metabolism [11]. The production of pharmaceutical-grade HSA is based on the isolation and purification of the protein from the plasma of donors, a process that includes a pasteurization step to inactivate viruses. The denaturation of HSA during the heat treatment (60 °C for 10 hours) is avoided by the addition of sodium octanoate and *N*-acetyltryptophan as thermal and antioxidant stabilizers, respectively [12].

A recently published crystal structure of the ternary complex of HSA with octanoate and *N*-acetyl-L-methionine shows that octanoate has a different binding pattern compared to long-chain fatty acids [13]. Octanoate binds at drug binding sites I and II of HSA, since the limited extension of its aliphatic chain prevents a full interaction with the main fatty acid binding sites; its binding modes are largely superimposed with those of site I- and site II-selective HSA ligands. Binding assays using fluorescent probes indicated site II as the primary binding site (K_{A_1} = 1.5 × 10^6 M^{-1}, in agreement with previous reports [14] and site I as the secondary binding site (K_{A_2} = 2.0 × 10^5 M^{-1}). *N*-acetyl-L-tryptophan also binds to site II, although its affinity is significantly lower (K_A = 9.1 × 10^4 M^{-1}) [12].

The presence of stabilizers in pharmaceutical-grade HSA can alter its non-oncotic properties with respect to the native protein [15,16]; such effects have also been observed *in vivo*, with a marked increase of the free circulating concentration of naproxen (a site II ligand) in patients treated with HSA for infusion [17]. Moreover, the long-term administration of pharmaceutical-grade HSA might increase the health risks related to the toxicological profiles of octanoate and *N*-acetyltryptophan, which have been deemed as pathogenic factors in patients with liver diseases and linked to hepatic encephalopathy and renal tubular toxicity [18]. Attempts at addressing these concerns are mainly devoted to the identification of alternative stabilizers [19] and to the development of depletion devices to remove stabilizers before infusion. A recent evaluation of several commercial adsorbents for the depletion of octanoate and *N*-acetyltryptophan from pharmaceutical-grade HSA showed that the simultaneous removal of both stabilizers cannot be fully achieved when a single adsorbent is employed in depletion devices for the purification of HSA formulations before infusion [16].

In the present article, a binding affinity assay based on circular dichroism (CD) spectroscopy was employed to gain further insight into the effect of octanoate on the binding properties of HSA at its drug binding sites, exploiting the peculiar sensitivity of CD spectroscopy toward the stereochemical features of high-affinity binding events; the assay could be applied to monitor the depletion of stabilizers from pharmaceutical-grade HSA, whose binding properties after ultrafiltration and dialysis were compared to those of fatty-acid-free HSA, used as reference.

The efficiency in the removal of stabilizers was quantified by HPLC-UV analysis, while the HSA binding affinity of selected site-specific markers (warfarin for site I, diazepam for site II and biliverdin for site III) was determined by means of induced CD measurements. Moreover, to enlarge the comprehension of site-II binding impairment caused by the strong modulation of octanoate, ketoprofen, which interacts with site II in a different binding mode as compared with diazepam [20], was also considered. The proposed approach should ensure a trustworthy monitoring of the binding properties of HSA, offering a deeper insight in the stabilizer cleaning process and supporting the selection of the optimal removal strategy.

4.2 Experimental section

4.2.1 Materials

Essentially fatty-acid-free HSA (*f*-HSA; product code A1887), biliverdin hydrochloride (BLV), *rac*-warfarin sodium salt (WRF), *rac*-ketoprofen (KPF), octanoic acid, *N*-acetyl-DL-tryptophan (NAT), formic acid (FA), trifluoroacetic acid (TFA), potassium dihydrogen phosphate (KH_2PO_4), dipotassium hydrogen phosphate trihydrate ($K_2HPO_4 \cdot 3\,H_2O$), disodium hydrogen phosphate (Na_2HPO_4), sodium chloride (NaCl), potassium chloride (KCl) and activated charcoal were purchased from Sigma-Aldrich (Milan, Italy).

Diazepam (DZP) was kindly supplied by Prof. Lucacchini (University of Pisa, Italy).

Pharmaceutical-grade HSA for infusion (*i*-HSA) was a 200 g L^{-1} solution form (Albital®; Kedrion Biopharma, Barga, Italy) containing sodium octanoate (16 mM) and *N*-acetyltryptophan (16 mM) as stabilizers.

Cellu·Sep® T4 regenerated cellulose tubular membranes with a 50 kDa molecular weight cut-off (MWCO) were supplied by Membrane Filtration Products, Inc. (Seguin, USA).

Amicon® Ultra 0.5 mL centrifugal filters with a 50 kDa MWCO were purchased from Millipore Merck (Darmstadt, Germany).

HPLC-grade (≥ 99.9%) 1-propanol (1-PrOH), methanol (MeOH) and acetonitrile (ACN) were supplied by Honeywell (Milan, Italy).

Aqueous solutions were obtained using deionized water purified by a Milli-Q purification system (Millipore, Milford, MA, USA).

Buffers were filtered through 0.22 μm membrane filters (Millipore, Milford, MA, USA) before use.

Spectroscopic measurements were carried out using high-performance quartz (QS) cells purchased from Hellma Analytics (Müllheim, Germany).

HSA samples prepared from *f*-HSA and *i*-HSA and used in the study are summarized in Table 1.

Table 1| List of all HSA samples employed in the study.

HSA sample	Description	Experimental section
i-HSA	pharmaceutical-grade HSA for infusion	4.2.1
i-HSA_{UF}	*i*-HSA after ultrafiltration	4.2.2
i-HSA_{dial}	*i*-HSA after dialysis	4.2.3
f-HSA	fatty-acid-free HSA	4.2.1
s-HSA	*f*-HSA with the addition of octanoic acid and NAT	4.2.3
s-HSA_{dial}	*s*-HSA after dialysis	4.2.3

4.2.2 Ultrafiltration

Ultrafiltration (UF) was performed with a Varifuge 3.0 r centrifuge (Heracus Sepatech, Hanau, Germany). 500 µL of *i*-HSA were ultrafiltered using Amicon Ultra centrifugal filters, which were washed with 1 mL Milli-Q water before use to remove glycerol from filter membranes. Each UF cycle was performed at room temperature, setting 4000×g for 15 min. After each cycle, 400 µL of phosphate buffered saline solution — PBS (pH 7.4) containing Na_2HPO_4 (10 mM), KH_2PO_4 (1.8 mM), KCl (2.7 mM) and NaCl (137 mM) — were added before resubmitting the solution to the following UF cycle. The residual content of NAT and octanoate in the ultrafiltered *i*-HSA samples (*i*-HSA_{UF}; Table 1) was monitored by HPLC-UV analysis on filtrates (see Section 4.2.4). Non-specific binding (NSB) to filter membranes was evaluated with a blank solution containing NAT and octanoate at the same concentrations. The concentration of each stabilizer in the receiver chamber was then quantified, and NSB was calculated by applying the following formula:

$$\text{NSB} = \frac{C_i - C_f}{C_i}, \quad (2)$$

where C_i is the concentration of the stabilizer in the loading chamber and C_f is its concentration in the filtrate.

4.2.3 Dialysis

Dialysis was carried out at room temperature on two different freshly prepared samples (Table 1): *i*-HSA diluted in deionized water at 500 µM and a solution containing *f*-HSA dissolved at 500 µM in deionized water with octanoic acid (2.7 mM) and NAT (2.7 mM), labeled *s*-HSA. Aliquots of 3.0 mL of each solution were transferred into 24-cm Cellu·Sep T4 tubular membranes and submitted to the dialysis procedure which consisted of fifteen steps (I–XV) of 2 h each, against 2 L of freshly prepared buffer, under gentle stirring. In detail, steps I–III were conducted in PB (pH 7.4; 10 mM); steps IV–IX were carried out in PB (pH 3.0; 10 mM):1-PrOH 80:20 (v/v) with 4 g of activated charcoal; step X was performed against PB (pH 3.0; 10 mM):1-PrOH 90:10 (v/v) with the addition of 4 g of activated charcoal; steps XI–XII were conducted in PB (pH 3.0; 10 mM); step XIII was carried out in PB (pH 4.6; 10 mM); steps XIV–XV were performed in PB (pH 7.4; 10 mM).

At the end of the procedure, dialyzed *i*-HSA (*i*-HSA_{dial}, Table 1) and dialyzed *s*-HSA (*s*-HSA_{dial}, Table 1) were spectrophotometrically quantified by a direct calibration method. For this purpose, a stock solution of *f*-HSA (15 µM) was prepared in PB (pH 7.4; 67 mM) and subsequently diluted in a series of two-fold dilutions (from 15 to 0.94 µM). A calibration curve was then derived by linear regression ($y = a\,x + b$; a = 31848.0; b = 0.00082; R^2 = 0.9993) based on the molar concentration of samples and the corresponding maximum absorbance at 280 nm (A_{280}, 1 cm pathlength).

To exclude the presence of stabilizers in the *i*-HSA_{dial} sample, the protein was removed by precipitation and the supernatant was analyzed by HPLC-UV (see Section 4.2.4). In detail, 400 µL of ice cold ACN were added to 100 µL of *i*-HSA_{dial}; the sample was vigorously vortexed for 1 min and centrifuged at 13000×g for 10 min at 4 °C; the concentration of stabilizers in the supernatant was then quantified.

4.2.4 HPLC-UV analysis

HPLC-UV analyses were carried out using a Zorbax Eclipse XDB-C18 column (150×2.1 mm, 3.5 µm I.D.; Agilent, Walbronn, Germany) on a Jasco PU-2089 Plus HPLC system (Tokyo, Japan) equipped with a CO-2067 Plus column thermostat. Data were processed using the ChromNAV software package (Jasco, Tokyo, Japan).

4.2.4.1 Quantitative determination of N-acetyltryptophan

The quantitative determination of NAT was performed setting the column temperature at 40 °C, the flow rate at 0.3 mL min^{-1} and the detection wavelength at 280 nm; an injection volume of 50 µL was used. Mobile phases A — H_2O:ACN:FA:TFA (99:1:0.1:0.025, v/v/v/v) — and B — ACN:H_2O:FA:TFA (99:1:0.1:0.025, v/v/v/v) — were employed to develop a gradient: the starting condition A–B (80:20, v/v) was kept for 4 min, then the percentage of mobile phase B was linearly incremented to 40% (v/v) in 2 min. The column was equilibrated with the mobile phase composition of the starting condition for 10 min before the next injection.

The stock solution of NAT (4.0 mM) was prepared in methanol. Standard solutions were prepared by diluting the stock solution in PBS (concentration range: 2.50–254 µM). Each standard solution was injected in duplicate; the derived average peak areas (in µV min) were plotted against the corresponding NAT concentration (in µM) to obtain the calibration curve by linear regression ($y = a\,x + b$; a = 54470; b = 127000; R^2 = 0.9999).

The quantification limit (LOQ, S/N = 10) was determined by performing LC–UV analysis on incremental dilutions of standard solutions and applying the formula:

$$\mathrm{LOQ} = 10\,\frac{a}{\sigma_b}, \tag{3}$$

where a is the slope and σ_b is the standard deviation of the *y*-intercept of the regression curve. The LOQ value resulted to be 1.78 µM.

4.2.4.2 Quantitative determination of octanoate

The quantitative determination of octanoate was performed in isocratic mode using a MeOH:H_2O:TFA (70:30:0.1, v/v/v) mobile phase at a flow rate of 0.3 mL min^{-1}. Analyses were

performed setting the column temperature at 40 °C and the detection wavelength at 214 nm; an injection volume of 50 µL was used.

The stock solution of octanoic acid (32 mM) was prepared in DMSO. Standard solutions were prepared by diluting the stock solution in PBS (concentration range: 0.0625–8.00 mM). Standard solutions were analyzed in duplicate; the derived average peak areas (in µV min) were plotted against the corresponding octanoate concentration (in mM) to obtain the calibration curve by linear regression ($y = a\,x + b$; a = 478000; b = −22980; R^2 = 0.9993). The LOQ value was derived as described in Section 4.2.4.1 and resulted to be 42 µM.

4.2.5 CD spectroscopy studies

All measurements for CD spectroscopy studies were performed on a Jasco J-810 spectropolarimeter (Tokyo, Japan) at room temperature. Samples were prepared by dilution from fresh stock solutions of HSA and of the selective ICD markers for its three drug binding sites: WRF (site I), DZP (site II), KPF (site II) and BLV (site III). The final concentration of organic modifier (1-PrOH or DMSO) in the samples never exceeded 0.5% (v/v) and 1% (v/v), respectively. Solutions containing BLV were protected from direct exposure to ambient light throughout the experiments.

Near-UV CD measurements were carried out using a 50 nm min^{-1} scanning speed (20 nm min^{-1} for WRF), a 2 nm spectral bandwidth, a 2 s data integration time, a 0.2 nm data pitch and an accumulation cycle of 3; spectral ranges were defined to include the peculiar ICD bands of each complex: 360–300 nm for WRF–HSA (λ_{max} = 308 nm), 350–250 nm for DZP–HSA (λ_{max} = 316 nm), 400–250 nm for KPF–HSA (λ_{max} = 340 nm) and 450–250 nm for BLV–HSA (λ_{max} = 385 nm). Far-UV CD measurements were carried out in the 260–195 nm spectral range using a 20 nm min^{-1} scanning speed, a 2 nm spectral bandwidth, a 2 s data integration time, a 0.2 nm data pitch and an accumulation cycle of 3. Spectra were processed using the Jasco Spectra Analysis software (Tokyo, Japan) and plotted using the Bezier smoothing algorithm provided by the Gnuplot software (version 5.2.2, http://gnuplot.sourceforge.net).

4.2.5.1 Affinity studies with ICD markers

The determination of the affinity constants for the three drug binding sites of HSA was carried out by near-UV CD measurements on equimolar (1:1) mixtures of the protein with the corresponding ICD marker in PB (pH 7.4; 67 mM).

Stock solutions of *f*-HSA, *i*-HSA_{UF} and *i*-HSA_{dial} were prepared in PB (pH 7.4; 67 mM) at a final concentration of 500 µM. Stock solutions of ICD markers were prepared as follows: WRF (10 mM)

in PB (pH 7.4; 67 mM); DZP (5 mM) in PB (pH 7.4; 67 mM)–(1-PrOH) (75:25, v/v); BLV (2 mM) in PB (pH 7.4; 67 mM)–DMSO (62:38, v/v).

Five 1:1 mixtures were analyzed for each marker–HSA complex; the pathlength and the initial concentration of analytes were changed simultaneously, while keeping their product constant. QS quartz cells with 10, 5, 2, 1 and 0.5 cm pathlengths were used, while concentrations were defined based on the binding properties and spectroscopic response of each complex: 5.0, 10, 25, 50 and 100 μM for WRF–HSA and DZP–(*i*-HSA_{UF}) complexes; 1.5, 3.0, 7.5, 15 and 30 μM for BLV–HSA and other DZP–HSA complexes. All markers were either non-chiral or used as racemic mixtures, so the ICD spectra of the marker–HSA complexes were obtained by subtraction of the CD spectrum of the protein from the CD spectra of the 1:1 mixtures.

The chemical equilibrium of the marker–HSA binding interaction was evaluated using a Benesi-Hildebrand mathematical method [21,22] based on the absolute values of maximum intensity for the ICD bands ($|\Delta A_{\mathrm{ind}}|$ at $\lambda_{\max}$). For interactions exhibiting a 1:1 stoichiometry, the concentrations of ligand and protein at equilibrium are equal ($[L] = [P]$) and the association constant is $K_{\mathrm{A}} = \frac{[LP]}{[P]^2}$. The initial concentration of the protein ($[P]_0$) can then be expressed as a function of the concentration of the ligand–protein complex at equilibrium ($[LP]$):

$$[P]_0 = [LP] + [P] = [LP] + \sqrt{\frac{[LP]}{K_{\mathrm{A}}}}\,. \tag{4}$$

The ICD signal is proportional to the concentration of the marker–protein complex; the combination of Equation 4 with the Beer–Lambert law gives:

$$[P]_0 = \frac{|\Delta A_{\mathrm{ind}}|}{|\Delta \varepsilon_{\mathrm{ind}}|\, l} + \sqrt{\frac{|\Delta A_{\mathrm{ind}}|}{K_{\mathrm{A}}\, |\Delta \varepsilon_{\mathrm{ind}}|\, l}}\,, \tag{5}$$

where $\Delta\varepsilon_{\mathrm{ind}}$ is the absolute value of the induced molar differential extinction coefficient for the binding complex (in M^{-1} cm^{-1}) and l is the pathlength (in cm). By setting $x = \sqrt{|\Delta A_{\mathrm{ind}}|/l}$ and dividing both terms by x, a linear Benesi-Hildebrand equation is obtained:

$$y = \frac{1}{|\Delta \varepsilon_{\mathrm{ind}}|}\, x + \sqrt{\frac{1}{|\Delta \varepsilon_{\mathrm{ind}}| \cdot K_{\mathrm{A}}}}\,, \tag{6}$$

where $y = [P]_0/x$.

The values of $\Delta\varepsilon_{\mathrm{ind}}$ and K_{A} for each marker–HSA complex were calculated from the slope $\left(m = \frac{1}{|\Delta \varepsilon_{\mathrm{ind}}|}\right)$ and intercept $\left(q = \sqrt{\frac{1}{|\Delta \varepsilon_{\mathrm{ind}}| \cdot K_{\mathrm{A}}}}\right)$ of Equation 6, as obtained by linear regression from the average x and y data of two independent assays ($n = 2$). The uncertainties of $\Delta\varepsilon_{\mathrm{ind}}$ and K_{A} were determined by propagation of the standard deviations of m and q values for the corresponding Benesi-Hildebrand equations.

4.2.5.2 Binding to HSA site II

The different binding capacities of *f*-HSA, *i*-HSA_{UF}, *s*-HSA, *i*-HSA_{dial} and *s*-HSA_{dial} at site II were evaluated by near-UV CD measurements on their equimolar mixtures (1:1, 50 μM) in PB (pH 7.4; 67 mM) with two site II-specific ICD markers, namely DZP and KPF. Spectra were recorded using a QS quartz cell with a 1 cm pathlength. The ICD spectra of the marker–HSA complexes were obtained by subtraction of the CD spectrum of the protein from the CD spectra of the 1:1 mixtures.

4.2.5.3 Secondary structure analysis

Far-UV CD measurements for the analysis of the secondary structure of HSA were performed on *f*-HSA, *i*-HSA_{UF}, *i*-HSA_{dial} and *s*-HSA_{dial} samples (5 μM) in PB (pH 7.4; 67 mM) using a QS quartz cell with a 0.05 cm pathlength.

4.3 Results and discussion

4.3.1 Depletion of N-acetyltryptophan and octanoate by ultrafiltration

Ultrafiltration (UF) is a common procedure used for protein concentration, buffer exchange and desalting. In the current study, UF was employed in the attempt to remove NAT and octanoate excess from *i*-HSA. The process was monitored by quantitating, after each UF cycle, the stabilizers concentration in the receiver chamber by means of the HPLC-UV methods described in Section 4.2.4. The optimized analytical approach allowed a fast determination of NAT and octanoate, whose chromatographic retention times were 4.0 (k = 2.9) and 3.8 min (k = 2.2), respectively. The assessment of UF efficacy was carried out by monitoring the residual concentration of each stabilizer in the *i*-HSA solution over 20 UF cycles (Fig. 7). Each stabilizer was quantified in the solutions collected in the receiver chamber, taking the effect of NSB on filter membranes into account.

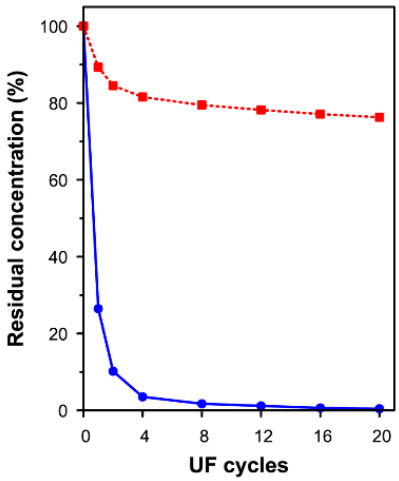

Figure 7| Progressive depletion followed by HPLC-UV analysis. Progressive depletion of *N*-acetyltryptophan (*solid line*) and octanoate (*dotted line*) from *i*-HSA by ultrafiltration.

N-acetyltryptophan and octanoate are present at the same declared starting concentration (16 mM), but the efficacy of UF was significantly different for the two stabilizers, as expected by their different binding affinities to HSA [12,13]. While the residual concentration of NAT fell below 1% after 12 cycles and reached 0.4% after 20 cycles, the removal of octanoate was significantly more difficult (Fig. 7) in agreement with data presented by Harm *et al.* [16]. The low removal efficiency is consistent with both the high affinity of octanoate for HSA and the high binding capacity of HSA. Based on the analysis of the concentration of octanoate in the receiver chamber after the first cycle of UF, only 10.7% of the stabilizer results to be free in solution, while the remaining fraction is bound to HSA.

4.3.2. Site-specific ICD markers as a tool for monitoring the removal of octanoate

CD spectroscopy can provide valuable information on both the structural features and the affinity of binding interactions in near-physiological conditions; the relatively higher information content that can be obtained through in solution CD binding assays represents an advantage over other popular techniques, such as isothermal titration calorimetry, fluorescence spectroscopy and surface plasmon resonance biosensing. Specifically, CD spectroscopy is a powerful technique for the investigation of the binding properties of HSA, thanks to the high degree of stereospecificity displayed by its main drug binding sites. The eventual onset of an induced circular dichroism (ICD) signal can be exploited to evaluate the binding parameters of a ligand–HSA complex and the bound conformation of the ligand; conversely, ligands with well-characterized ICD spectra can be used as selective markers to investigate the competition for the binding sites of HSA by other small molecules [21].

The availability of specific ICD markers for the three drug binding sites of HSA allowed a thorough comparison of the binding properties of samples derived from *i*-HSA with those of *f*-HSA by means of CD affinity studies. The simultaneous determination of K_A and $\Delta\varepsilon_{ind}$ values by the Benesi-Hildebrand method allows a reliable evaluation of the binding affinity and capacity of HSA at each binding site, with the additional advantage of monitoring highly stereoselective binding events; nevertheless, it must be noted that the reliability of ICD affinity studies using this approach strongly depends on the nature of the binding complex under investigation. Indeed, the analysis must be carried out on strictly equimolar marker–protein mixtures in a concentration range where the binding complex is not close to saturation and the resulting ICD signal is sufficiently intense to be accurately monitored; situations where these requirements are not fulfilled will lead to significant errors in the estimation of binding affinities.

Table 2| Affinity constant (K_A), induced molar differential extinction coefficients ($\Delta\varepsilon_{ind}$) and linear regression parameters of the Benesi-Hildebrand equations for the binding of site-specific ICD markers to *f*-HSA, as obtained by CD spectroscopic analysis ($n = 2$). Affinity data available from literature are also listed for comparison.

Marker	Site	K_A (M^{-1})	$\Delta\varepsilon_{ind}$ (M^{-1} cm^{-1})	λ_{max} (nm)	m	q	R^2	Literature K_A (M^{-1}) for HSA
WRF	I	$(8.62 \pm 0.81) \times 10^4$	1.84 ± 0.05	308	$(5.44 \pm 0.13) \times 10^{-1}$	$(2.51 \pm 0.09) \times 10^{-3}$	0.9982	1.1×10^5 (**a**)
DZP	II	$(1.09 \pm 0.15) \times 10^6$	-7.45 ± 0.14	316	$(1.34 \pm 0.03) \times 10^{-1}$	$(3.50 \pm 0.21) \times 10^{-4}$	0.9989	6.6×10^5 (**b**)
BLV	III	$(1.93 \pm 0.45) \times 10^6$	62.1 ± 1.5	385	$(1.61 \pm 0.04) \times 10^{-2}$	$(9.12 \pm 0.95) \times 10^{-5}$	0.9982	1.5×10^6 (**c**)

(**a**) determined by surface plasmon resonance biosensing [23].
(**b**) determined by equilibrium dialysis [24].
(**c**) determined by HSA fluorescence quenching [25].

The calculated K_A values for the marker–(*f*-HSA) complexes (Table 2) were found to be in good agreement with affinity values determined with orthogonal techniques, showing that the ICD approach can provide accurate estimates for the affinity of small molecules to HSA.

The $\Delta\varepsilon_{ind}$ obtained from the slopes of the Benesi-Hildebrand equations highlighted that the presence of octanoate in the *i*-HSA_{UF} samples affects the binding of markers [14]: the binding capacity of site II was found to be significantly lower in *i*-HSA_{UF} than in *f*-HSA (Table 3).

Table 3| Affinity constant (K_A), induced molar differential extinction coefficients ($\Delta\varepsilon_{ind}$) and linear regression parameters of the Benesi-Hildebrand equations for the binding of site-specific ICD markers to *i*-HSA_{UF}, as obtained by CD spectroscopic analysis ($n = 2$). K_A and $\Delta\varepsilon_{ind}$ values for *f*-HSA are also listed for comparison.

Marker	Site	K_A (M^{-1})	$\Delta\varepsilon_{ind}$ (M^{-1} cm^{-1})	λ_{max} (nm)	m	q	R^2	K_A ($\Delta\varepsilon_{ind}$) for *f*-HSA
WRF	I	$(1.07 \pm 0.23)\times 10^5$	2.58±0.13	308	$(3.87 \pm 0.19)\times 10^{-1}$	$(1.90 \pm 0.15)\times 10^{-3}$	0.9927	8.62×10^4 (1.84)
DZP	II	$(3.60\pm10.00)\times10^7$	−1.73 ± 0.06	316	$(5.77 \pm 0.21)\times 10^{-1}$	$(1.26 \pm 1.72)\times 10^{-4}$	0.9961	1.09×10^6 (−7.45)
BLV	III	$(3.36 \pm 0.93)\times 10^6$	62.0 ± 1.4	385	$(1.61 \pm 0.04)\times 10^{-2}$	$(6.93 \pm 0.88)\times 10^{-5}$	0.9985	1.93×10^6 (62.1)

The strong decrease of $\Delta\varepsilon_{ind}$ observed for the DZP–(*i*-HSA_{UF}) complex (Fig. 8) is consistent with a mechanism of direct binding competition between octanoate and DZP at site II: indeed, the presence of a high-affinity competitor (octanoate) in the *i*-HSA_{UF} sample breaks one of the requirements of the Benesi-Hildebrand approach, i.e. the equimolar ratio between the ligand and the available binding sites. The saturation of the ICD signal for the DZP–HSA complex is therefore reached at a lower concentration, resulting in a significant overestimation of K_A and a marked increase of the uncertainty for the values derived by linear regression analysis.

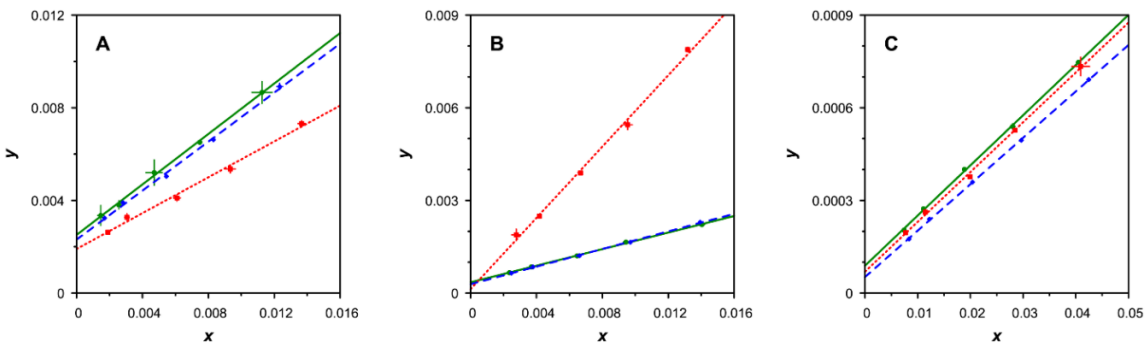

Figure 8| Benesi-Hildebrand curves. Benesi Hildebrand curves for the ICD affinity studies on 1:1 mixtures of *f*-HSA (*solid lines*), *i*-HSA_{UF} (*dotted lines*) and *i*-HSA_{dial} (*dashed lines*) with site-specific ICD markers. (**A**) WRF (site I; λ_{max} = 308 nm). (**B**) DZP (site II; λ_{max} = 316 nm). (**C**) BLV (site III; λ_{max} = 385 nm). $x = \sqrt{|\Delta A_{ind}|/l}$; $y = [P]_0/x$.

The binding capacity of *i*-HSA at site II is heavily influenced by the efficiency of the purification method used for the removal of stabilizers. CD measurements on *i*-HSA$_{UF}$ samples subjected to 8 UF cycles yielded a lower $\Delta\varepsilon_{ind}$ value (-0.86 ± 0.06 M^{-1} cm^{-1}) than samples obtained after 20 UF cycles (-1.73 ± 0.06 M^{-1} cm^{-1}). These results confirm that UF is only partially successful in depleting octanoate from *i*-HSA samples due to the high affinity of octanoate to HSA.

The presence of octanoate influenced the binding properties of site I as well, although the K_A and $\Delta\varepsilon_{ind}$ values of WRF–HSA complexes increased going from *f*-HSA to *i*-HSA$_{UF}$ (Fig. 8). Previous studies on the effect of stabilizers on the binding properties of HSA at site I reported a small reduction in the fluorescence emission of WRF bound to excess HSA in the presence of octanoate [13]. Considering the racemic nature of the marker, the behavior observed in the ICD affinity assay might be explained by a change in the binding enantioselectivity for the two enantiomers of WRF [26], resulting in a variation of the overall ICD signal of the mixture. The analysis of BLV–HSA complexes, on the other hand, showed minor differences between the binding properties of *f*-HSA and *i*-HSA$_{UF}$ (Fig. 8). Therefore, the presence of octanoate in *i*-HSA$_{UF}$ does not seem to interfere significantly with the binding capacity of site III.

The results of ICD affinity assays strongly support the usefulness of site II-specific ICD markers to monitor the removal of octanoate from *i*-HSA and the recovery of its optimal binding capacity. Site II-specific ICD markers are ideal in this framework thanks to the strong stereospecificity observed at this site and the strong modulation of its binding properties displayed by octanoate. An additional proof of the usefulness of site II-specific ICD markers for this application was given by the observation that the binding of DZP to *s*-HSA (where octanoate is added to *f*-HSA) displays a similar reduction in the intensity of ICD response compared to *i*-HSA$_{UF}$ (Fig. 9A).

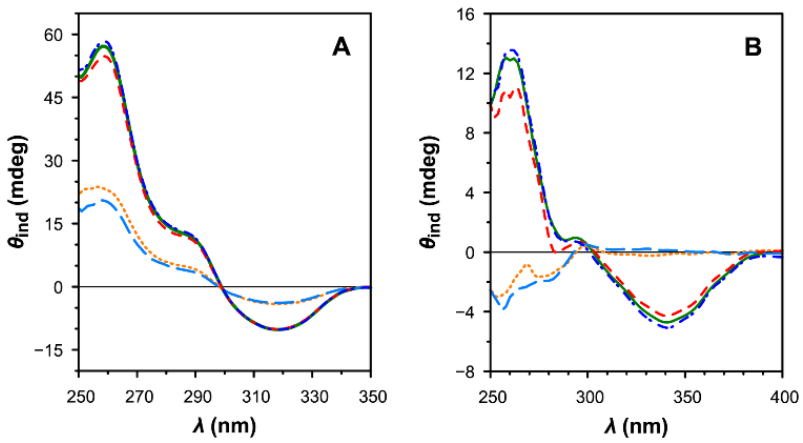

Figure 9| ICD spectra for site-II specific markers. ICD spectra for the 1:1 mixtures (50 μM) of HSA samples with site II-specific ICD markers (solvent: PB 67 mM pH 7.4; cell pathlength: 1 cm). (**A**) DZP. (**B**) KPF. *Solid*: *f*-HSA. *Dotted*: *i*-HSA$_{UF}$. *Short-dashed*: *i*-HSA$_{dial}$. *Long-dashed*: *s*-HSA. *Dash-dotted*: *s*-HSA$_{dial}$.

The binding impairment at HSA site II caused by the presence of octanoate was further investigated using an additional site II-specific ICD marker, i.e. KPF. An even more dramatic effect was observed: the presence of octanoate in *i*-HSA_{UF} and *s*-HSA caused the complete disappearance of the peculiar negative ICD band of the complex at around 340 nm (Fig. 9B) [27]. The different extents of the binding impairment at site II triggered by octanoate can be explained by the differences in the binding modes of benzodiazepines and non-steroidal anti-inflammatory drugs [20,28]; the evidence of competition by octanoate for both classes of drugs gives additional strength to the choice of site-II specific ICD markers as excellent tools in the evaluation of the effect of stabilizers on the binding properties of *i*-HSA.

4.3.3 Removal of stabilizers by dialysis

The efficiency in the removal of stabilizers, quantified by HPLC-UV analysis (Fig. 1), revealed that ultrafiltration was ineffective in depleting octanoate (residual concentration 80 % after 20 cycles) due to its strong affinity with HSA [13,14]. Analogous results were obtained by means of adsorbent devices and common protocols of equilibrium dialysis, in which octanoate bound to the protein proved to be 27 ± 3 % and 17 ± 6 % of its starting concentration in *i*-HSA, respectively [16]. Aiming at improving the removal of octanoate, a more drastic and extensive protocol of dialysis was performed, which allowed to exploit the reversible unfolding of HSA as a function of pH [29].

Dialysis was carried out on *i*-HSA and *s*-HSA. Initial steps were performed at pH 7.4 to eliminate excess of octanoate and NAT, similarly to UF. Then, the pH of dialysis buffer was decreased to 3.0, where HSA undergoes a reversible transition from its physiological fold (normal or *N* form; pH 8–4.3) to a transiently unfolded conformation characterized by a larger solvent-accessible surface area and a partial loss of α-helical structure (fast-migrating or *F* form; pH 4.3–2.7) [2]. Moreover, octanoate is mostly protonated in this acidic environment ($pK_a = 4.9$), and the adsorption of octanoic acid by charcoal further promotes the dissociation of octanoate from HSA [30]. Subsequent dialysis steps carried out against buffer with increasing pH values enabled protein refolding to the *N* form.

The initial HSA concentration submitted to dialysis proved to be crucial to obtain a successful removal of stabilizers: since the solubility of the *F* form is significantly lower than the *N* form [2], different concentrations were tested to avoid protein precipitation at pH 3.0, which hampered the efficient extraction of octanoic acid (data not shown). Based on this experimental evidence, *i*-HSA and *s*-HSA solutions were dialyzed at an initial concentration of 500 μM. At the end of the procedure, *i*-HSA_{dial} and *s*-HSA_{dial} were spectrophotometrically quantified and the final concentrations ranged from 80 to 85% (w/w) of the initial amount.

The secondary structure of *i*-HSA$_{dial}$ and *s*-HSA$_{dial}$ was investigated by CD spectroscopy to verify the recovery of the physiological conformation of HSA after dialysis; the excellent agreement of the recorded spectra with those of *f*-HSA and *i*-HSA$_{UF}$ (Fig. 10), which displayed the typical features of α-helix-rich proteins with negative bands centered at 208 and 222 nm [31], confirmed that the secondary structure of HSA was completely restored after dialysis.

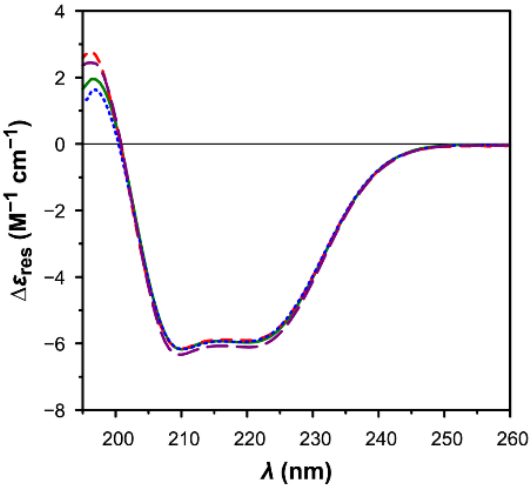

Figure 10| Secondary structure spectra. Far-UV CD spectra (in *molar* units per residue) of *f*-HSA (*solid*), *i*-HSA$_{UF}$ (*short-dashed*), *i*-HSA$_{dial}$ (*dotted*) and *s*-HSA$_{dial}$ (*long-dashed*). Solvent: PB 67 mM pH 7.4. Cell pathlength: 0.05 cm.

The binding capacity for DZP and KPF at site II was analyzed to verify the total removal of stabilizers from dialyzed samples. The excellent overlapping of the ICD spectra obtained with *i*-HSA$_{dial}$, *s*-HSA$_{dial}$ and *f*-HSA (Fig. 9) proved the successful removal of octanoate. LC-UV analysis excluded the presence of octanoate at detectable concentrations.

Table 4| Affinity constant (K_A), induced molar differential extinction coefficients ($\Delta\varepsilon_{ind}$) and linear regression parameters of the Benesi-Hildebrand equations for the binding of site-specific ICD markers to *i*-HSA$_{dial}$, as obtained by CD spectroscopic analysis ($n = 2$). K_A and $\Delta\varepsilon_{ind}$ values for *f*-HSA are also listed for comparison.

Marker	Site	K_A (M^{-1})	$\Delta\varepsilon_{ind}$ (M^{-1} cm^{-1})	λ_{max} (nm)	m	q	R^2	K_A ($\Delta\varepsilon_{ind}$) for *f*-HSA
WRF	I	$(9.91 \pm 1.24) \times 10^4$	1.89 ± 0.05	308	$(5.29 \pm 0.15) \times 10^{-1}$	$(2.31 \pm 0.11) \times 10^{-3}$	0.9975	8.62×10^4 (1.84)
DZP	II	$(1.71 \pm 0.28) \times 10^6$	-7.02 ± 0.13	316	$(1.42 \pm 0.03) \times 10^{-1}$	$(2.88 \pm 0.21) \times 10^{-4}$	0.9991	1.09×10^6 (−7.45)
BLV	III	$(5.58 \pm 0.68) \times 10^6$	66.5 ± 0.5	385	$(1.50 \pm 0.01) \times 10^{-2}$	$(5.19 \pm 0.30) \times 10^{-5}$	0.9998	1.93×10^6 (62.1)

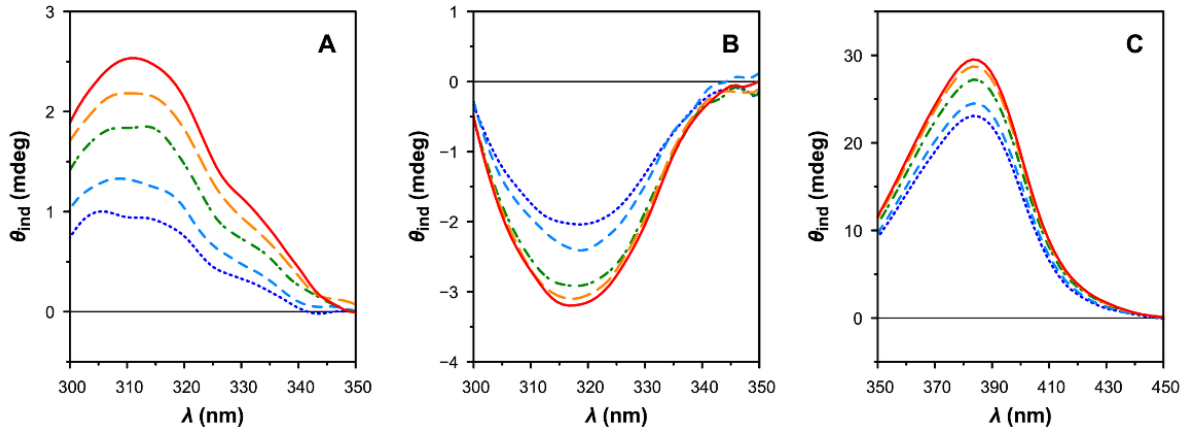

Figure 11| ICD spectra of site-specific markers. ICD spectra for the 1:1 mixtures of *i*-HSA_{dial} with site-specific ICD markers, as measured using different cell pathlengths (solvent: PB 67 mM pH 7.4). **(A)** WRF, site I marker. *Solid*: 100 μM (0.5 cm). *Long-dashed*: 50 μM (1 cm). *Dash-dotted*: 25 μM (2 cm). *Short-dashed*: 10 μM (5 cm). *Dotted*: 5 μM (10 cm). **(B)** DZP, site II marker. *Solid*: 30 μM (0.5 cm). *Long-dashed*: 15 μM (1 cm). *Dash-dotted*: 7.5 μM (2 cm). *Short-dashed*: 3 μM (5 cm). *Dotted*: 1.5 μM (10 cm). **(C)** BLV, site III marker. *Solid*: 30 μM (0.5 cm). *Long-dashed*: 15 μM (1 cm). *Dash-dotted*: 7.5 μM (2 cm). *Short-dashed*: 3 μM (5 cm). *Dotted*: 1.5 μM (10 cm).

4.4 Conclusions

A full characterization of the ADMET profile of a drug requires a comprehensive study of plasma bioavailability, which is strongly affected by the binding to serum proteins. The presence of fatty acids or the addition of stabilizers in pharmaceutical formulations may compete with the binding of drugs to HSA, causing an impairment in the assessment of the binding capacity. Analytical approaches able to quantify binding parameters, detect concomitant interactions and provide a deeper insight on the availability of the binding sites offer clear advantages toward a better characterization of drug–target interactions; the application of CD spectroscopy to binding affinity studies has an enormous potential in this respect. Indeed, the highly stereoselective responses of well-characterized ICD markers allow the direct assignment of the observed signal to a specific binding event, a feature that other biophysical techniques cannot provide.

The comparison between the binding parameters (K_A, $\Delta\varepsilon_{ind}$) achieved for all site-specific ICD markers (warfarin, diazepam, biliverdin) and those obtained for fatty-acid-free HSA proved the inefficiency of ultrafiltration in removing octanoate, which affected the binding capacity at site II and, to a lesser extent, at site I. Conversely, the proposed dialysis protocol, that involves the reversible unfolding of the protein in acidic conditions, successfully granted both stabilizers depletion. The reversible conformational transition of HSA, from the *N* to the *F* form, proved to be necessary to remove octanoate strongly bound to HSA. The recovery of binding capacity of HSA was further verified for all site-specific ICD markers as a proof of the totally restored availability of the binding sites, enhancing previous results reported in the literature based on different purification methods such as marketed adsorbent devices or common protocols of equilibrium dialysis.

The use of CD spectroscopy guaranteed a thorough site-specific assessment of the availability of the high-affinity binding sites, as well as to verify the recovery of the physiological conformation of HSA after removal of the stabilizers. The approach proposed proved to be trustworthy for studying drug–HSA interactions, when the modulation of the binding properties needs to be assessed. The clear competition displayed by octanoate at site II makes site-II specific ICD markers excellent tools in the evaluation of the effect of stabilizers on the binding properties of *i*-HSA, providing an easy method to monitor the depletion of stabilizers from pharmaceutical-grade HSA submitted to different purification methods. In the attempt to develop more efficient devices for the removal of stabilizers, the proposed ICD approach might be employed as a method to selectively monitor the full availability of the binding sites of HSA after purification, thus ensuring further progress in the connection between *in vitro* studies and the use of HSA in clinical applications.

References

[1] A. Tramarin, D. Tedesco, M. Naldi, M. Baldassarre, C. Bertucci, M. Bartolini, New insights into the altered binding capacity of pharmaceutical-grade human serum albumin: site-specific binding studies by induced circular dichroism spectroscopy, J. Pharm. Biomed. Anal. 162 (2019) 171–178.

[2] T. Peters Jr., All about albumin, First ed., Academic Press, London, 1996.

[3] M. Naldi, M. Baldassarre, M. Domenicali, M. Bartolini, P. Caraceni, Structural and functional integrity of human serum albumin: analytical approaches and clinical relevance in patients with liver cirrhosis, J. Pharm. Biomed. Anal. 144 (2016) 138–153.

[4] T.W. Evans, Review article: Albumin as a drug-biological effects of albumin unrelated to oncotic pressure, Aliment. Pharmacol. Ther. 16 (2002) 6–11.

[5] G. Fanali, A. Di Masi, V. Trezza, M. Marino, M. Fasano, P. Ascenzi, Human serum albumin: from bench to bedside, Mol. Aspects Med. 33 (2012) 209–290.

[6] M. Fasano, S. Curry, E. Terreno, M. Galliano, G. Fanali, P. Narciso, S. Notari, P. Ascenzi, The extraordinary ligand binding properties of human serum albumin, IUBMB Life. 57 (2005) 787–796.

[7] F. Zsila, Subdomain IB is the third major drug binding region of human serum albumin: toward the three-sites model, Mol. Pharm. 10 (2013) 1668–1682.

[8] S. Fujiwara, T. Amisaki, Identification of high affinity fatty acid binding sites on human serum albumin by MM-PBSA method, Biophys. J. 94 (2008) 95–103.

[9] J.R. Simard, P.A. Zunszain, J.A. Hamilton, S. Curry, Location of high and low affinity fatty acid binding sites on human serum albumin revealed by NMR drug-competition analysis, J. Mol. Biol. 361 (2006) 336–351.

[10] E. Fabini, U.H. Danielson, Monitoring drug–serum protein interactions for early ADME prediction through Surface Plasmon Resonance technology, J. Pharm. Biomed. Anal. 144 (2017) 188–194.

[11] P. Caraceni, O. Riggio, P. Angeli, C. Alessandria, S. Neri, F.G. Foschi, F. Levantesi, A. Airoldi, S. Boccia, G. Svegliati-Baroni, S. Fagiuoli, R.G. Romanelli, R. Cozzolongo, V. Di Marco, V. Sangiovanni, F. Morisco, P. Toniutto, A. Tortora, R. De Marco, M. Angelico, I. Cacciola, G. Elia, A. Federico, S. Massironi, R. Guarisco, A. Galioto, G. Ballardini, M. Rendina, S. Nardelli, S. Piano, C. Elia, L. Prestianni, F.M. Cappa, L. Cesarini, L. Simone, C. Pasquale, M. Cavallin, A. Andrealli, F. Fidone, M. Ruggeri, A. Roncadori, M. Baldassarre, M. Tufoni, G. Zaccherini, M. Bernardi, Long-term albumin administration in decompensated cirrhosis (ANSWER): an open-label randomised trial, Lancet. 391 (2018) 2417–2429.

[12] M. Anraku, Y. Tsurusaki, H. Watanabe, T. Maruyama, U. Kragh-Hansen, M. Otagiri, Stabilizing mechanisms in commercial albumin preparations: octanoate and N-acetyl-L-tryptophanate protect human serum albumin against heat and oxidative stress, Biochim. Biophys. Acta Proteins Proteomics. 1702 (2004) 9–17.

[13] A. Kawai, V.T.G. Chuang, Y. Kouno, K. Yamasaki, S. Miyamoto, M. Anraku, M. Otagiri, Crystallographic analysis of the ternary complex of octanoate and N-acetyl-L-methionine with human serum albumin reveals the mode of their stabilizing interactions, Biochim. Biophys. Acta Proteins Proteomics. 1865 (2017) 979–984.

[14] U. Kragh-Hansen, Octanoate binding to the indole- and benzodiazepine-binding region of human serum albumin, Biochem. J. 273 (1991) 641–644.

[15] M.R. Ashrafi-Kooshk, F. Ebrahimi, S. Ranjbar, S. Ghobadi, N. Moradi, R. Khodarahmi, Comparative studies on drug binding to the purified and pharmaceutical-grade human serum albumins: bridging between basic research and clinical applications of albumin, Biologicals. 43 (2015) 1–11.

[16] S. Harm, C. Schildböck, J. Hartmann, Removal of stabilizers from human serum albumin by adsorbents and dialysis used in blood purification, PLoS One. 13 (2018) 1–18.

[17] P.A. Reine, U.E. Kongsgaard, A. Andersen, A.K. Thøgersen, H. Olsen, Infusions of albumin increase free fraction of naproxen in healthy volunteers: a randomized crossover study, Acta Anaesthesiol. Scand. 54 (2010) 430–434.

[18] J. Stange, M. Stiffel, A. Goetze, S. Strube, J. Gruenert, S. Klammt, S. Mitzner, S. Koball, S. Liebe, E. Reisinger, Industrial stabilizers caprylate and N-acetyltryptophanate reduce the efficacy of albumin in liver patients, Liver Transplant. 17 (2011) 705–709.

[19] Y. Kouno, M. Anraku, K. Yamasaki, Y. Okayama, D. Iohara, H. Nakamura, T. Maruyama, F. Hirayama, U. Kragh-Hansen, M. Otagiri, N-acetyl-L-methionine is a superior protectant of human serum albumin against post-translational oxidation as compared to N-acetyl-L-tryptophan, Biochem. Biophys. Reports. 6 (2016) 266–

274.

[20] K. Maruyama, H. Nishigori, M. Iwatsuru, Characterization of the benzodiazepine binding site (diazepam site) on human serum albumin, Chem. Pharm. Bull. 33 (1985) 5002–5012.

[21] D. Tedesco, C. Bertucci, Induced circular dichroism as a tool to investigate the binding of drugs to carrier proteins: classic approaches and new trends, J. Pharm. Biomed. Anal. 113 (2015) 34–42.

[22] H.A. Benesi, J.H. Hildebrand, A spectrophotometric investigation of the interaction of iodine with aromatic hydrocarbons, J. Am. Chem. Soc. 71 (1949) 2703–2707.

[23] Å. Frostell-Karlsson, A. Remaeus, H. Roos, K. Andersson, P. Borg, M. Hämäläinen, R. Karlsson, Biosensor analysis of the interaction between immobilized human serum albumin and drug compounds for prediction of human serum albumin binding levels, J. Med. Chem. 43 (2000) 1986–1992.

[24] U. Kragh-Hansen, Evidence for a large and flexible region of human serum albumin possessing high affinity binding sites for salicylate, warfarin, and other ligands., Mol. Pharmacol. 34 (1988) 160–71.

[25] C.E. Ahlfors, Competitive interaction of biliverdin and bilirubin only at the primary bilirubin binding site on human albumin, Analyitical Biochem. 110 (1981) 295–307.

[26] T.A. Noctor, I.W. Wainer, D.S. Hage, Allosteric and competitive displacement of drugs from human serum-albumin by octanoic-acid, as revealed by high-performance liquid affinity-chromatography, on a human serum albumin-based stationary phase, J. Chromatogr. B Biomed. Sci. Appl. 577 (1992) 305–315.

[27] C. Bertucci, M. Pistolozzi, Species-dependent stereoselective drug binding to albumin: a circular dichroism study, Chirality. 20 (2008) 552–558.

[28] W. Müller, U. Wollert, Characterization of the binding of benzodiazepines to human serum albumin, Naunyn-Schmiedebergs Arch. Pharmacol. 280 (1973) 229–237.

[29] C. Bertucci, M.C. Barsotti, A. Raffaelli, P. Salvadori, Binding properties of human albumin modified by covalent binding of penicillin, Biochim. Biophys. Acta. 1544 (2001) 386–392.

[30] R.F. Chen, Removal of fatty acids from serum albumin by charcoal treatment, J. Biol. Chem. 242 (1967) 173–181.

[31] N. Greenfield, G.D. Fasman, Computed circular dichroism spectra for the evaluation of protein conformation, Biochemistry. 8 (1969) 4108–4116.

Chapter 5

Characterization of the interaction between glycated HSA and the receptor for advanced glycation end products (RAGE) by SPR and affinity-MS spectrometry

Abstract

Due to RAGE role as pattern recognition receptor and its involvement in pathological setting of many chronic diseases, many efforts have been made to define structural requirements for RAGE binding and activation. The current lack of a clear picture is partially related to AGEs heterogeneity. Based on these premises, the current study aimed to investigate the interaction between the VC1, i.e. RAGE ectodomain, and a form of glycated albumin (HSAgly), recently released on the market, by a tailored multimethodological strategy able to provide affinity parameters along with structural features for VC1 recognition. Four sites of glycation, including glycation at K525, were identified by 2D-LC-ESI-MSMS while top down LC-MS approach allowed the definition of glycation extent. The ability of the HSAgly to interact with VC1 was confirmed by surface plasmon resonance (SPR) studies using a HSAgly sensing surface and affinity proteomics employing a purposely developed VC1 column. The related steady state dissociation constant (K_D) highlighted a moderate affinity between the two interactants while displacement studies using chondroitin sulphate, a known RAGE binder, validated the VC1–HSAgly interaction assessed by the SPR-based assay. The combination of epitope extraction method with LC-MSMS analysis allowed further insights into the region(s) of HSAgly involved in the binding. Specifically, preliminary outcomes of these analyses highlighted that glycation at K525 and subdomain IA may be important for VC1 biorecognition.

The study is still *in fieri*. However, so far obtained outcomes showed that the proposed multimethodological strategy can be a suitable approach to shed light on requirements for VC1 biorecognition and it may be further employed to investigate the interaction with different glycated interactants including AGEs.

5.1 Introduction

Circulating glycated human serum albumin (HSA) is the result of the non-enzymatic glycation of the native protein by reducing sugars, mainly glucose, over the course of albumin life-time. The glycation process initially leads to the formation of chemically reversible Schiff bases and Amadori adducts, which are also known as early stage glycation products. Amadori adducts slowly undergo further irreversible rearrangements such as dehydration, oxidation, polymerization and intra/inter molecular crosslinking, which result in the formation of the so-called advanced glycation end products (AGEs), a generic name indicating the heterogeneous class of products resulting from this process. Early glycation products can also undergo oxidation, i.e. glycoxidation reaction, forming advanced glycoxidation products. In addition to this complex framework, AGEs can also directly derive from irreversible reactions between proteins and glucose-based reactive dicarbonyls (e.g. methylglyoxal) [1]. Protein glycation occurs at a limited extent in healthy subjects and glycation products accumulate with aging, contributing to the aging process itself. However, in specific pathological conditions, such as in diabetes, this process is accelerated [2]. Indeed, the main hallmark of diabetes is the dysregulation of plasma glucose levels, which strongly influences protein glycation rate and AGEs formation [3]. Since HSA is the most abundant circulating protein in plasma, accounting for more than 50 % of the total plasma protein content, and its primary structure contains aminoacid residues targeted by glycation, i.e. arginine and lysine residues, this protein is highly sensitive to glycation and albumin-derived AGEs are commonly found in human body [4].

AGEs are considered as biomarkers of several diseases including kidney failure, arteriosclerosis, cancer or Alzheimer's disease. Moreover, emerging data suggest that AGEs play a role in the onset of diabetic complications such as nephropathy, retinopathy and cardiomyopathy, acting as pathogenic factors and/or as damaging-intermediates [2,5]. In this scenario, structural characterization of the different AGEs, their quantification along with the elucidation of their role in pathological conditions constitute an emerging need of paramount importance [6].

AGE accumulation-related damages arise from multiple pathological mechanisms including loss of proteins function, proteins dysregulation, aggregation and signaling mediated by the activation of receptors such as the receptor for advanced glycation end product (RAGE) [7,8]. RAGE is a transmembrane receptor which belongs to the immunoglobulin superfamily and plays a role in innate immunity and inflammatory response [9]. It consists of an extracellular region, which is composed by one ligand-binding V-type Ig domain and two Ig-like constant domains (C1 and C2), a transmembrane domain and a cytosolic signal-transducing tail. The V and C1 domains form an integrated structural unit (VC1) involved in the binding of the majority of RAGE ligands including

AGEs [10,11]. Recent studies have suggested that the activation of RAGE by AGEs plays a role in the pathogenesis of some chronic diabetes complications [7]. Despite the advances in the understanding of AGE–RAGE axis, the pathological role of specific AGEs as well as AGEs structural requirements for AGE-RAGE interaction and RAGE activation still mostly remain unclear. The lack of a clear picture is partially related to AGEs heterogeneity, their chemical and metabolic instability along with the negligible amounts of circulating AGEs and complexity of biological matrices from which they need to be isolated [7]. *In vitro* studies involving RAGE are most commonly performed using BSA- or HSA-derived AGEs as reference ligands. However, BSA-AGEs and HSA-AGEs are commonly prepared in house by *in vitro* glycation [11–14] and the obtained AGE mixtures are usually employed without any further characterization of the formed AGEs species. This lack of a detailed knowledge on the AGE species used for binding experiments dramatically hampers the comprehension of the biorecognition phenomenon, preventing the rational design of new RAGE antagonists.

In this scenario, the use of structurally well characterized ligands seems to be compulsory. With this in mind, we decided to investigate glycated HSA–RAGE interaction in order to possibly highlight the structural features involved in such interaction.

To achieve this goal the binding between VC1 from human RAGE, expressed by Degani *et al.*[15], and a form of glycated albumin, recently released on the market (HSAgly), was studied. LC-MS was employed to define glycation sites on the commercial product, a prerequisite for the comprehension of the observed recognition phenomenon. Taking advantages of peculiar features of SPR [16,17], a HSAgly-sensing surface was employed to estimate binding affinity towards VC1. A competition assay involving the reference RAGE binder chondroitin sulphate [18,19] was used to further validate the binding between VC1 and HSAgly. Affinity chromatography coupled with mass spectrometry (affinity-MS) approach [20] was further developed in order to highlight the region(s) of the protein scaffold involved in such interaction. The outcome of the current study is the development of a multimethodological strategy to characterize HSAgly–VC1 binding with the aim of getting to elucidate molecular basis of AGE–RAGE interactions.

5.2 Experimental section

5.2.1 Materials

Glycated human serum albumin lyophilized powder (product code A8301) and trypsin from bovine pancreas were purchased from Sigma-Aldrich (Milan, Italy). Human recombinant RAGE ectodomain, i.e.VC1, was expressed in *Pichia Pastoris* and was kindly supplied by Prof. Popolo (University of Milan, Italy) [15].

Analytical grade racemic warfarin sodium salt (rac-WRF), chondroitin sulphate sodium salt from shark cartilage (CND), N-2-hydroxyethylpiperazine-N′-2-ethanesulfonic acid (HEPES), potassium dihydrogen phosphate (KH_2PO_4), disodium hydrogen phosphate (Na_2HPO_4), sodium chloride (NaCl), polyoxyethylenesorbitan monolaurate (p-20), formic acid (FA), trifluoroacetic acid (TFA), ammonium bicarbonate (AMBIC, NH_4HCO_3), sodium bicarbonate ($NaHCO_3$), ammonium acetate (NH_4OAc), sodium hydroxide (NaOH), sodium acetate (NaOAc), ethylenediaminetetracetic acid (EDTA), dithiothreitol (DTT) and iodoacetamide (IAA) were supplied by Sigma-Aldrich (Milan, Italy). HPLC-grade (≥ 99.9%) acetonitrile (ACN) was supplied by Honeywell (Milan, Italy).

Research-grade CM5 sensor surface, *N*-ethyl-*N*-(3-dimethylaminopropyl)-carbodiimide (EDC), *N*-hydroxysuccinimide (NHS), ethanolamine hydrochloride (pH 8.5, 1 M), CNBr-activated sepharose™ 4B were purchased from GE Healthcare Bio-Sciences (Uppsala, Sweden). 2,5-Dihydroxybenzoic acid (DHB) and super 2,5-dihydroxybenzoic acid (SDHB) were supplied by Bruker Daltonics (Bremen, Germany).

Amicon® Ultra 0.5 mL centrifugal filters (50 kDa MWCO) were supplied by Millipore Merck (Darmstadt, Germany).

Mobicol-Classic columns (cod.1002) and filter (small) 35 μm pore size (cod. M513515) were purchased from MoBiTec GmbH (Göttingen, Germany).

Deionized water was obtained by Milli-Q system (Millipore, Milford, MA, USA) and all aqueous solutions were filtered through 0.22 μm membrane filters before use.

5.2.2 Surface plasmon resonance-based analyses

SPR measurements were carried out on a Biacore™ X100 system (GE Healthcare Bio-Sciences, Uppsala, Sweden) provided with an in-line degasser and thermostated at 25°C. Data elaboration was performed using Biacore™ X100 2.0 evaluation software and GraphPad Prism 6.0 software (GraphPad Software Inc.).

5.2.2.1 Preparation and validation of HSAgly-biosensing surface

For the preparation of HSAgly-functionalized surface, HSAgly was solubilized in NaOAc buffer (0.01 M) at various pH (pH range 4.0–5.5) at a 30 μg mL^{-1} concentration in order to test the electrostatic pre-concentration over the chip surface (*pH scouting*). Ligand pre-concentration was evaluated by injecting stock solutions at different pH values at 5 μL min^{-1} for a contact time of 180 s, using as running buffer phosphate buffered saline solution (PBS) (pH 7.4), which contains Na_2HPO_4 (10 mM), KH_2PO_4 (1.8 mM), KCl (2.7 mM) and NaCl (137 mM). After each injection, the baseline was restored injecting twice a NaOH solution (0.05 M) at the same flow rate and setting 20 s as contact time. The NaOAc (pH 4.5; 0.01 M) proved to be the best immobilization condition and was used for HSAgly immobilization. HSAgly was immobilized on a carboxymethyl dextran CM5 sensor chip through amine coupling reaction [21]. Briefly, the sensor surface was activated by flushing a freshly prepared mixture of EDC (0.4 M) and NHS (0.1 M) for 7 min at flow rate of 10 μL min^{-1}. Then, a solution of HSAgly 30 μg mL^{-1} in NaOAc (pH 4.5; 0.01 M) was injected until the required amount of immobilized protein was obtained, i.e. 5500 response units (RUs). After the immobilization step, residual active esters were quenched by treating the surface with a solution of ethanolamine hydrochloride (1 M; pH 8.5) which was injected for 7 min at the same flow rate. Besides the flow cell with immobilized HSAgly (*active flow cell*), to account for non-specific binding events, a *reference flow cell* was prepared using the same protocol apart from HSAgly injection. Finally, sensor surface was allowed to stabilize overnight by flowing PBS buffer to obtain a steady baseline.

Before further use, the functionality of the HSAgly-sensing surface was verified using rac-WRF as test compound. Analysis conditions were set as follow: PBS (pH 7.4) with the addition of p-20 0.05 % (v/v) was used as running buffer, 75 μL min^{-1} as flow rate and 45 s and 60 s as association and dissociation time, respectively. rac-WRF was dissolved directly in running buffer (600 μM), diluted in three-fold serial dilutions (from 30.0 to 0.50 μM) and injected over the surface. Data achieved were processed as described in Section 5.2.2.4.

5.2.2.2 Analysis of VC1–HSAgly binding

Affinity assays were carried out in multi-cycle kinetic (MCK) mode employing HEPES (0.02 M), NaCl (0.15 M), EDTA (50 μM) and p-20 0.05 % (v/v) (pH 7.1), labeled HEPES buffered saline (HBS-E-T), as running buffer. HSAgly–VC1 affinity studies were performed setting the flow rate at 20 μL min^{-1}. Stock solution of VC1 1.00 mg mL^{-1} in HEPES buffered saline (pH 7.1) without EDTA and p-20 (HBS) was diluted in running buffer by two-fold serial dilutions from 4.00 μM to 0.016 μM and injected in ascending order over the sensing surface. The contact time and the

dissociation time were set at 300 s and 1300 s, respectively. At the end of each injection, NaOH (0.05 M) was injected twice (contact time = 20 s) in order to re-establish the baseline before starting a new cycle. In between VC1 cycles, blank injections of running buffer were made to monitor baseline stability and to enable double-reference subtraction [22]. VC1–HSAgly affinity studies were carried out in duplicate. Data achieved were processed as described in Section 5.2.2.4.

5.2.2.3 SPR-based displacement assay using chondroitin

A 1.0 mM stock solution of chondroitin sulphate from shark cartilage (CND) (Sigma-Aldrich) was prepared in running buffer (HBS-E-T, pH 7.1) while VC1 stock solution, which consisted of 1.00 mg mL^{-1} in HBS (pH 7.1), was diluted at 2 μM in HBS-E-T (pH 7.1). VC1-CND mixtures at increasing concentrations of CND (1 μM, 2 μM, 5 μM) and constant concentration (1 μM) of VC1 were also prepared in running buffer in order to obtain final [CND]/[VC1] molar ratios equal to 0/1, 1/1, 2/1 and 5/1. Moreover, in order to account for possible CND direct binding to HSAgly, a CND solution at the highest used concentration (5 μM) was also prepared in running buffer (blank solution). Displacement experiments were performed injecting the CND/VC1 mixtures and the CND blank solution over the HSAgly-sensing surface in the following experimental conditions: flow rate 10 μL min^{-1}, contact time and dissociation time 240 s and 800 s, respectively. At the end of each injection, NaOH (0.05 M) was injected for 20 s in order to re-establish the baseline before the next cycle.

5.2.2.4 SPR data analysis

The binding capacity of immobilized HSAgly was questioned injecting rac-WRF as reference compound. The experimentally determined R_{max}, which corresponds to the maximal response (RU) achievable, was compared with the theoretical value, calculated as follow (Eq. (7)):

$$R_{max} = \frac{MW_{analyte}}{MW_{ligand}} * RU_{immobilized} * stoichiometry \quad (7)$$

Sensorgrams dataset for both rac-WRF and VC1 binding to HSAgly were processed according to the same protocol. Firstly, SPR responses were double corrected for responses obtained from both reference channel and blank injections [22]. Then, responses recorded at the steady state were plotted against concentration. The equilibrium dissociation constant (K_D) of the ligand–HSAgly complex was extrapolated assuming a 1:1 isotherm binding model, as defined in Eq. (8):

$$R_{eq} = (R_{max} * c)/(K_D + c) + R_{bulk} \quad (8)$$

where c (M) is analyte concentration, R_{eq} and R_{max} (RU) correspond to SPR responses at the steady state and upon ligand saturation respectively and R_{bulk} refers to the response resulting from the bulk contribution of analyte solutions (RU).

VC1–HSAgly binding analysis was repeated in duplicate and each dataset was independently fitted in the theoretical binding model. Achieved K_D values were averaged and reported with the corresponding standard deviation (±SD).

5.2.3 HSAgly–VC1 interaction studies by affinity-MS approach

5.2.3.1 HSAgly in solution tryptic digestion.

Trypsin stock solution (1.0 mg mL^{-1}) was prepared dissolving trypsin in HCl (2 mM). The solution was stored at -20°C until use. A 2.0 mg mL^{-1} stock solution of HSAgly was prepared by dissolving the lyophilized powder in ultrapure water. Working solution was prepared by diluting HSAgly stock solution 0.5 mg mL^{-1} in AMBIC (pH 8.5; 0.05 M). 800 µL of HSAgly working solution were treated with 40 µL of DTT (0.1 M, in AMBIC pH 8.5; 0.05 M) and incubated at 56 °C for 30 min, under gentle shaking (600 rpm). Afterwards, 40 µL of freshly prepared IAA solution (10 mg mL^{-1} in AMBIC pH 8.5; 0.05 M) were added and the solution was incubated for 40 min in the dark at room temperature. Lastly, 8 µL of trypsin stock solution were added and the sample was incubated overnight at 37 °C, under shaking (600 rpm). Digestion was stopped by rapidly freezing the solution at -80°C. In the digested samples, the final concentration of each component resulted: HSAgly 0.45 mg mL^{-1}, DTT 4.50 mM, iodoacetamide 0.45 mg mL^{-1} and trypsin 0.01 mg mL^{-1}. HSAgly/trypsin ratio (p/p) was 45:1.

HSAgly peptides were analyzed by 2D-LC-ESI-MSMS (Section 5.2.4.3) and were used for affinity-MS analysis (Section 5.2.3.3).

5.2.3.2 Preparation and validation of immobilized VC1 affinity column

VC1 stock solution (1.00 mg mL^{-1} in HBS) was ultrafiltered (UF) for buffer exchanging. HBS was replaced with sodium bicarbonate (0.2 M) and NaCl (0.5 M) (pH 8.3) (coupling buffer). UF was carried out with a Varifuge 3.0 R centrifuge (Heracus Sepatech, Hanau, Germany). 150 µL of VC1 stock solution were diluted up to 500 µL with the coupling buffer and submitted to UF using Amicon Ultra centrifugal filters membranes. Four UF cycles were performed setting 6000xg for 15 min at 25 °C. At the end of each cycle, an aliquot of 400 µL of coupling buffer was added before resubmitting the solution to UF.

VC1 immobilization onto sepharose beads was carried out *via* amine coupling following a previous developed protocol [23]. Briefly, 30 mg of dry CNBr-activated sepharose beads were transferred

into an empty spin column (Mobicol-Classic, MoBiTec GmbH, Göttingen, Germany) with a volume of 800 μL in which a small lower filter of 35 μm was inserted to avoid bead leakage. The beads were pre-treated with 0.5 mL of HCl (0.1M) for 15 min, under shacking (450 rpm). Beads were washed ten times with 0.4 mL NaOAc (pH 4.0; 0.2 M) containing NaCl (0.5 M) (washing buffer) and ten times with 0.4 mL of coupling buffer (pH 8.3). At the end of the washes, coupling buffer was drained and 127.8 μL of VC1 sample, now diluted in coupling buffer at 0.88 mg mL^{-1}, was transferred into the column and incubated with activated beads for 3 h at room temperature, under gentle shacking (450 rpm). The ratio (w/w) VC1/beads was chosen according to previous developed protocols for which 3.75 μg of target ligand were added for each mg of beads [23]. A blank column was also prepared following the same experimental procedure (except for VC1 addition) in order to account for non-specific interactions. After immobilization, the coupling buffer was drained and columns (test column and blank column) were washed ten times with 0.4 mL of washing buffer and ten times with 0.4 mL of blocking buffer, i.e. ethanolamine (0.2 M) and NaCl (0.5 M) (pH 8.3) to remove the unbound receptor. Then, an aliquot of 0.4 mL of blocking buffer was added and columns were incubated 3 h at room temperature, under shacking, to quench residual active cyanate esters. Finally, columns were washed 20 times with 0.4 mL AMBIC (pH 8.5; 0.05 M).

To test VC1 functionality after immobilization, the binding to HSAgly was verified. To this aim, 30 μL of a 2 mg mL^{-1} HSAgly solution in AMBIC (pH 8.5; 0.05 M), corresponding to 60 μg of HSAgly, was added to the VC1-beads and incubated overnight at room temperature, under gentle shacking. The theoretical ratio (w/w) HSAgly/VC1 was 0.5. Afterwards, the supernatant was drained, and the column was washed 40 times with 0.4 mL of ammonium acetate (pH 7.2; 0.05 M). Last wash was subjected to Matrix-Assisted Lased Desorption/Ionization Mass Spectrometry (MALDI-TOF MS) analysis to confirm the absence of unbound protein or other contaminants. Finally, the bound fraction was eluted with 0.3 mL of H_2O:FA (99.9:0.1 v/v). and was analyzed by MALDI-TOF MS as described at Section 5.2.4.1.

5.2.3.3 VC1–HSAgly binding studies by epitope extraction method

The characterization of the interaction between HSAgly and VC1-based column was studied following the epitope extraction method [23,24]. Briefly, the column was washed ten times with 0.4 mL of AMBIC (pH 8.5; 0.05 M), last wash was drained. 60 μg of tryptic digested HSAgly [0.45 mg mL^{-1} in AMBIC (pH 8.5; 0.05 M)] (Section 5.2.3.1) were transferred into the VC1 column and incubated overnight at room temperature, under gentle shacking (450 rpm). The tryptic peptides/VC1 ratio (w/w) was 0.5. After overnight incubation, the supernatant containing unbound

peptides was collected and the column was washed 40 times with 0.4 mL of ammonium acetate (pH 7.2; 0.05 M). Last wash was analyzed by MALDI-TOF MS to confirm the total clearance of unbound peptides. Bound peptides were eluted with 0.3 mL of H_2O:FA (99.9:0.1 v/v). An identical experiment was performed on a blank column to account for non-specific interactions with sepharose beads. The protocol (Fig. 17-A) was repeated in duplicate for two freshly prepared VC1 and blank columns. All collected fractions (unbound and bound) were analyzed by HPLC-ESI-MSMS (Section 5.2.4.4) and data were processed as described in Section 5.2.4.5.

Elution fractions were also resubmitted to trypsin digestion (Fig. 17-B). Briefly, both fractions were diluted 1:2 (v/v) in AMBIC (pH 8.5; 0.5M), treated with 10 μL of DTT (0.1 M) in AMBIC (pH 8.5; 0.5 M), incubated at 56 °C for 30 min, under agitation (600 rpm), further treated with 10 μL of IAA [10 mg mL^{-1} in AMBIC (pH 8.5; 0.5 M)] and incubated 40 min in the dark at room temperature. Finally, 5 μL of trypsin (1 mg mL^{-1}) in HCl (2 mM) were added to each sample and they were incubated overnight at 37°C, under shacking (rpm 600). All digested fractions collected from VC1 and blank columns were dried at room temperature by a SpeedVac vacuum concentrator, resolubilized in bidistilled water and analyzed by HPLC-ESI-MSMS (5.2.4.3). Data were processed as described in Section 5.2.4.4.

5.2.4 MS-based analysis

5.2.4.1 MALDI-TOF MS detection

MALDI-TOF MS analyses were performed with a Brucker Autoflex Smartbeam linear TOF mass spectrometer (Bruker Daltonics, Bremen, Germany) equipped with external scout fully automated X-Y target stage MALDI pulsed collision gas. A nitrogen UV laser (λ_{max} = 337 nm) was used and ions were generated by 10 laser shots for 0.5–1 s at 30 V and extracted at 15 V. MS spectra were recorded setting 10 laser shots for each scan and accumulating 30-60 scans. Mass range was set at 0-70 kDa *m/z* for the detection of intact HSAgly (Section 5.2.3.2) and at 0-7 kDa when HSAgly tryptic peptides were analyzed (Section 5.2.3.3). A freshly prepared 50 mg mL^{-1} SDHB solution in ACN:H_2O:TFA (50:49.9:0.1 v/v) was used as matrix solution for the MS analysis of intact HSAgly while a 20 mg mL^{-1} DHB in ACN:H_2O:TFA (50:49.9:0.1 v/v) was used for the analysis of the digested peptides. In both cases, 0.5 μL of matrix solution was mixed with 0.5 μL of sample solution. The mixture was lodged on the MALDI target plate and the drop was allowed to dry at room temperature. MS analyses were performed using a 20 kV acceleration voltage and 1.5 kV detector voltage. Spectra were processed by Bruker Daltonic flexAnalysis software 3.3.80.0 and corresponding evaluation program was used for mass calculation, data calibration and processing. Spectra were re-elaborated by mMass software (version 5.5.0). Before measurements, external

calibration was carried out using monoisotopic masses of the singly protonated ions of human angiotensin I, angiotensin II, neurotensin, bradykinin, bovin insulin β-chain (oxidized) and bovin insulin.

5.2.4.2 LC-ESI-MS characterization of HSAgly

10 µL aliquots of HSAgly dissolved at 0.1 mg mL^{-1} in bidistilled water were analyzed by LC-MS approach using an Agilent 1200 HPLC system (Walbronn, Germany) and a monolithic CIMac C4 Analytical column (5 mm × 5.3 mm I.D.; pores size 1.3 µm). Mobile phases A [water/acetonitrile/FA (99:1:0.1, v/v/v)] and B [water/acetonitrile/FA (2:98:0.1, v/v/v)] were used to develop a gradient as follow: 30%–70% B, 10 min; 70%–20% B, 1 min; 20% B, 1 min. The column was re-equilibrated with the starting conditions of analysis for 3 min before the next injection. Flow rate was set at 0.4 mL min^{-1} and the injection volume was 3 µL. MS analyses were performed on a Q-TOF Micro quadrupole time-of-flight (Q-TOF) hybrid analyzer (Micromass, Manchester, UK) equipped with a Z-spray electrospray ion source (ESI). Analysis parameters were set as follow: source temperature 120°C, capillary voltage 3.5 kV, cone voltage 45 V. The scan time and the interscan time were set at 2.4 s and 0.1 s, respectively. The cone gas flow was set at 120 L/h and the desolvation gas at 500 L/h. Mass chromatograms were recorded in total ion current (TIC) within 1000-1700 *m/z* range. The HSA baseline-subtracted spectrum (*m/z* 1000–1500) was deconvoluted onto a true mass scale using the maximum entropy (MaxEnt1)-based software supplied with MassLynx 4.1 software. The abundance of single isoforms was calculated as the ratio between their fractional intensity and the sum of the intensities of all isoforms, expressed as percentage. Data were analyzed by Microsoft Excel software.

5.2.4.3 2D-LC-ESI-MSMS analysis of HSAgly

A 2D chromatographic approach was used to resolve the HSAgly peptides obtained from the tryptic digestion. The first dimension consisted of reverse phase liquid chromatography (RP-LC) analyses performed on Jasco PU-1585HPLC system (Jasco Corporation, Tokyo, Japan) equipped with a Rheodyne 7281 injection valve (50 µL sample loop). The peptide separation was carried out by using a Zorbax Extend-C18 RP column (5 µm, 250 mm × 4.6 mm I.D.; column porosity 100 Å). Mobile phases A [water/acetonitrile (98/2) (v/v), adjusted to pH 10.0 using ammonium hydroxide] and B [acetonitrile/water (98/2) (v/v), adjusted to pH 10.0 using ammonium hydroxide] were used for gradient development. The solvent gradient was set as follow: 2%–70% B, 20 min; 70% of B, 2 min. The column was equilibrated for 10 min before the next injection. The analysis flow rate was 0.5 mL min^{-1}. The chromatogram was monitored at 214 nm and the eluate was collected every 2

min into 1.5 mL Eppendorf tubes. Samples were dried under vacuum and reconstituted in 50 µL of water for subsequent second dimension analyses as describe in the Section 5.2.4.4.

5.2.4.4 LC-ESI-MSMS analysis

LC-ESI-MSMS analysis was carried out by using an Agilent 1200 Series (Walbronn, Germany) equipped with a CO-2067 Plus Jasco column oven and a G1329A Agilent autosampler. Analyses were performed on Aeris Peptide XB-C18 (3.6 µm; 150 x 2.1 mm I.D.; column porosity 100 Å) at 40 °C. Mobile phases A [water/acetonitrile/FA (99:1:0.1) (v/v)] and B [acetonitrile/water/FA (99:1:0.1) (v/v)] were used to develop a gradient set as follow: 0–5% B, 1 min; 5–40% B, 59 min; 40–70% B, 5 min. Column was re-equilibrated with the starting conditions for 12 min before the next injection. The injection volume was 50 µL.

MS analyses were performed on a QTOF spectrometer (Micromass, Manchester, UK) equipped with a Z-spray ion source. The source temperature was set at 120 °C, the desolvation temperature at 280 °C, the capillary voltage at 3.0 kV, and the cone voltage at 35 V.

Peptides endowed with 2, 3 and 4 charges with *m/z* values within 600-1900 and an intensity higher than 10 counts/sec were selected for fragmentation and MSMS analyses. Scan time was 1 s for the parent ion and 1 s for the MSMS ions. Collision energy was selected using charge state recognition.

5.2.4.5 Data processing

Raw files from LC-ESI-MSMS analyses were processed using Mascot Distiller 2.5.1.0 (Matrix Science, London, UK), a software program that reduces MS raw data to high-quality peak lists for database searching. Data bank search was performed on the human SWISSPROT database (2018_10; 558590 sequences; 200544181 residues; http://www.uniprot.org) allowing five missed cleavages. The precursor and fragment ion tolerance were 0.5 and 0.3 Da, respectively. Cysteine carbamidomethylation was selected as fixed modification while methionine oxidation, cysteine sulfonylation, cysteine trioxidation, lysine and arginine glycation were selected as variable modifications.

5.3 Results and discussion

5.3.1 Characterization of HSAgly by LC-ESI MS and 2D-LC-ESI-MSMS

The lack of a clear picture concerning AGE-HSA–RAGE interaction is partially related to AGE-HSA heterogeneity. Indeed, the use of not well-characterized albumin-AGEs in *in vitro* studies hampers the identification of structural requirements for interaction and RAGE activation. To partially overcome this problem, we focused our attention on a commercially available glycated HSA (HSAgly), which has been recently released on the market, as possible reference compound for interaction studies. Based on the vendor specifications, the commercial HSAgly was produced by reaction with glucose as reducing sugar. Hence, it is expected to present fructosyl-lysines in its structure. Nevertheless, no other information is available from the supplier and the glycation extent as well as the specific aminoacid residues involved in glycation were unknown. For this reason, before studying HSAgly–VC1 interaction, the structure of the commercial product was investigated by both top-down and bottom-up approaches.

At first, the glycation extent of the protein was determined by analyzing the intact protein by LC-ESI-MS. The protein was resolved by RP chromatography. From the multicharged mass spectrum acquired under the HSAgly chromatographic peak, the deconvoluted ESI-MS spectrum was derived, enabling the evaluation of protein micro-heterogeneity. Along with the native unmodified protein, other modified isoforms were detected and the most abundant were the cysteinylated and glycated forms. Focusing on the glycated isoforms, their relative abundance was calculated, as reported in Fig. 12. The overall albumin glycation was found to be 51.4 %.

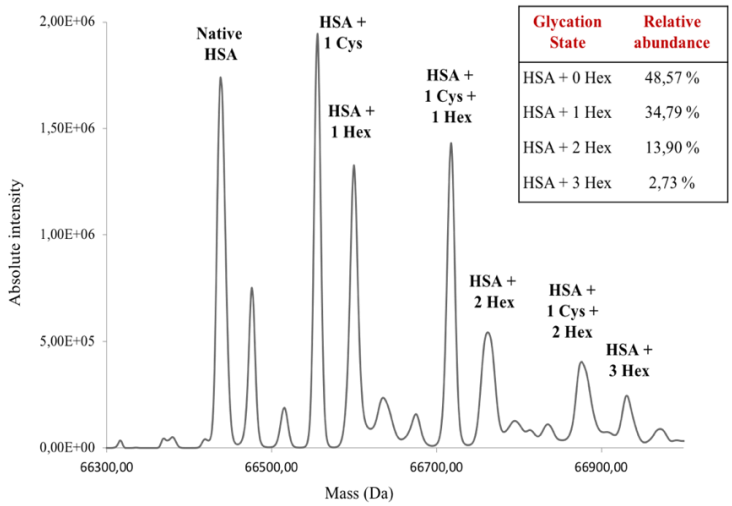

Figure 12| Representative deconvoluted ESI-MS spectrum for HSAgly. The HSAgly micro-heterogeneity was identified by LC-ESI-MS (see Section 5.2.4.2). In addition to the native HSA, isoforms displaying cysteinylation at the cysteine-34 residue (HSA+ Cys), glycation with different hexose molecules (HSA + nHex), and combination of both (HSA+ cys + nHex) were detected. The insert table lists the glycation state along with the relative abundance (%) calculated for the various glycated isoforms.

To identify sites of glycation, a two-dimensional liquid chromatography separation coupled with mass spectrometry detection (2D-LC-ESI-MSMS) was employed. 2D separation prior to MSMS analysis facilitates the resolution of complex mixtures, offering advantages in terms of sensitivity [25]. This method previously proved to be suitable for the analysis of the glycated proteome notwithstanding the complexity of clinical samples and the low abundance of *in vivo* glycated proteins [26]. Tryptic mixture was first resolved in basic conditions, eluates were collected every 2 min, dried under vacuum, reconstituted in water and analyzed by ESI-MSMS in acidic conditions. The databank search confirmed a 75 % coverage of HSAgly sequence. The 2D-LC-MSMS approach allowed the identification of four glycated residues: K137, K414, K525, K574 (Table 5). No carboxymethyl/carboxyethyl lysines (CML/CEL), which are the most abundant AGEs *in vivo* [27], were detected by 2D-LC-ESI-MSMS analysis, pointing out the early glycation state of the commercial product.

Table 5. Tryptic peptides of HSAgly, containing glycated residues on their sequence, identified by 2D-LC-ESI-MSMS. The corresponding observed *m/z* value, molecular weight (MW), retention time (RT) and sequence with the glycated residues involved along with Mascot search score are reported.

Peptide	Observed *m/z*	Peptide MW	t_R (min)	Score[a]	Sequence
137-144	609,57	1217,13	19.48	42	**K**.KYLYEIAR.R + [+162.1256 at N-term]
413-428	867.39	1801.73	24.53	50	K.**K**VPQVSTPTLVEVSR.N [+162.1256 at K2]
525-534	646,19	1290,36	20.53	43	**K**.KQTALVELVK.H + [+162.0528 at N-term]
574-585	652,86	1303,70	26.66	41	**K**.KLVAASQAALGL.+ [+162.0528 at N-term]

[a]t_R stands for retention time. [b]Score is derived from Mascot database and is based on the calculated probability, P, that the observed match between the experimental data and the database sequence is a random event. Score greatest than 35 indicates high probability of identity.

Among the found glycated residues, K525, which is the most common glycated lysine residue of albumin both in *in vitro* glycation and in clinical samples, was detected [2]. In particular, clinical studies showed that glycation at K525 accounts for 33% of the total glycated HSA in patients with unstable blood glucose and that K137, K414, K574 are common glycation sites, frequently detected in HSA from diabetic patients [2,26,28]. The similarity between the glycation pattern observed in the commercial HSAgly and diabetic patients makes the former a good reference compound to correlate the role of early glycated albumin with RAGE activation in diabetes.

5.3.2 Biosensing surface preparation and validation

HSAgly sensing surface was prepared via amine coupling reaction. The covalent binding between the amine groups of lysines on the surface of target molecule and the carboxymethyl dextran layer is the most commonly used approach for target immobilization on sensor chips. Indeed, thanks to

the high stability and high surface density, this strategy has been previously exploited to investigate binding parameters of small molecules to HSA [29–31].

To assess the best immobilization conditions, a pH scouting procedure was carried out by diluting HSAgly in several immobilization solutions at different pH. To obtain an adequate pre-concentration of the protein over the surface, immobilization buffer requires a pH above the isoelectric point (pI) of the dextran layer and below pI of the protein. pH scouting evaluation showed that the NaOAc (pH 4.5; 0.01 M) solution granted the best conditions for immobilization, providing a stable, high and time-dependent pre-concentration of the protein over the surface (data not shown).

For HSAgly immobilization the surface was activated by treatment with EDC/NHS mixture prior injection of a HSAgly solution to reach an immobilization level of 5500 RUs (Fig. 13). According to classic amine coupling protocol, residual active esters were quenched by flushing a solution of ethanolamine hydrochloride (pH 8.5; 1 M) [22] and the sensing surface was stabilized overnight in PBS. The overnight stabilization is required to stabilize the baseline and remove the residual HSAgly not covalently bound to the surface. Final immobilization level resulted 5000 RUs, approximatively corresponding to a surface density of 5.0 ng mm^{-2} [21].

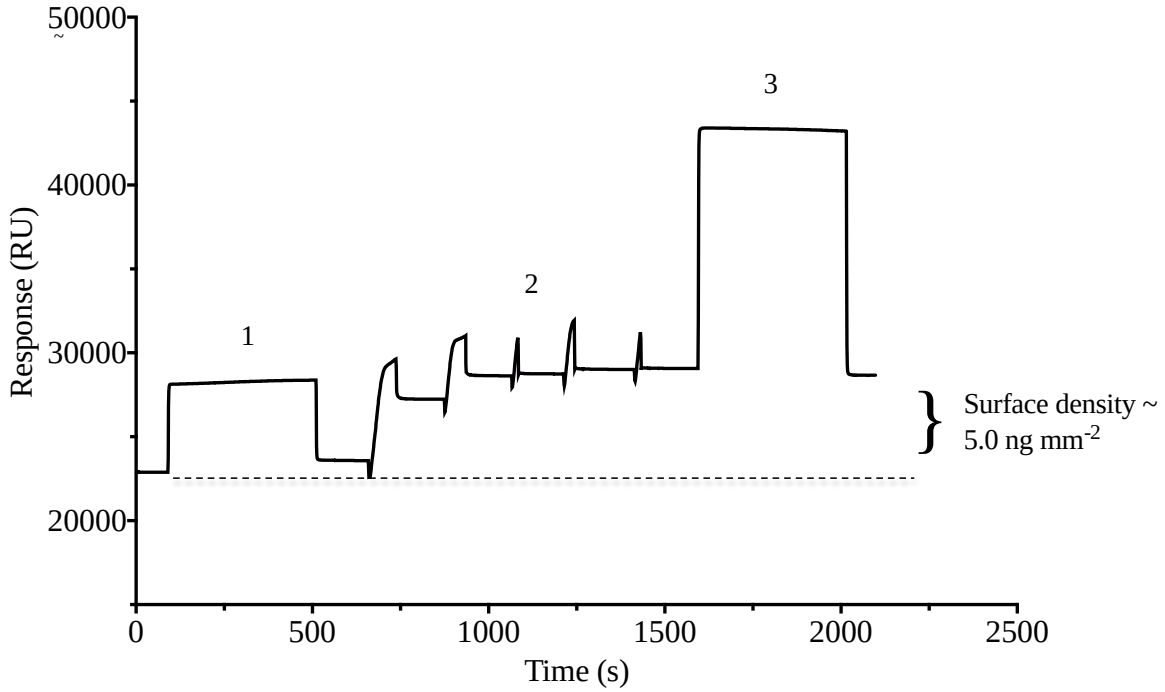

Figure 13| Sensorgram of HSAgly immobilization to a CM5 sensor chip. HSAgly was immobilized according to amine coupling procedure which involves (1) activation of the sensor surface by EDC/NHS mixture, (2) injections of a HSAgly solution in NaOAc (pH 4.5; 0.01 M), (3) quenching of residual activated esters by treatment with an ethanolamine solution. After overnight stabilization the surface density was estimated to be about 5.0 ng mm^{-2}.

After covalent immobilization, the validation of the sensing surface is required to assess if the covalent anchorage to the surface has preserved target binding properties. To evaluate HSAgly functionality, rac-WRF, which is one of the mostly used markers to assess HSA binding capacity at binding site I [31], was used as test compound. The measured K_D value (11.5×10^{-6} M) resulted in agreement with previously reported SPR analysis of the interaction of rac-WRF and HSA [31]. Altogether, the comparison between the experimental R_{max} value with the theoretical maximal response and the affinity for rac-WRF confirmed that the functionality of the surface was maintained.

It is worth to note that commercial HSAgly is in an early stage of glycation (see Section 5.3.1). This fact may explain the comparable binding capacity of HSAgly and native protein. The obtained K_D resulted in agreement with affinity values reported by Joseph K.S *et al.* [32] for WRF–HSAgly and WRF–HSA, quantified by high performance affinity chromatography (HPAC).

5.3.3 Characterization of VC1–HSAgly binding by SPR

SPR biosensing is the gold standard method to *real time* monitor biorecognition phenomena. This highly informative technique allows easy access to affinity and kinetic data on complex formation/disruption [33]. Despite the great interest on RAGE–AGE interaction, a limited amount of SPR-based studies are available in the literature [13,14,34]. In the current work, SPR biosensor was used to investigate HSAgly binding to the ectodomain VC1 of RAGE. HSAgly was chosen as immobilized target instead of VC1 because of the lack of commercially well-characterized AGE-albumin binders to validate the VC1-sensing surface after immobilization. Conversely, using the opposite system (immobilization of HSAgly) the resulting sensing surface could be validated (see Section 5.3.2).

VC1 (MW= 28 kDa measured by ESI-MS) was firstly diluted in HBS-E-T at 1 μM and injected over HSAgly sensing surface. The obtained double-reference corrected sensorgram resulted well discernable from background noise confirming the interaction between the two biomolecules. To our knowledge, this is the first time that the interaction between VC1 and this form of commercially glycated albumin was analyzed and, as consequence, no data are available regarding the affinity of the complex and the range of concentrations for VC1-HSAgly affinity studies. The higher tested concentration was 4.00 μM, because responses recoded at higher concentrations resulted compromised, making unreliable the sensorgrams related to the binding event. Possible explanation of that may be high steric hindrance, crowding and possible aggregation at the functionalized surface when high concentrations were used [22].

VC1–HSAgly affinity analysis were carried out diluting VC1 in HBS-E-T in two-fold serial dilutions from 4.00 μM to 0.016 μM. All measured interactions reached the steady-state condition within the selected injection and dissociation time, i.e. 300 s and 1300 s, respectively (Fig. 14-A). Two injections of regeneration solution (NaOH, 0.05 M) were required to re-establish the baseline condition. Responses recorded at equilibrium were plotted against concentration and the equilibrium dissociation constant (K_D) was calculated applying a 1:1 binding model (Fig. 14-B) resulting in the averaged value of (6.05 ± 0.96) $\times 10^{-7}$ M (n= 2).

Moreover, preliminary evaluation of association and dissociation events suggested a slow interaction, which required a long VC1 injection (300 s) before reaching the steady state as well as a long dissociation time (1300 s) to allow the disruption event.

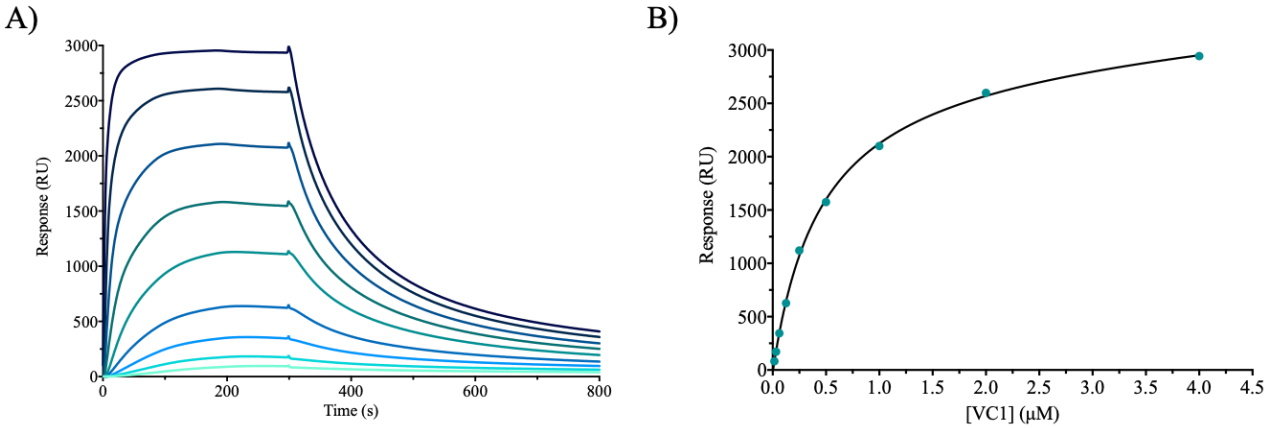

Figure 14| SPR sensorgrams and corresponding 1:1 isotherm for VC1–HSAgly interaction. A) Different VC1 concentrations (0.016–4.00 μM) were injected in ascending order over the sensing surface. Increasing concentrations (0.016, 0.031, 0.063, 0.125, 0.250, 0.500, 1.00, 2.00, 4.00) are denoted by different shade of blue (from light to dark). K_D value for VC1–HSAgly complex was extrapolated by plotting the double-reference corrected responses (RUs) recorded at the equilibrium as function of VC1 concentration. A simple 1:1 binding model, which fitted the experimental data, was applied, according to Eq. (8).

To our knowledge, no affinity datum is available from literature regarding the interaction of VC1 with this form of glycated albumin. Hence, to further validate the VC1–HSAgly binding, a SPR-based displacement assay was performed using CND, a selective RAGE binder, as displacing agent. Affinity for the CND–RAGE interaction has been previously assessed by Mizumoto S. *et al*. by a SPR-based approach, which highlighted a K_D value of (3.06 ± 1.63) x 10^{-7} M [18,19]. On the other hand, CND is not a HSAgly binder, as proved by our studies. Indeed, injection of CND over the HSAgly-sensing surface did not result in any significant interaction. This finding makes CND a suitable agent for displacement studies.

Displacement study was carried out monitoring VC1–HSAgly binding as a function of increasing concentrations of CND (Fig. 15). A concentration-dependent competition of CND towards HSAgly-VC1 binding was observed, inferring a specific interaction involving overlapped binding sites. Indeed, solutions of [CND]/[VC1] molar ratios of 1/1, 2/1, 5/1 reduced SPR response of the VC1–HSAgly complex recorded in the absence of CND ([CND]/[VC1] = 0/1) by 15.1 %, 31.8 %, 66.7 %, respectively (Fig. 15).

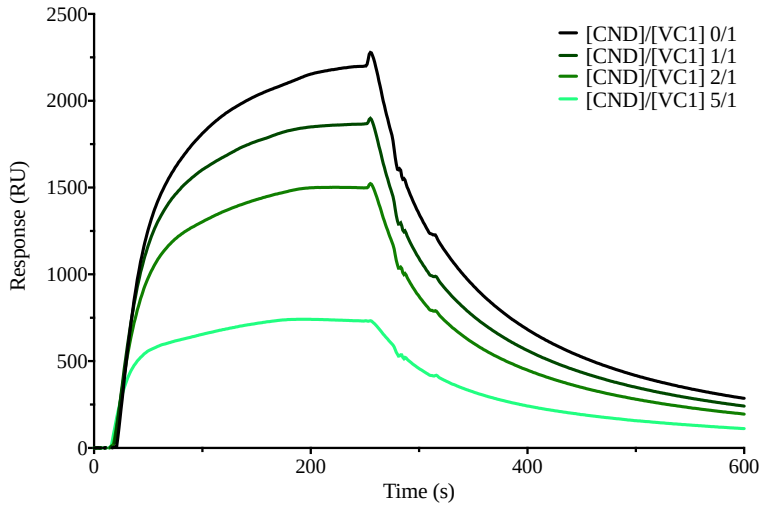

Figure 15| SPR-based displacement assay for the VC1–HSAgly interaction. Competition assay was carried out injecting CND/VC1 mixtures at increasing stoichiometry molar ratios. Reference SPR response in the absence of CND is depicted as black line while signals recorded at increasing [CDN]/[VC1] ratios are depicted as green lines of decreasing shades as detailed in the graph.

Results proved VC1–HSAgly interaction is specific and can be hampered by a VC1 known RAGE binder.

Commercial glycated albumin is an early stage glycation product as compared to AGEs and, as consequence, it is unrepresentative of advanced glycation end products which may form in vivo in severe hyperglycemia. Nevertheless, preliminary data obtained by the SPR-based assay allowed to make some considerations on the binding of this early stage product with VC1, thus laying the basis for subsequent investigations on AGE–RAGE interaction.

5.3.4 HSAgly–VC1 interaction studies by affinity-MS approach

The immobilization strategy chosen for affinity-MS approach envisaged VC1 covalent immobilization onto CNBr-activated sepharose beads pre-packed into a microcolumn. Moreover, the strategy enabled to reduce VC1 consumption, usually higher when the receptor is selected as analyte instead of as immobilized target. Covalent immobilization of VC1 onto CNBr-activated

sepharose beads through amine coupling [23] granted VC1 stability, enabling the reusability of the VC1-based column for multiples analyses. The effectiveness of immobilization procedure was confirmed by affinity-MS approach (Fig.16) [20].

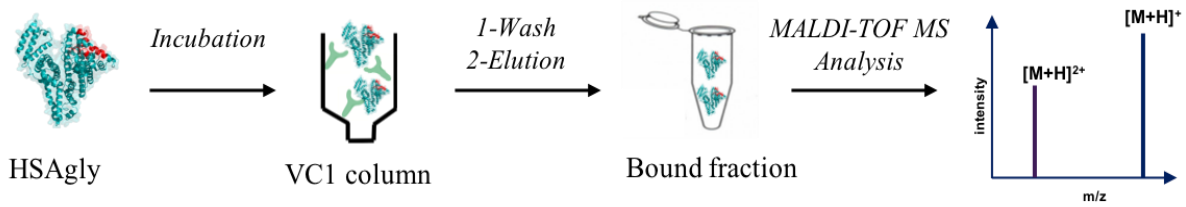

Figure 16| Schematic representation affinity-MS approach used to test VC1 column functionality. The method briefly consisted of incubation of the intact HSAgly, the removal of unretained protein (or peptides) as well as washing steps to remove not specifically bound analytes, the disruption of the binding complex by acidic conditions, the collection of the bound fraction and the analysis by MALDI-TOF MS.

In order to validate the VC1 column, the interaction with HSAgly was studied. In the preliminary set up of the method, the effectiveness of washing steps was confirmed by analyzing washings by MALDI-TOF MS and confirming the absence of any protein in the last wash (Fig. 17-B). In the optimized procedure, HSAgly was added to the VC1 column and incubated overnight, unbound fraction was washed and, finally, HSAgly–VC1 binding was disrupted in acidic condition. The eluted fraction was collected and analyzed by MALDI-TOF MS (Fig. 17-A).

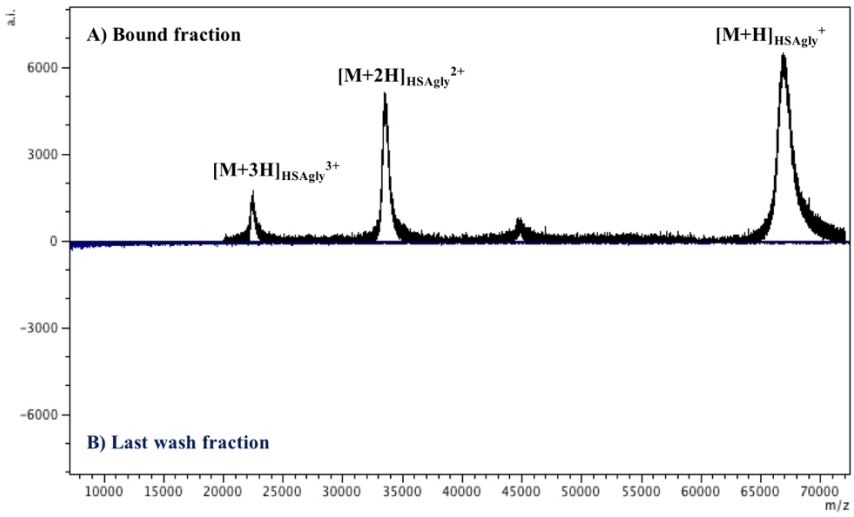

Figure 17| Comparison of MALDI-TOF MS spectra obtained by Affinity-MS approach for VC1 column validation. A) Elution of bound fraction was analyzed by MALDI-TOF MS and HSAgly intact protein was recorded (black spectrum). Monocharged ion $[M+H]^{+}$ = 66925.4 Da, doubly charged ion $[M+2H]^{2+}$ = 33480.4 Da and triply charged ion $[M+3H]^{3+}$ = 22369.3 Da were detected, validating VC1 column. **B)** The flip spectrum (blue) corresponds to the analysis of the last washing step. The absence of any residual unbound protein or contaminant confirmed that washing protocol was efficient in removing any unbound analyte from the column before elution.

The detection of the intact protein in the bound fraction confirmed the binding of HSAgly with immobilized VC1, supporting the results achieved by SPR-based assay. Most importantly, the retained binding capacity of VC1 towards HSAgly confirmed that VC1 was functional after immobilization. A blank column was also prepared following the same procedure and was used as negative control for the determination of non-specific interactions.

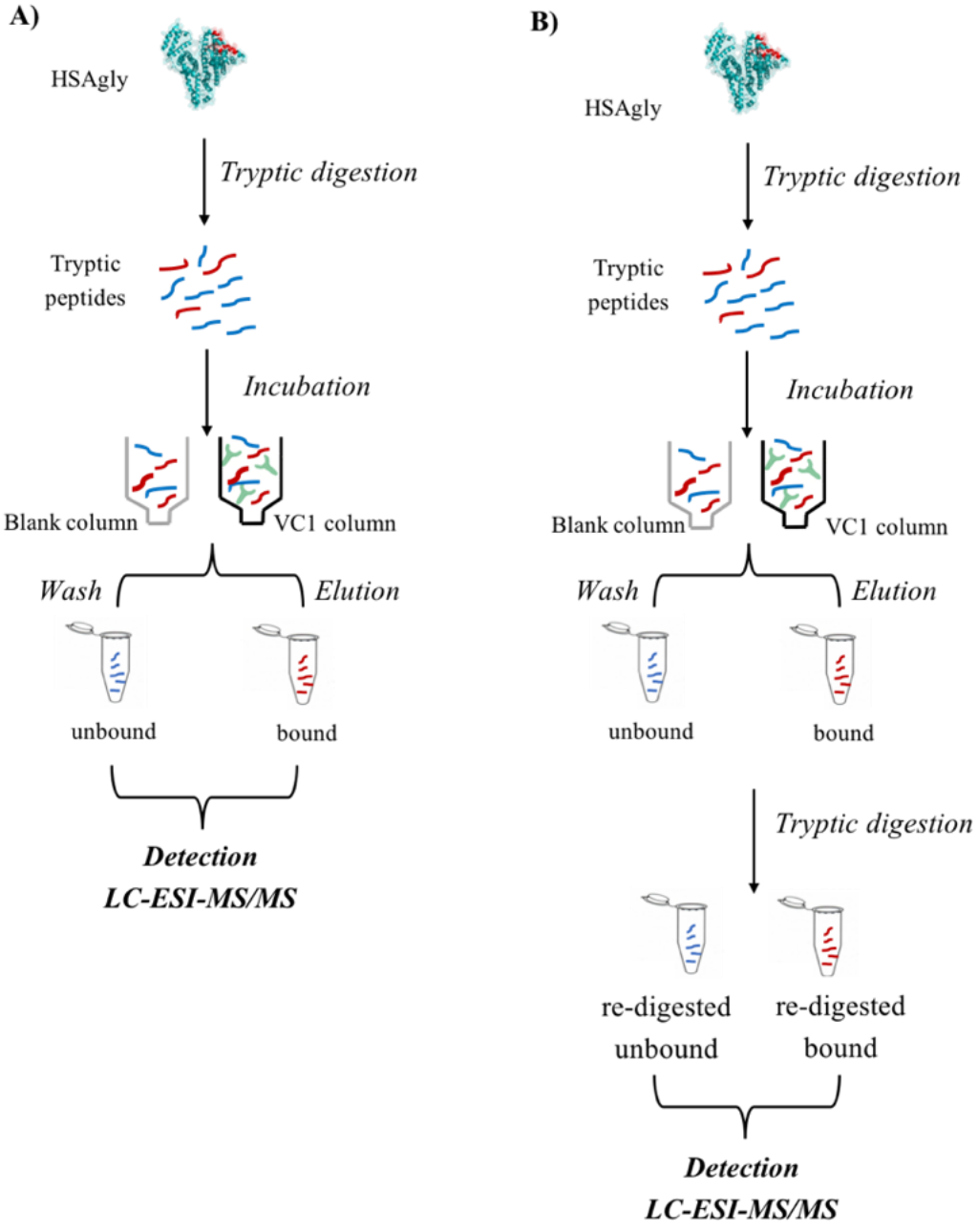

Figure 18| Schematic representation of the tailored epitope extraction method described in Section 5.2.3.3. Epitope extraction method was exploited to isolate tryptic peptides of HSAgly involved in the binding with VC1. **A)** Supernatant (unbound) and elution (bound) were directly analyzed by LC-ESI-MSMS. **B)** Supernatant (unbound) and elution (bound) were re-digested with trypsin before analysis by LC-ESI-MSMS.

Once assessed the functionality of immobilized VC1, the column could be applied to further studies, in particular to the determination of the protein region involved in HSAgly–VC1 recognition. To this purpose, the so-called epitope extraction method was applied [23,35]. This approach has been set up to identify the epitope involved in antigen-antibody interaction. Briefly, the method consists of target (i.e., antibody) immobilization onto a microcolumn packed with sepharose beads, the incubation of the peptide mixture derived from proteolytic digestion of the ligand protein, the isolation of the bound peptides, their elution and the identification of the epitope sequence by MS analysis of the eluates [23,24,35,36]. Herein, a slightly modified set up was used to identify the surface region of HSAgly involved in the binding with VC1 receptor to shed light on protein structural requirements necessary for HSAgly–VC1 recognition.

In Figure 18 the tailored experimental workflow for epitope extraction method is reported. In detail, the peptide mixture obtained by tryptic digestion of HSAgly was overnight incubated on VC1 and blank columns. The unbound peptides were collected and the columns were washed. Before eluting the bound peptides, the effectiveness of washing procedure was assessed by MALDI-TOF MS analysis of the last washing. Finally, the bound fraction was eluted in acidic conditions and analyzed by LC-ESI-MSMS. Figure 19 shows the chromatographic profile of the bound fraction collected from the VC1 column in comparison with the bound fraction collected from the blank column. The absence of significant signals in the bound fraction of the blank column highlighted negligible non-specific interactions between HSAgly peptides and sepharose beads.

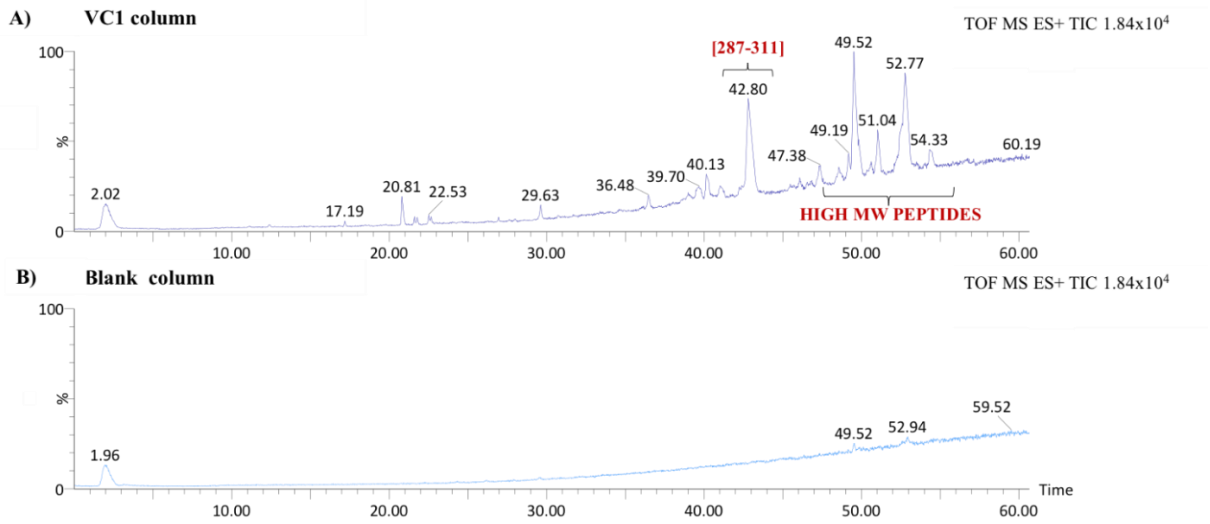

Figure 19| LC-ESI-MSMS total ion chromatogram of the bound fractions eluted from VC1 and blank columns. Bound fractions eluted from **A)** VC1 and **B)** blank column were analyzed. Retention time values are displayed on relative peak apexes. The peak at 42.80 min was identified as peptide [287-311]. High MW peptides, for which further studies were required, were eluted at higher retention time and their corresponding peaks are pointed out. Analysis conditions are reported in Section 5.2.4.4.

The LC-MSMS analysis of the bound fraction and the following MASCOT database search allowed the identification of only one peptide, namely peptide [287-311] eluting at 42.8 min (Table 6). The good score ensured the peptide identification.

Bound fraction also contained high MW (HMW) peptides, which eluted with longer retention times, which were not selected from further fragmentation. The experimental set-up, indeed, involves the fragmentation of $[M+2H]^{2+}$, $[M+3H]^{3+}$ and $[M+4H]^{4+}$ ions (Section 5.2.4.4) while these HMW peptides are characterized by a higher charge state. As example, Fig 20-A shows the multicharged mass spectrum acquired under the peek apex eluting at 52.77 min and the corresponding deconvolution spectrum (Fig. 20-B).

Table 6. Characteristics of the peptide [287-313] identified by the epitope extraction method as interactant with VC1. Mascot search score is also reported.

Peptide	Observed *m/z*	Peptide MW	t_R (min)	Score[a]	Sequence
287-313	992.2	2973.33	42.7	63	K.SHCIAEVENDEMPADLPSLAADFVESK.D

[a]t_R stands for retention time. [b]Score is derived from Mascot database and is based on the calculated probability, P, that the observed match between the experimental data and the database sequence is a random event. Score greatest than 35 indicates high probability of identity.

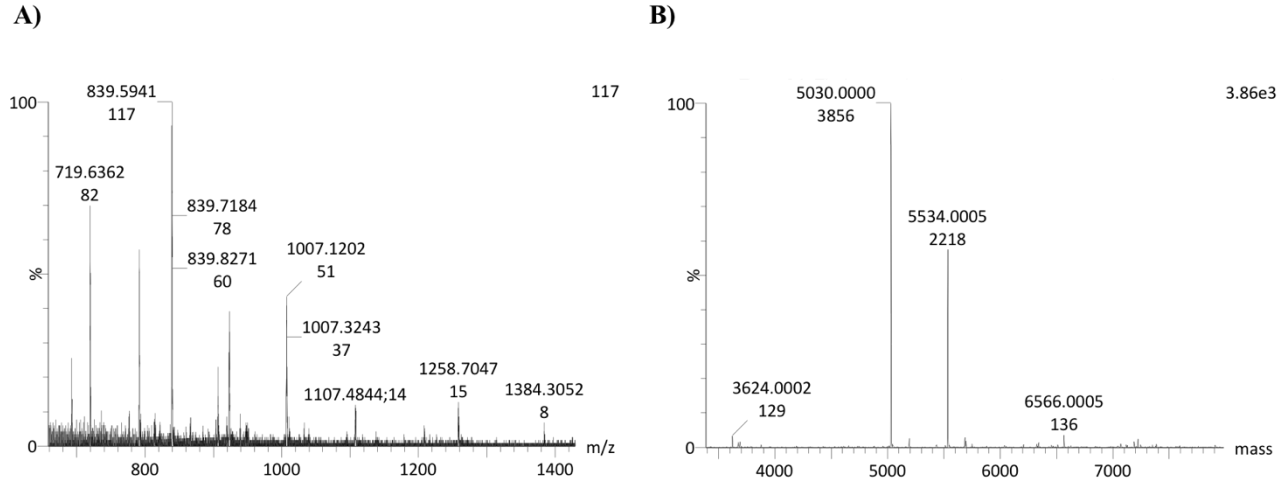

Figure 20| ESI-MS analysis of high MW peptide eluted at 52.77 min and found in bound fraction. A) Multi-charged mass spectrum, acquired on peak apex eluting at 52.77 min, and **B)** corresponding deconvoluted ESI-MS spectrum. For analyses condition see Section 5.2.4.4.

In order to identify these HMW peptides, the bound fraction was re-digested to get peptides with lower MW and facilitated their identification by subsequent LC-ESI-MSMS analysis (Fig. 18-B). This approach led to the identification of a number of peptides which are summarized in Figure 21.

Among glycated peptides identified by 2D-LC-MSMS, only the one containing K525, the most common lysine residue involved in glycation reaction of albumin [1], was identified in the bound

fraction. This suggest that this residue (and region of the protein around this region) is the most likely involved in the interaction with VC1.

It should be also mentioned that tryptic digestion makes available for the interaction also peptides otherwise not exposed on the protein surface. This explains the identification of a number of peptides which are not located at the protein surface. Although they clearly cannot play a role in the biorecognition of VC1 when the protein if correctly folded, it cannot be excluded at this stage of the study that these peptides may be involved in the stabilization of the interaction between AGE-albumins which are characterized by an extensive alteration of the native structure including dimerization, oligomerization and misfolding. Furthermore, interaction of VC1 with these embedded peptides also opens the possibility of identifying structure requirements for binding to VC1.

Finally, among HSA domains, the subdomain IA is that with the higher degree of identified amino acid sequence (63%). This observation suggests this region may be the most likely involved in the interaction with VC1.

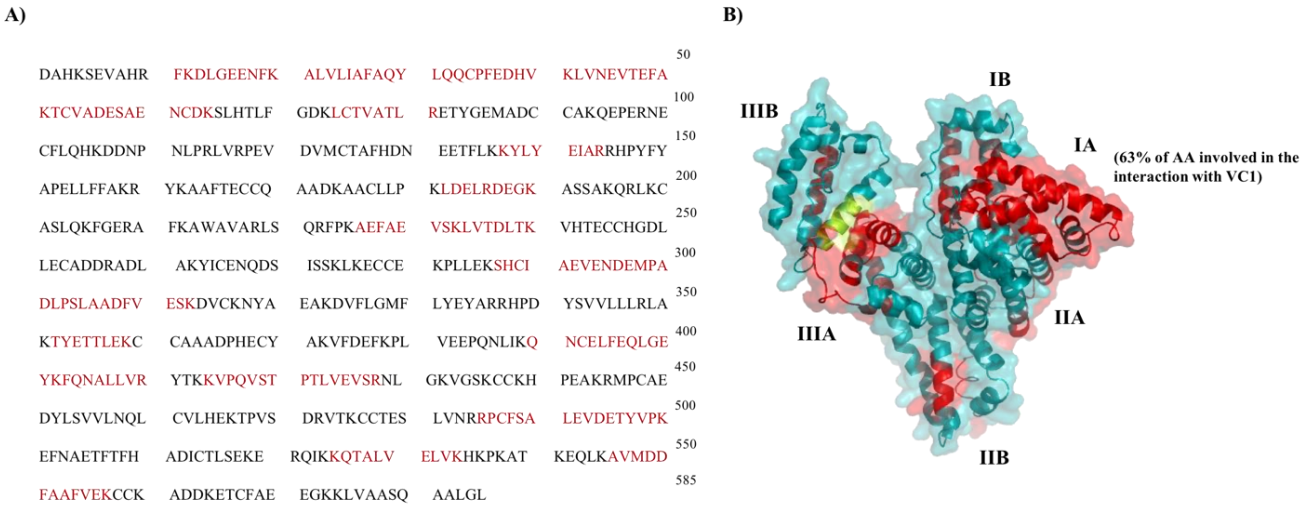

Figure 21| Aminoacidic sequence and tridimensional structure of the HSAgly highlighting bound peptides identified by epitope extraction procedure. A) Aminoacidic sequence of HSAgly. The peptides identified by LC-ESI-MSMS after the re-digestion of the bound fraction are depicted in bold (red). **B)** HSAgly tridimensional structure in which regions corresponding to peptides identified in the bound fraction are highlighted in red. The glycated peptide corresponding to sequence [525-534], detected in the bound fraction, is depicted in light green. Identified peptides from bound fraction cover 63% of aminoacidic sequence of subdomain IA.

5.4 Conclusions and perspectives

In the current study we set up a multimethodological strategy to investigate the binding between the ectodomain of human RAGE, i.e. VC1, expressed in *Pichia Pastoris* by Degani *et al*. [15], and a glycated albumin recently released on the market. The interest on such ligand arises from its commercial availability and its similarity in terms of glycation pattern and glycation degree with the average glycated HSA forms found in diabetic patients. Indeed, 2D-LC-ESI-MSMS analysis allowed the identification of four site of glycation, among which the residue K525, i.e. the most commonly glycated lysine residue detected in glycated albumins both obtained by *in vitro* glycation and found in diabetic patients.

Although HSAgly is not an advanced glycation end product, SPR-biosensing studies using a HSAgly-sensing surface highlighted HSAgly can interact with VC1 with a moderate affinity (K_D = $6.05x10^{-7}$) and with a slow association and dissociation rate. Observed interaction was confirmed to be specific as proved by displacement studies with a well-known RAGE binder, i.e. chondroitin. Application of affinity-proteomics, involving the use of a purposely developed VC1-affinity column and subsequent MS analysis of the retained protein or peptides, allowed further insights into HSAgly–VC1 biorecognition. In details, the study identified the glycated peptide [525-534], with glycation at residue K525, as the only glycated peptide of HSAgly able to interact with VC1. Furthermore, and quite interestingly, preliminary results also highlighted a possible involvement of the area including subdomain IA in VC1 biorecognition (63% coverage of the subdomain). This area does not contain glycated lysine residues. This observation, if confirmed by further studies, may open new considerations on a possible more complex biorecognition pattern.

The identification of peptides normally embedded into the protein as possible interactants of VC1 arises from the exposure of these peptides upon protein denaturation prior to tryptic digestion. Although interesting information on the structural requirements for VC1 binding may be obtained from the analysis of these peptides, they obviously cannot contribute to VC1 recognition by native HSAgly. Therefore, to overcome the latter limitation, further experiments, which will include analysis of peptides obtained from HSAgly digestion in non-denaturing conditions, will be carried out.

As general consideration, the outcomes of this study showed that combination of VC1-affinity column for interactants isolation, HPLC-ESI-MSMS for the identification of the binding region(s) along with SPR technology for affinity quantification of the binding complex, may be a useful strategy to elucidate structural requirements for VC1 binding. In particular, the proposed approach may be further employed to investigate the interaction between VC1 and *in vitro* albumin-AGEs formed at different stages of glycation, including the forms more representative of diabetes

conditions. Finally, the availability of increasing information on biorecognition mechanisms involving RAGE, or its ectodomain VC1, although partial, are useful to start fulfilling the gap between circulating glycated species (either early glycation products or end products) and the pathological pathways triggered by RAGE activation.

References

[1] J. Anguizola, R. Matsuda, O.S. Barnaby, K.S. Hoy, C. Wa, E. DeBolt, M. Koke, D.S. Hage, Review: glycation of human serum albumin, Clin. Chim. Acta. 425 (2013) 64–76.

[2] R. Kisugi, T. Kouzuma, T. Yamamoto, S. Akizuki, H. Miyamoto, Y. Someya, J. Yokoyama, I. Abe, N. Hirai, A. Ohnishi, Structural and glycation site changes of albumin in diabetic patient with very high glycated albumin, Clin. Chim. Acta. 382 (2007) 59–64.

[3] P. Rondeau, E. Bourdon, The glycation of albumin: structural and functional impacts, Biochimie. 93 (2011) 645–658.

[4] C. Wa, R.L. Cerny, W.A. Clarke, D.S. Hage, Characterization of glycation adducts on human serum albumin by matrix-assisted laser desorption/ionization time-of-flight mass spectrometry, Clin. Chim. Acta. 385 (2007) 48–60.

[5] G. Aldini, G. Vistoli, M. Stefek, N. Chondrogianni, T. Grune, J. Sereikaite, I. Sadowska-Bartosz, G. Bartosz, Molecular strategies to prevent, inhibit, and degrade advanced glycoxidation and advanced lipoxidation end products, Free Radic. Res. 47 (2013) 93–137.

[6] S. Yamagishi, Role of advanced glycation end products (AGEs) and receptor for AGEs (RAGE) in vascular damage in diabetes, Exp. Gerontol. 46 (2011) 217–224.

[7] G. Degani, A.A. Altomare, M. Colzani, C. Martino, A. Mazzolari, G. Fritz, G. Vistoli, L. Popolo, G. Aldini, A capture method based on the VC1 domain reveals new binding properties of the human receptor for advanced glycation end products (RAGE), Redox Biol. 11 (2017) 275–285.

[8] C. Ott, K. Jacobs, E. Haucke, A. Navarrete Santos, T. Grune, A. Simm, Role of advanced glycation end products in cellular signaling, Redox Biol. 2 (2014) 411–429.

[9] G. Fritz, RAGE: A single receptor fits multiple ligands, Trends Biochem. Sci. 36 (2011) 625–632.

[10] M. Koch, S. Chitayat, B.M. Dattilo, A. Schiefner, J. Diez, W.J. Chazin, G. Fritz, Structural basis for ligand recognition and activation of RAGE, Structure. 18 (2010) 1342–1352.

[11] J. Xie, S. Reverdatto, A. Frolov, R. Hoffmann, D.S. Burz, A. Shekhtman, Structural basis for pattern recognition by the receptor for advanced glycation end products (RAGE), J. Biol. Chem. 283 (2008) 27255–69.

[12] J. V Valencia, S.C. Weldon, D. Quinn, G.H. Kiers, J. DeGroot, J.M. TeKoppele, T.E. Hughes, Advanced glycation end product ligands for the receptor for advanced glycation end products: biochemical characterization and formation kinetics., Anal. Biochem. 324 (2004) 68–78.

[13] E. Uetz-Von Allmen, M. Koch, G. Fritz, D.F. Legler, V domain of RAGE interacts with AGEs on prostate carcinoma cells, Prostate. 68 (2008) 748–758.

[14] Y. Murakami, T. Fujino, T. Hasegawa, R. Kurachi, A. Miura, T. Daikoh, T. Usui, F. Hayase, H. Watanabe, Receptor for advanced glycation end products (RAGE)-mediated cytotoxicity of 3-hydroxypyridinium derivatives, Biosci. Biotechnol. Biochem. 82 (2018) 312–319.

[15] G. Degani, M. Colzani, A. Tettamanzi, L. Sorrentino, A. Aliverti, G. Fritz, G. Aldini, L. Popolo, An improved expression system for the VC1 ligand binding domain of the receptor for advanced glycation end products in Pichia pastoris, Protein Expr. Purif. 114 (2015) 48–57.

[16] P. Singh, SPR biosensors: historical perspectives and current challenges, Sensors Actuators B Chem. 229 (2016) 110–130.

[17] R.L. Rich, Y.S. Day, T.A. Morton, D.G. Myszka, High-resolution and high-throughput protocols for measuring drug/human serum albumin interactions using BIACORE, Anal. Biochem. 296 (2001) 197–207.

[18] S. Mizumoto, K. Sugahara, Glycosaminoglycans are functional ligands for receptor for advanced glycation end-products in tumors, FEBS J. 280 (2013) 2462–2470.

[19] S. Mizumoto, J. Takahashi, K. Sugahara, Receptor for advanced glycation end products (RAGE) functions as receptor for specific sulfated glycosaminoglycans, and anti-RAGE antibody or sulfated glycosaminoglycans delivered in vivo inhibit pulmonary metastasis of tumor cells, J. Biol. Chem. 287 (2012) 18985–18994.

[20] M. Macht, A. Marquardt, S.O. Deininger, E. Damoc, M. Kohlmann, M. Przybylski, “Affinity-proteomics”: direct protein identification from biological material using mass spectrometric epitope mapping, Anal. Bioanal. Chem. 378 (2004) 1102–1111.

[21] S. Löfås, A. Mcwhirter, The art of immobilization for SPR sensors, in: Surf. Plasmon Reson. Based Sensors, Springer, Berlin, Heidelberg, 2006: pp. 117–151.

[22] D.G. Myszka, Improving biosensor analysis, J. Mol. Recognit. 12 (1999) 279–284.

[23] S. Dhungana, J.G. Williams, M.B. Fessler, K.B. Tomer, Epitope mapping by proteolysis of antigen-antibody complexes, in: Ep. Mapp. Protoc., second ed., Springer New York, Berlin, 2009.

[24] M. Macht, W. Fiedler, K. Kürzinger, M. Przybylski, Mass spectrometric mapping of protein epitope structures of myocardial infarct markers myoglobin and troponin T, Biochemistry. 35 (1996) 15633–15639.

[25] C. Delahunty, J.R. Yates III, Protein identification using 2D-LC-MS/MS, Methods. 35 (2005) 248–255.

[26] L. Zhang, C.-W. Liu, Q. Zhang, Online 2D-LC-MS/MS platform for analysis of glycated proteome, Anal. Chem. 90 (2018) 1081–1086.

[27] J. Xue, V. Rai, S. Frolov, D. Singer, S. Chabierski, J. Xie, S. Reverdatto, D.S. Burz, A.M. Schmidt, R. Hoffman, Advanced glycation end product (AGE) recognition by the receptor for AGEs (RAGE), Structure. 19 (2012) 722–732.

[28] E.C. Keilhauer, P.E. Geyer, M. Mann, HCD fragmentation of glycated peptides, J. Proteome Res. 15 (2016) 2881–2890.

[29] E. Fabini, G.M.L. Fiori, D. Tedesco, N.P. Lopes, C. Bertucci, Surface plasmon resonance and circular dichroism characterization of cucurbitacins binding to serum albumins for early pharmacokinetic profiling, J. Pharm. Biomed. Anal. 122 (2016) 166–172.

[30] C. Bertucci, S. Cimitan, Rapid screening of small ligand affinity to human serum albumin by an optical biosensor, J. Pharm. Biomed. Anal. 32 (2003) 707–714.

[31] Å. Frostell-Karlsson, A. Remaeus, H. Roos, K. Andersson, P. Borg, M. Hämäläinen, R. Karlsson, Biosensor analysis of the interaction between immobilized human serum albumin and drug compounds for prediction of human serum albumin binding levels, J. Med. Chem. 43 (2000) 1986–1992.

[32] K.S. Joseph, D.S. Hage, The effects of glycation on the binding of human serum albumin to warfarin and l-tryptophan, J. Pharm. Biomed. Anal. 53 (2010) 811–818.

[33] E. Fabini, U.H. Danielson, Monitoring drug–serum protein interactions for early ADME prediction through Surface Plasmon Resonance technology, J. Pharm. Biomed. Anal. 144 (2017) 188–194.

[34] L. Yatime, G.R. Andersen, Structural insights into the oligomerization mode of the human receptor for advanced glycation end-products, FEBS J. 280 (2013) 6556–6568.

[35] F. Rinaldi, L. Lupu, H. Rusche, Z. Kukačka, S. Tengattini, R. Bernardini, L. Piubelli, T. Bavaro, S. Maeser, L. Pollegioni, E. Calleri, M. Przybylski, C. Temporini, Epitope and affinity determination of recombinant Mycobacterium tuberculosis Ag85B antigen towards anti-Ag85 antibodies using proteolytic affinity-mass spectrometry and biosensor analysis, Anal. Bioanal. Chem. 411 (2019) 439–448.

[36] M.I. Iurașcu, O. Marroquin Belaunzanar, C. Cozma, U. Petrausch, C. Renner, M. Przybylski, An HLA-B27 homodimer specific antibody recognizes a discontinuous mixed-disulfide epitope as identified by affinity-mass spectrometry, J. Am. Soc. Mass Spectrom. 27 (2016) 1105–1112.

PART III

Human cholinesterases

Chapter 6

Introduction

6.1 General remarks

Cholinesterase (ChE) is a generic name for a family of enzymes implicated in the hydrolysis of the neurotransmitter acetylcholine (ACh) both in the central and in the peripheral nervous system. These serine hydrolases play a key role in the catalysis of ACh into choline and acetic acid, thus promoting the termination of the neurotransmission at cholinergic synapses and the restoration of the resting state [1] (Fig. 22).

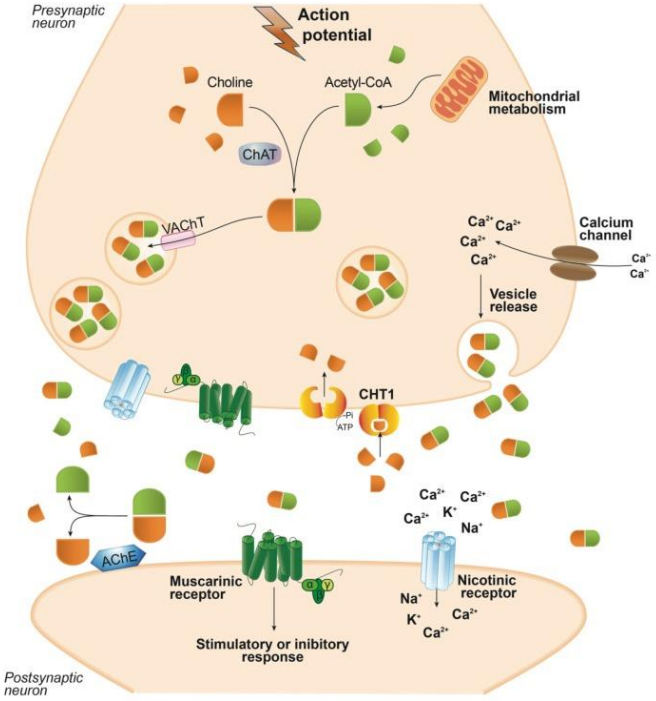

Figure 22| Graphical representation of biological mechanisms involved in ACh neurotransmission. After the synthesis of ACh in the cytosol of pre-synaptic cholinergic neurons, the neurotransmitter is incorporated into synaptic vesicles. Due to depolarization induced by calcium ions, ACh exocytosis releases ACh into synaptic cleft. The neurotransmitter can bind two different receptors, namely nicotinic and muscarinic receptor, thus promoting ACh-based cascade response. The role of AChE grants ACh hydrolysis with the subsequent reuptake of acetate and choline into the pre-synaptic neurons. Reprinted with permission from [1].

Cholinesterase includes two types of enzymes, namely acetylcholinesterase (AChE) and butyrylcholinesterase (BuChE), which are located ubiquitously through human body regulating different functions. The former, which is the most abundant enzyme belonging to this family, is located both in central and peripheral neurons. [2]. BuChE, also known as plasma cholinesterase, is

predominantly located in liver, blood plasma and central nervous system where it is associated with glial cells. In the nervous system, it directly acts as co-regulator of ACh levels in brain, although to a lesser extent compared with AChE [3]. Since ACh plays a key role in cognitive process, impairment of the cholinergic system is considered an important hallmark in dementia including Alzheimer's disease (AD).

AD is a progressive age-related neurological syndrome, marked by a gradual memory loss. Pathological hallmarks of AD include neuronal death, decrease of ACh levels with consequent impairment of the central cholinergic tone and accumulation of plaques in the brain (especially amyloid-beta aggregates).

Inhibitors of AChE (AChEIs) represent the major class of compounds released on the market and approved to treat AD with the aim of increasing ACh levels by reducing AChE hydrolysis rate. Nevertheless, current marketed inhibitors can only temporally reduce cognitive deficits, thus enhancing the quality of life [4]. Recently, the possibility of hitting BuChE instead of/or simultaneously with AChE for the treatment of AD and related dementias has been highlighted. Compounds with risen selectivity for BuChE, e.g. cymserine-like molecules, or dual inhibitors towards both ChEs, e.g. rivastigmine, revealed potential beneficial effects in AD treatment and related dementias. Therefore, efforts in the design of new dual inhibitors towards AChE and BuChE are increasing with the purpose of developing new and more efficient treatment options [3].

Despite the continuous progress in the comprehension of the multiple networks involved in AD, this form of dementia represents one of the major public health concerns [5]. Indeed, the increasing number of patients and the lack of effective treatment for cure challenge medicinal chemists to design new chemical scaffolds. Several hypotheses have been suggested to rationalize clinical failure. Among these, the multifactorial nature of AD along with the various molecular targets involved have been proposed as reasons for clinical withdrawn of drug candidates [6]. This knowledge has laid the foundation of a novel design strategy, the so-called multi-target-directed ligands (MTDLs). This rational strategy aims to synthesize heterogeneous class of compounds which are able to simultaneously target more than a single molecular target in the pursuit of the development of new molecules endowed with better pharmacological effect [7–9]. Advantages in using multipotent drugs with respect to the administration of a combination of drugs are also ascribed to the decrease of drug–drug interactions and the simplification of ADMET studies.

In this scenario, continuous efforts in developing chemical entities are paralleled by the efforts in developing analytical strategies able to better assess drug–target interaction. Concerning the identification of new ChE inhibitor in the early phase of the drug discovery process, in solution assays to assess the half-maximal inhibitory concentration (IC_{50}) and the binding mode (reversible

or pseudo-irreversible; competitive, non-competitive or mixed type) are the most common approaches [10]. In particular, IC_{50} is the classical parameter which is quantified to rank inhibitors during first screening and SAR studies. Recently, the interest in the development of highly-informative screening methodology is rising. In particular the availability of robust methodologies which can provide kinetic information on drug binding events, thus providing additional information which may better predict the *in vivo* duration of action may help the correct prioritization of favorite chemical scaffolds to be further developed, thus reducing the attrition rate in the first phased of the drug discovery process.

6.2 Structure and catalytic function of AChE

The main biological function of AChE is the termination of impulse transmission by the rapid hydrolysis of ACh (into choline and acetate) at cholinergic synapses (Fig. 23). In physiological conditions, its role as serine hydrolase is marked by highly significant activity, getting closer to the limit of diffusion-controlled reaction. Indeed, almost 25000 molecules of ACh neurotransmitter are hydrolyzed per second by each enzyme [11].

AChE secondary structure is formed by 14 α helices which centrally encircle 12 stuck parallel and antiparallel β sheets, thus conferring to the molecule a ellipsoid-like form [12]. Typical feature of AChE structure is a narrow and ~20 Å deep gorge which extends for half the enzyme length and widens near the base. The wall of the gorge is lined by 14 aromatic residues, highly conserved across the species [12].

Early kinetic studies showed that AChE active site is formed by two main subsites, namely esteratic and anionic subsites. The esteratic subsite acts as catalytic machinery and contains three amino acids which forms the so-called catalytic triad: serine at position 200 (Ser200), histidine at position 440 (His440) and glutamate at position 327 (Glu327) of AChE backbone (the amino acid numbering in this section, if not otherwise specified, refers to AChE from *Torpedo californica,* as first form of AChE to have been crystallized) [13]. Corresponding amino acids forming the catalytic triad in human AChE are Ser203, His447 and Glu334 [14].

Substrate hydrolysis starts with the nucleophilic substitution promoted by the serine residue towards the ACh carbonyl group, forming the so-called tetrahedral intermediate which has the oxygen of the carbonyl group of the neurotransmitter negatively charged. This intermediate further undergoes the breakup between acetyl- and choline moieties, thus resulting in the release of choline. Finally, the hydrolysis of the acyl-based intermediate with AChE grants the displacement of acetic acid, thus restoring the resting state of AChE (Fig. 23). The proximity of His440 increases the nucleophilicity of serine residue, thus enhancing the reaction. Instead, Glu327 grants the stabilization of the

transition through hydrogen bond. Similarly, His440 favors the nucleophilic attack by water molecule due to its acid-base catalyst function (Fig. 23) [15,16].

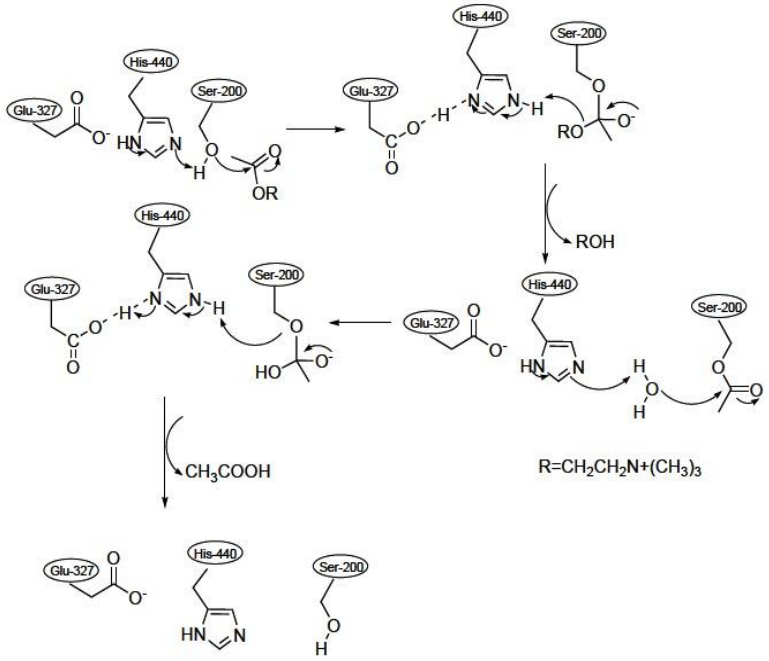

Figure 23 | Mechanism of ACh degradation promoted by the so-called catalytic triad. Reprinted with permission from [4].

The anionic subsite, also known as choline-binding pocket, is an uncharged lipophilic portion able to interact with choline via the charged quaternary nitrogen moiety. Among amino acidic residues which constitute this site, tryptophan at position 84 (Trp84) plays a key role in the choline binding. Experimental evidence has also proved that its replacement with an alanine residue decreases the activity rate of more than three thousand times [17–19]. Moreover, the permanent dipole displayed by AChE is aligned with the active-site gorge, suggesting that the electrostatic field facilitates the substrate guidance down the aromatic gorge to the active site [20]. This mechanism may also explain the fast interaction between AChE and cationic molecules.

In addition to the catalytic center, AChE holds an additional binding site, the so-called peripheral anionic site (PAS) [21]. PAS is involved in the binding with ACh as well as with other ligands which can modulate AChE activity in an allosteric way. Binding of the natural substrate (at high concentration) to PAS also determine AChE activity inhibition [22,23].

ACh substrate is larger than the narrowest part of gorge. For this reason, fluctuations of gorge wall are required to allow substrate guidance down this portion and subsequent interaction with the active site. Since the early 1990s, molecular dynamics simulations and X-ray crystallography studies indicated the presence of the so-called backdoor, a channel located at the thin part of the

gorge, adjacent to the active site, probably involved in the transit of substrate, solvent and products by its constant fluctuation between opening and shutting state. This evidence may explain the high turnover of AChE [24–26].

Despite AChE is encoded from a single gene, it exists in several polymorphism of quaternary structures as consequence of different mRNA splicing and diverse subunits combination. Catalytic subunits, which can also differ in glycosylation extent, can oligomerize thus forming dimmer- or tetramer-based globular structures, namely G1, G2 and G4. These structures can be further divided depending on their amphiphilicity [27,28]. In the brain of healthy subjects, the G4 quaternary structure is the most abundant. However, in elderly people and especially AD patients, G4 form progressively decreases while G1 form seems to have growing importance both in ACh hydrolysis at cholinergic neurons and disease progression [29].

6.3 Alzheimer's disease

Alzheimer's disease (AD) is the most frequent form of neurodegenerative disorder. This incurable age-related dementia is usually diagnosed in people over 65 years of age even if, in case of early-onset AD, it arises much earlier [30]. Due to aging increase in the world population, AD is becoming significantly much more common. It is estimated that in 2050 AD will affect 1 in every 85 people [5].

Since its discovery, three main hallmarks have been underlined: (i) the neurodegeneration of the central nervous system which particularly affects the cholinergic tone, (ii) the extracellular deposits of protein aggregates of human beta-amyloid (Aβ) peptides, i.e. senile plaques, (iii) the intracellular formation of protein deposits, i.e. neurofibrillary tangles. Over the years, different theories have been postulated, e.g. the amyloid cascade hypothesis, the cholinergic hypothesis and the hyperphosphorylation hypothesis [31–34]. Recently, the understanding that not only a single theory but combinations of multifactorial events contribute in disease etiology is widely accepted. Indeed, many factors are thought to play a role in the pathogenesis of the disease including inflammation, overproduction of free radicals induced by oxidative stress, mitochondrial failure, metal dyshomeostasis, cholesterol-based lipid rafts [35]. The consciousness that further potential targets are engaged in the progression of AD shows that polypharmacological treatment is likely a more promising strategy to be pursued for drug research. Nowadays, only palliative drugs aimed at alleviating AD symptoms and countering memory loss have been released on the market. Nevertheless, drug development for AD therapies is steadily increasing and several potential compounds are in different stages of clinical trials, namely phases I, II, III (Fig. 24) [5].

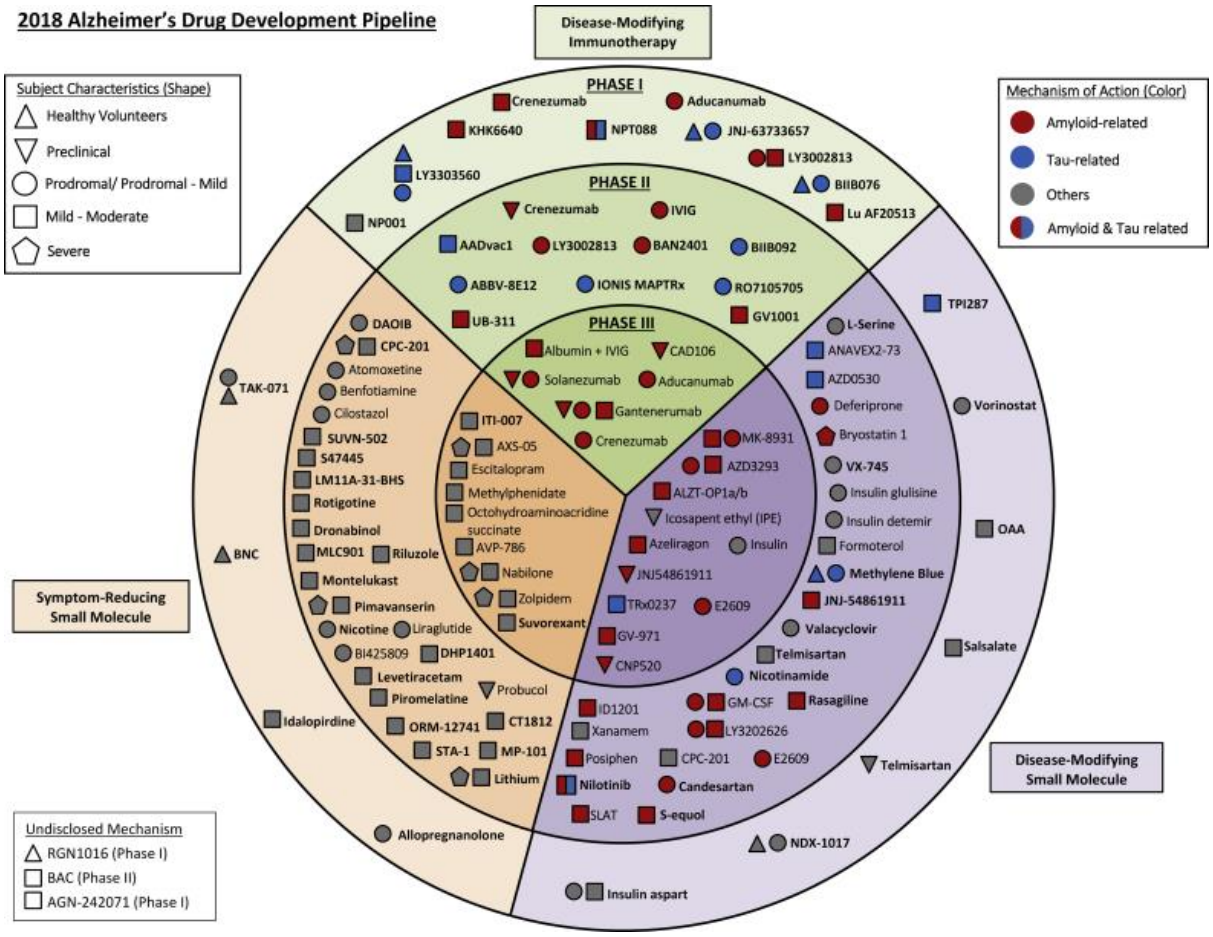

Figure 24 | Chemical compounds in clinical trials for AD therapy in 2018. Currently 112 agents are under investigation in clinical trials: 26 agents in phase III, 65 agents in phase II, 23 agents in phase I. Reprinted with permission from [5].

6.3.1 AD treatment: targeting AChE

In terms of clinical therapy, the rational design which has so far generated the majority of drugs released on the market is based on the cholinergic hypothesis, postulated over 20 years ago [32]. The hypothesis is based on the evidence that AD patients, compared with healthy elderly subjects, have a significant decrease of the enzyme responsible for ACh synthesis, namely choline acetyltransferase (ChAT) and of the corresponding neurotransmitter. Indeed, these reductions have been observed in AD brain, especially in the cholinergic forebrain area and their projections to the cerebral cortex, as a result of a significant loss of cholinergic neurons [36]. Coupled with the latter, a decrease of AChE levels, in particular the G4 form, occurs and it is partially due to the overall loss of cholinergic activity. The formation of plaques and tangles as well as the progression of the disease correlate with these losses [37]. Moreover, it has been reported that AChE may act as molecular chaperone promoting the aggregation of beta-amyloid (Aβ) peptides. In particular, the recognition site for Aβ seems to be PAS [38,39]. Although the cholinergic impairment only partially accounts for some clinical aspects of the pathology, cholinergic hypothesis has promoted

the research and the development of drugs targeting the cholinergic system. In this scenario, compounds which target muscarinic or nicotinic receptors as well as compounds which indirectly increase ACh levels in the synaptic cleft by inhibiting the activity of AChE have been widely studied and are still under investigation [1].

Inhibitors of AChE (AChEIs) were the first class of drugs successfully released on the market for treating AD symptoms (Fig. 25). Currently, four AChEIs have been approved by the U.S. Food and Drug Administration (FDA) for pharmacologic therapy, namely tacrine, donepezil, rivastigmine and galantamine [4]. All these inhibitors are involved in the centrally inhibition of AChE, thus increasing ACh availability in the brain. From a symptomatic point of view, they can temporally improve memory and cognitive performance in subjects with mild to moderate AD, enhancing their quality of life. Despite they belong to the same drug class, i.e. inhibitors of AChE, they differ in many aspects, from adverse effects to inhibition modes (reversible or pseudo-irreversible; competitive, non-competitive or mixed type). A different pharmacological response induced by these inhibitors is usually observed across AD patients, thus requiring case-by-case custom dosing and treatment.

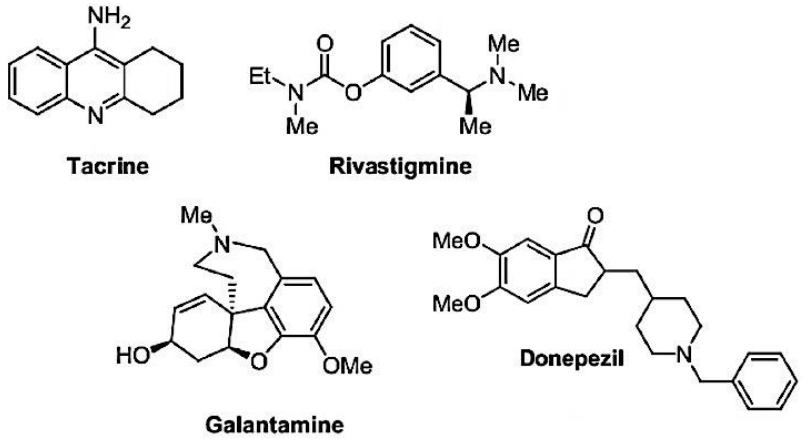

Figure 25| Chemical structures of AChE inhibitors approved for AD treatment**.**

Tacrine (Fig. 25) is a reversible inhibitor towards both AChE and BuChE. Tacrine hydrochloride (Cognex®, Park-Davis) was the first drug approved (in 1993) for treating AD. Nowadays, its administration has been abandoned due to hepatotoxicity (~50 % of patients) and gastrointestinal side effects [40]. Nevertheless, tacrine has been employed as reference compound in the development of further AChEIs and many tacrine analogues are involved in preclinical and clinical trials [41]. In recent years, tacrine-based structures are also used in the rational design of hybrids based of MTDLs strategy [42–44]. An example is also reported in chapter 9.

Donepezil hydrochloride (Aricept®, Eisai-Pfizer) was the second marketed drug for treating AD. Donepezil (Fig. 25) is a reversible inhibitor highly selective for AChE beyond BuChE: indeed, the affinity to the former target is almost one thousand greater. This inhibitor binds both the catalytic and the peripheral anionic site exerting a mixed type inhibition towards AChE. Moreover, it seems involved in the delaying of amyloid plaques accumulation [45,46]. Although donepezil is usually prescribed to patients with mild/moderate AD, clinical evidence has shown that it can ameliorate cognition also in patients affected by severe AD [47]. Donepezil has long duration of action and a long half-life time (~70 h), thus allowing once-daily dose. Side effects are much less severe compared to tacrine and include nausea, diarrhea, abdominal pain and bradycardia [4]. Currently, the drug is on the market as oral tablets (5 or 10 mg) and transdermal patches [48]. For a long time, donepezil has been the most administered drug for AD treatment. Nowadays, the treatment with other FDA-approved drugs is growing. Moreover, donepezil-based hybrids have been recently developed according to the MTDLs approach [49,50]. An example is also presented in chapter 8.

Rivastigmine (Exelon®, Novartis) is a pseudo-irreversible inhibitor, acting at the central nervous system, that displays activity towards both AChE and BuChE (Fig. 25). In particular, the inhibition of central BuChE is thought to contribute the efficacy of AD treatment [51]. Interestingly, it exhibits selectivity for the G1 form versus G4 of both ChE. Rivastigmine belongs to carbamate-based AChEI class of inhibitors. The inhibition mode consists of the carbamoylation of Ser200 within the catalytic triad [4] leading to the formation of a carbamoylated adduct. Although covalent, inhibition by rivastigmine is reversible, owning a short half-life time (~1.5 h) [52]. Its efficiency is comparable with that of donepezil even if it results less tolerated when administered at high doses [51]. Adverse reactions are typically those common for all cholinergic drugs such as diarrhea, nausea, anorexia. Rivastigmine is marketed in oral formulations or transdermal patches [53]. The administration regimen requires a gradual dosing increase: usually from 1.5 mg twice a day to 6.0 mg twice a day in case of severe AD. A remarkable feature is its different metabolism, which is not relied on hepatic isoenzymes, but granted by cholinesterase hydrolysis. As consequence, in case of liver or kidney failure, no adjustment of the dosing is required. Furthermore, rivastigmine constitutes one of the pharmacologic approaches for Parkinson's disease and Lewy bodies [51].

Galantamine (Reminyl®, Janssen) is a natural compound isolated from *Galanthus woronowii* plant (Fig. 25). It is a tertiary alkaloid able to interact with both the anionic subsite and the aromatic residues along the gorge, resulting in a reversible competition, selective for AChE [54]. Galantamine is proposed for treating mild to moderate AD. Besides, this inhibitor acts as allosteric modulator for nicotinic receptors of cholinergic neurons. Indeed, it binds a different site compared to those of ACh and nicotinic agonists, enhancing the activity of nicotinic receptors when ACh is

bound. This dual mechanism grants additional benefits for AD treatment since a loss of nicotinic receptors also occurs in severe AD [55]. Galantamine shows about ~8h of half-life time in plasma and high bioavailability. It is administered twice/day and the treatment usually starts from 4 mg up to 12 mg. The positive symptomatic effects in terms of cognition, memory and behavior seem to be retained for 3-6 months. Instead, adverse effects include gastrointestinal symptoms [55].

Besides these ChE inhibitors, it is worth mentioning that also a non-competitive antagonist for N-methyl-D-aspartate receptor (NMDA), namely memantine, was approved by FDA for treating moderate to severe AD [56].

Despite it is not related to the aim of the present dissertation, it is worth mentioning that other design strategies based on cholinergic hypothesis have been explored to overcome clinical failure. In particular agonists for M_1 muscarinic and nicotinic receptors, located on membranes of post-synaptic neurons, along with antagonists for M_2 receptors, located on membranes of pre-synaptic neurons have been widely investigated. The rationale relies on the importance of finding other strategies to enhance cholinergic tone, by prolonging receptors activation in the former case or, in the latter, by increasing synaptic levels of ACh [57,58]. Indeed, AChE inhibition grants the prolonging of ACh life-time, only for a short period [1]. Furthermore, attempts to promote ACh synthesis have been achieved by dosing ACh precursors, e.g. choline [59]. Despite many limits have been reported so far for all these compounds, such as low bioavailability, limited efficacy and several side effects, the pursuit of non-inhibitor AChE molecules constitutes an important area of investigation.

6.3.2 AD treatment: the role of BuChE

Butyrylcholinesterase (BuChE) is the sister enzyme of AChE, with whom shares 65% of homology. It is a non-specific cholinesterase able to hydrolyze different choline esters besides ACh. Moreover, compared to AChE it has different topology in terms of kinetic, location and activity. It ubiquitously exists throughout the human body even if it is predominantly situated in human liver, pancreas, blood and central nervous system. In the brain it is mainly detected in glial and endothelial cells [3,60]. It is able to catalyze butyrylcholine faster compared to ACh substrate, hence the name. Currently, BuChE role still remains unclear since butyrylcholine is not a physiological constituent of the brain and since subjects which have a silent form of this enzyme show analogues functions compared to healthy people.

In healthy people the 90% of ACh hydrolysis depends on the activity of AChE, mainly located in neurons. BuChE has a lower concentration than AChE also displaying a more restricted distribution in the central nervous system. Nevertheless, it has been shown that the 10-15% from all cholinergic

neurons in amygdala and hippocampus contain BuChE instead of AChE as synaptic enzyme involved in ACh metabolism. BuChE has proved to compensate AChE functions in case of AChE failures. In particular, it shows a remarkable activity at high substrate concentrations, interesting fact since these two ChEs have different kinetic responses as function of ACh concentrations. Indeed, AChE decreases its efficiency in case of neurotransmitter excess, while BuChE becomes highly efficient, thus supporting AChE activity. Similar to its ‘‘sister’’, BuChE exists in different isoforms and, among them, the G4 form is the most abundant in the brain of healthy people whereas the G1 form becomes more important in AD [61].

Owing to its low expression in the central nervous system, the importance of central BuChE has not been considered at first. However, different studies confirmed its remarkable role in the brain, in particular regarding the co-regulation of ACh levels in AD. Indeed, if the abundance ratio of BuChE to AChE is almost 0.3 in normal conditions, in the case of AD this value increases to 11 in cortical areas [60]. With AD progression, AChE activity is reduced of almost 55%–65%. In these conditions, ACh hydrolysis is almost exclusively carried out by BuChE which becomes of functional importance. The alteration in AChE/BuChE ratio affects ACh metabolism, thus contributing to cholinergic failure [60]. The association of BuChE to AD has been investigated in several ethnic groups. Outcomes of these studies have underlined how this enzyme may promote the risk of late-AD onset, both alone or in synergic association with a variant form (i.e. K variant), in particular in humans who carry the apolipoprotein E4 allele (ApoE4) [62,63]. Moreover, BuChE co-localizes with amyloid plaques, dystrophic neurons and neurofibrillary tangles, which constitute the main hallmarks of AD. Moreover, studies carried out comparing the brains (temporal cortex) of demented and normal subjects demonstrated that Aβ peptides found in patients had a BuChE-based reactivity 6 times higher compared to non-demented individuals [64]. However, controversial *in vitro* and *in vivo* studies have been reported regarding BuChE role in promoting or inhibiting amyloid fibril formations [65].

Due to BuChE central activity in the hydrolysis of ACh as well as its involvement in the disorder progression, this enzyme has been proposed as a viable therapeutic target for treating AD. In particular, according to cholinergic hypothesis, inhibitors of BuChE should prolong ACh activity at synaptic clefs, thus ameliorating AD-related symptoms, with particular beneficial effect in patients with moderate-to-severe forms of AD-type dementia [66]. Among drugs approved by FDA for AD treatment, already discussed in the previous paragraph, rivastigmine acts as dual inhibitor for both ChEs. Moreover, its inhibition role towards BuChE seems to have an additional role in protecting the formation of Aβ plaques [51]. As consequence, the clinical therapy with rivastigmine provides long-term symptomatic effects in the treatment of subjects with AD-related dementia.

In this scenario, various selective BuChE inhibitors have been recently developed as potential candidates for AD treatment [65]. Nevertheless, the interest in designing selective inhibitors for BuChE seem a viable and promising strategy.

6.3.3 AD treatment: multi-target-directed ligands (MTDLs)

Over the years, the accumulating insights into the pathogenesis and the progression of AD have highlighted the multifactorial nature of this disorder, promoted by several elements such as genetic, environmental and endogenous factors. The multiple etiologies include protein misfolding and aggregation, formation of free radicals induced by oxidative stress, neuroinflammatory processes, mitochondrial anomalies, cholesterol-based lipid rafts, calcium dyshomeostasis [35]. The complexity of the picture has been proposed as one of the possible reasons why the currently available drugs have turned out to be palliative instead of healing. In this scenario, alongside drug development focuses on agents able to specifically counteract amyloid and tau aggregation, a rational approach based on the ‘‘one molecule multiple targets’’ concept has increasingly attracted the attention of medicinal chemists. The rational design to obtaining ligands towards multiple targets, is usually based on the synthesis of new compounds by combining distinct known pharmacophores selective for different targets. This approach, which should lead to the identification of the so-called multi-target-directed ligands (MTDLs), can be considered closely related to the known multiple-medication therapy (MMT), well-accepted in clinical [67]. Indeed, the use of MMT to treat AD, i.e. memantine (NMDA antagonist) in combination with AChEI, has already shown additional benefits with respect to the use of single drugs, ameliorating tolerance and effectiveness of the treatment [68]. MTDLs strategy may thus provide advantages over the MMT approach. Indeed, the administration of a single drug, which possesses multiple biological properties, may limit drug–drug interaction, facilitate ADMET studies and simplify therapeutic regimen.

In this scenario, MTDLs have emerged as an intriguing drug discovery avenue to treat AD and several MTDLs have been recently developed [69]. So far, the most common strategy has been based on the synthesis of compounds endowed with inhibitory potency towards ChE in combination with different activities towards one of the multiple targets involved in AD etiology.

In the MTDLs rational design context, the first strategy has been focused on the synthesis of the so-called dual binding sites AChEIs, aimed at simultaneously interacting with AChE catalytic and the peripheral site [69]. These AChEIs might mitigate cognitive impairment by restoring cholinergic activity and, most importantly, might reduce Aβ aggregation, important mechanism involved in AD, through the interaction with PAS. In this class of compounds, AP2238 was the first developed

dual inhibitor towards AChE which successfully displayed inhibitory potency along with the capacity of countering Aβ protein misfolding and aggregation [70]. Since then, a variety of dual inhibitors has been synthesized [69]. Nevertheless, it is worth to remark that compound capacity to bind both CAS and PAS is a not sufficient condition to call them MTDLs. Dual site inhibitors, however, can be considered MTDLs if their peripheral binding allows slowing and countering Aβ assembly.

Thenceforth, hybrids able to simultaneously interact with different targets involved in AD etiology have been developed. Among these, active molecules towards other neurotransmitter systems, besides the cholinergic one, have been considered. Indeed, the neuropsychiatric abnormalities observed in AD patients are not related only to the huge loss of cholinergic neurons but also to impairment in the serotoninergic, noradrenergic and glutamatergic systems. For instance, AD-related serotoninergic failures steam from raphe atrophy and lead to depression and psychosis. AD-related noradrenergic failures is related to *locus ceruleus* atrophy and lead to depression [71,72]. In this context, rational design strategies aiming at combining inhibitors of AChE with: (i) inhibitors of monoamine oxidase (MAO), namely dual AChE/MAO inhibitors, (ii) inhibitors of serotonin transporter (SERT), i.e. AChE/SERT, (iii) agonists or antagonists exerting a modulation on the serotoninergic or histaminergic pathways, have been widely investigated [73].

Another widely investigated class of MTDLs is constituted by multifunctional compounds endowed with anti-AChE activity and antioxidant properties. Indeed, molecules able to contrast oxidative damage and, in the meantime, enhance cholinergic tone have emerged as promising multipotent compounds [74]. An example of donepezil-lipoic acid hybrids is presented in chapter 8.

One of the major class of MTDLs designed for AD treatment is represented by AChEIs endowed with the capacity of regulating calcium homeostasis. Indeed, since the connection between calcium dyshomeostasis and AD etiology is well-supported [75], different AChE inhibitors also possessing a moderate ability to block calcium channels have been developed [73]. An example of hybrids synthetized with this dual goal is presented in chapter 9.

However, the mentioned class of multifunctional compounds only account for a small part of all MTDLs strategies investigated over recent years. Indeed, it is worth to mention that several other MTDLs designed to hit different targets such as amyloid peptide production and aggregation, tau hyperphosphorylation and aggregation, metal dyshomeostasis, neuroinflammation and mitochondrial disfunction have been developed. Further details can be retrieved in some recent reviews [69,73,76,77].

Regardless of the rationale which promotes design strategies, synthesis of new lead compounds requires, in parallel, the development of analytical methods to assess drug–target interaction. To

rank AChE/BuChE inhibitors, definition of the inhibitory potency by classic in solution assay (Ellman's assay) [78] is the mostly used approach. Recently, accessing kinetic information on drug binding events at initial stages of the drug discovery process is gaining increasing interest among pharmaceutical chemists. The possibility of counting on additional information which may better predict the *in vivo* duration of action (e.g. kinetic constants and residence time), indeed, facilitates the prioritization process and the selection of favorite chemical scaffolds.

With this regard, following chapters include different studies carried out during my PhD program and based on the characterization of different AChE/BuChE inhibitors. In particular, classical in solution assay and a developed SPR-based assay, which proved to be a suitable approach for nicely complement classic inhibition studies, have been employed.

References

[1] T. H. Ferreira-Vieira, I. M. Guimaraes, F. R. Silva, F. M. Ribeiro, Alzheimer's disease: targeting the cholinergic system, Curr. Neuropharmacol. 14 (2016) 101–115.

[2] C.W. Goh, C.C. Aw, J.H. Lee, C.P. Chen, E.R. Browne, Pharmacokinetic and pharmacodynamic properties of cholinesterase inhibitors donepezil, tacrine, and galantamine in aged and young lister hooded rats, Drug Metab. Dispos. 39 (2011) 402–411.

[3] N.H. Greig, D.K. Lahiri, K. Sambamurti, Butyrylcholinesterase: an important new target in Alzheimer's disease therapy, Int. Psychogeriatr. 14 (2002) 77–91.

[4] M.B. Colovic, D.Z. Krstic, T.D. Lazarevic-Pasti, A.M. Bondzic, V.M. Vasic, Acetylcholinesterase inhibitors: pharmacology and toxicology, Curr. Neuropharmacol. 11 (2013) 315–335.

[5] J. Cummings, G. Lee, A. Ritter, K. Zhong, Alzheimer's disease drug development pipeline: 2018, Alzheimer's Dement. Transl. Res. Clin. Interv. 4 (2018) 195–214.

[6] J. Cummings, G. Lee, T. Mortsdorf, A. Ritter, K. Zhong, Alzheimer's disease drug development pipeline: 2017, Alzheimer's Dement. Transl. Res. Clin. Interv. 3 (2017) 367–384.

[7] C. Rochais, C. Lecoutey, F. Gaven, P. Giannoni, K. Hamidouche, D. Hedou, E. Dubost, D. Genest, S. Yahiaoui, T. Freret, V. Bouet, F. Dauphin, J. Sopkova de Oliveira Santos, C. Ballandonne, S. Corvaisier, A. Malzert-Fréon, R. Legay, M. Boulouard, S. Claeysen, P. Dallemagne, Novel multitarget-directed Llgands (MTDLs) with acetylcholinesterase (AChE) inhibitory and serotonergic subtype 4 receptor (5-HT 4 R) agonist activities as potential agents against Alzheimer's disease: the design of donecopride, J. Med. Chem. 58 (2015) 3172–3187.

[8] X. Lu, S. He, Q. Li, H. Yang, X. Jiang, H. Lin, Y. Chen, W. Qu, F. Feng, Y. Bian, Y. Zhou, H. Sun, Investigation of multi-target-directed ligands (MTDLs) with butyrylcholinesterase (BuChE) and indoleamine 2,3-dioxygenase 1 (IDO1) inhibition: the design, synthesis of miconazole analogues targeting Alzheimer's disease, Bioorg. Med. Chem. 26 (2018) 1665–1674.

[9] A. Agis-Torres, M. Sölhuber, M. Fernandez, J.M. Sanchez-Montero, Multi-target-directed ligands and other therapeutic strategies in the search of a real solution for Alzheimer's disease, Curr. Neuropharmacol. 12 (2014) 2–36.

[10] M. Bartolini, V. Cavrini, V. Andrisano, Characterization of reversible and pseudo-irreversible acetylcholinesterase inhibitors by means of an immobilized enzyme reactor, J. Chromatogr. A. 1144 (2007) 102–110.

[11] D.M. Quinn, Acetylcholinesterase: enzyme structure, reaction dynamics, and virtual transition states, Chem. Rev. 87 (1987) 955–979.

[12] P. Manavalan, P. Taylor, W. Curtis Johnson, Circular dichroism studies of acetylcholinesterase conformation. Comparison of the 11 S and 5.6 S species and the differences induced by inhibitory ligands, Biochim. Biophys. Acta Protein Struct. Mol. Enzymol. 829 (1985) 365–370.

[13] J.L. Sussman, M. Harel, F. Frolow, C. Oefner, A. Goldman, L. Toker, I. Silman, J. Sussman, Atomic structure of acetylcholinesterase from Torpedo californica: a prototypic acetylcholine-binding protein, Science. 253 (1991) 872–9.

[14] J. Wiesner, Z. Kříz, K. Kuca, D. Jun, J. Koca, Acetylcholinesterases - The structural similarities and differences, J. Enzyme Inhib. Med. Chem. 22 (2007) 417–424.

[15] Y. Zhang, J. Kua, J.A. McCammon, Role of the catalytic triad and oxyanion hole in acetylcholinesterase catalysis: an ab initio QM/MM study, J. Am. Chem. Soc. 124 (2002) 10572–7.

[16] C. Bartolucci, E. Perola, L. Cellai, M. Brufani, D. Lamba, Back doors opening implied by the crystal structure of a carbamoylated acetylcholinesterase, Biochemistry. 38 (1999) 5714–9.

[17] V. Tougu, Acetylcholinesterase: mechanism of catalysis and inhibition, Curr. Med. Chem. Nerv. Syst. Agents. 1 (2001) 155–170.

[18] A. Ordentlich, D. Barak, C. Kronman, N. Ariel, Y. Segall, B. Velan, A. Shafferman, Contribution of aromatic moieties of tyrosine 133 and of the anionic subsite tryptophan 86 to catalytic efficiency and allosteric modulation of acetylcholinesterase, J. Biol. Chem. 270 (1995) 2082–91.

[19] N. Ariel, A. Ordentlich, D. Barak, T. Bino, B. Velan, A. Shafferman, The "aromatic patch" of three proximal residues in the human acetylcholinesterase active centre allows for versatile interaction modes with inhibitors,

Biochem. J. 335 (1998) 95–102.

[20] D.R. Ripoll, C.H. Faerman, P.H. Axelsen, I. Silman, J.L. Sussman, An electrostatic mechanism for substrate guidance down the aromatic gorge of acetylcholinesterase, Proc. Natl. Acad. Sci. U. S. A. 90 (1993) 5128–32.

[21] P. Taylor, S. Lappi, Interaction of fluorescence probes with acetylcholinesterase. Site and specificity of propidium binding, Biochemistry. 14 (1975) 1989–1997.

[22] E. Reiner, N. Aldridge, V. Simeon, Z. Radic, P. Taylor, Cholinesterases : structure, function, mechanism, genetics, and cell biology, in: Cholinesterases Struct. Funct. Mech. Genet. Cell Biol., American Chemical Society, 1991: pp. 227–228.

[23] H. Dvir, I. Silman, M. Harel, T.L. Rosenberry, J.L. Sussman, Acetylcholinesterase: from 3D structure to function, Chem. Biol. Interact. 187 (2010) 10–22.

[24] L. Alisaraie, G. Fels, Molecular docking study on the "back door" hypothesis for product clearance in acetylcholinesterase, J. Mol. Model. 12 (2006) 348–354.

[25] B. Sanson, J.-P. Colletier, Y. Xu, P.T. Lang, H. Jiang, I. Silman, J.L. Sussman, M. Weik, Backdoor opening mechanism in acetylcholinesterase based on X-ray crystallography and molecular dynamics simulations, Protein Sci. 20 (2011) 1114–8.

[26] C. Kronman, A. Ordentlich, D. Barak, B. Velan, A. Shafferman, The "back door" hypothesis for product clearance in acetylcholinesterase challenged by site-directed mutagenesis, J. Biol. Chem. 269 (1994) 27819–27822.

[27] P. Taylor, Z. Radic, The cholinesterases: from genes to proteins, Annu. Rev. Pharmacol. Toxicol. 34 (1994) 281–320.

[28] J. Massoulié, L. Pezzementi, S. Bon, E. Krejci, F.M. Vallette, Molecular and cellular biology of cholinesterases, Prog. Neurobiol. 41 (1993) 31–91.

[29] T. Arendt, M.K. Brückner, M. Lange, V. Bigl, Changes in acetylcholinesterase and butyrylcholinesterase in Alzheimer's disease resemble embryonic development-a study of molecular forms, Neurochem. Int. 21 (1992) 381–96.

[30] R. Brookmeyer, S. Gray, C. Kawas, Projections of Alzheimer's disease in the United States and the public health impact of delaying disease onset, Am. J. Public Health. 88 (1998) 1337–42.

[31] E. Karran, M. Mercken, B. De Strooper, The amyloid cascade hypothesis for Alzheimer's disease: an appraisal for the development of therapeutics, Nat. Rev. Drug Discov. 10 (2011) 698–712.

[32] A. Contestabile, The history of the cholinergic hypothesis, Behav. Brain Res. 221 (2011) 334–340.

[33] G. Šimić, M. Babić Leko, S. Wray, C. Harrington, I. Delalle, N. Jovanov-Milošević, D. Bažadona, L. Buée, R. de Silva, G. Di Giovanni, C. Wischik, P.R. Hof, Tau protein hyperphosphorylation and aggregation in Alzheimer's disease and other tauopathies, and possible neuroprotective strategies, Biomolecules. 6 (2016) 6.

[34] E. Mohandas, V. Rajmohan, B. Raghunath, Neurobiology of Alzheimer's disease, Indian J. Psychiatry. 51 (2009) 55–61.

[35] A. Cavalli, M.L. Bolognesi, A. Mìnarini, M. Rosini, V. Tumiatti, M. Recanatini, C. Melchiorre, Multi-target-directed ligands to combat neurodegenerative diseases, J. Med. Chem. 51 (2008) 347–372.

[36] R.T. Bartus, R.L. Dean, B. Beer, A.S. Lippa, The cholinergic hypothesis of geriatric memory dysfunction, Science. 217 (1982) 408–14.

[37] J.R. Atack, E.K. Perry, J.R. Bonham, J.M. Candy, R.H. Perry, Molecular forms of acetylcholinesterase and butyrylcholinesterase in the aged human central nervous system, J. Neurochem. 47 (1986) 263–77.

[38] N.C. Inestrosa, A. Alvarez, C.A. Pérez, R.D. Moreno, M. Vicente, C. Linker, O.I. Casanueva, C. Soto, J. Garrido, Acetylcholinesterase accelerates assembly of amyloid-beta-peptides into Alzheimer's fibrils: possible role of the peripheral site of the enzyme, Neuron. 16 (1996) 881–91.

[39] E. Viayna, I. Sola, M. Bartolini, A. De Simone, C. Tapia-Rojas, F.G. Serrano, R. Sabaté, J. Juárez-Jiménez, B. Pérez, F.J. Luque, V. Andrisano, M.V. Clos, N.C. Inestrosa, D. Muñoz-Torrero, Synthesis and multitarget biological profiling of a novel family of rhein derivatives as disease-modifying anti-alzheimer agents, J. Med. Chem. 57 (2014) 2549–2567.

[40] P.B. Watkins, H.J. Zimmerman, M.J. Knapp, S.I. Gracon, K.W. Lewis, Hepatotoxic effects of tacrine administration in patients with Alzheimer's disease, JAMA. 271 (1994) 992–8.

[41] N. Guzior, A. Wieckowska, D. Panek, B. Malawska, Recent development of multifunctional agents as potential drug candidates for the treatment of Alzheimer's disease, Curr. Med. Chem. 22 (2015) 373–404.

[42] X. Li, H. Wang, Y. Xu, W. Liu, Q. Gong, W. Wang, X. Qiu, J. Zhu, F. Mao, H. Zhang, J. Li, Novel Vilazodone–tacrine hybrids as potential multitarget-directed ligands for the treatment of Alzheimer's disease accompanied with depression: design, synthesis, and biological evaluation, ACS Chem. Neurosci. 8 (2017) 2708–2721.

[43] K. Spilovska, J. Korabecny, E. Nepovimova, R. Dolezal, E. Mezeiova, O. Soukup, K. Kuca, Multitarget tacrine hybrids with neuroprotective properties to confront Alzheimer's disease, Curr. Top. Med. Chem. 17 (2017) 1006–1026.

[44] C. Quintanova, R.S. Keri, S.M. Marques, M. G-Fernandes, S.M. Cardoso, M. Luísa Serralheiro, M. Amélia Santos, Design, synthesis and bioevaluation of tacrine hybrids with cinnamate and cinnamylidene acetate derivatives as potential anti-Alzheimer drugs, Medchemcomm. 6 (2015) 1969–1977.

[45] A. Castro, A. Martinez, Targeting beta-amyloid pathogenesis through acetylcholinesterase inhibitors, Curr. Pharm. Des. 12 (2006) 4377–87.

[46] M.P. Arce, M.I. Rodríguez-Franco, G.C. González-Muñoz, C. Pérez, B. López, M. Villarroya, M.G. López, A.G. García, S. Conde, Neuroprotective and cholinergic properties of multifunctional glutamic acid derivatives for the treatment of Alzheimer's disease, J. Med. Chem. 52 (2009) 7249–7257.

[47] B. Winblad, Review: donepezil in severe Alzheimer's disease, Am. J. Alzheimer's Dis. Other Dementiasr. 24 (2009) 185–192.

[48] P. Sozio, L.S. Cerasa, L. Marinelli, A. Di Stefano, Transdermal donepezil on the treatment of Alzheimer's disease, Neuropsychiatr. Dis. Treat. 8 (2012) 361–8.

[49] L. Piemontese, D. Tomás, A. Hiremathad, V. Capriati, E. Candeias, S.M. Cardoso, S. Chaves, M.A. Santos, Donepezil structure-based hybrids as potential multifunctional anti-Alzheimer's drug candidates, J. Enzyme Inhib. Med. Chem. 33 (2018) 1212–1224.

[50] E. Mezeiova, K. Spilovska, E. Nepovimova, L. Gorecki, O. Soukup, R. Dolezal, D. Malinak, J. Janockova, D. Jun, K. Kuca, J. Korabecny, Profiling donepezil template into multipotent hybrids with antioxidant properties, J. Enzyme Inhib. Med. Chem. 33 (2018) 583–606.

[51] M.L. Onor, M. Trevisiol, E. Aguglia, Rivastigmine in the treatment of Alzheimer's disease: an update, Clin. Interv. Aging. 2 (2007) 17–32.

[52] M. Bond, G. Rogers, J. Peters, R. Anderson, M. Hoyle, A. Miners, T. Moxham, S. Davis, P. Thokala, A. Wailoo, M. Jeffreys, C. Hyde, The effectiveness and cost-effectiveness of donepezil, galantamine, rivastigmine and memantine for the treatment of Alzheimer's disease (review of Technology Appraisal No. 111): a systematic review and economic model, Health Technol. Assess. (Rockv). 16 (2012).

[53] R. Khoury, J. Rajamanickam, G.T. Grossberg, An update on the safety of current therapies for Alzheimer's disease: focus on rivastigmine, Ther. Adv. Drug Saf. 9 (2018) 171–178.

[54] C. Pilger, C. Bartolucci, D. Lamba, A. Tropsha, G. Fels, Accurate prediction of the bound conformation of galanthamine in the active site of Torpedo californica acetylcholinesterase using molecular docking, J. Mol. Graph. Model. 19 (2001) 288–96, 374–8.

[55] M. Pohanka, Cholinesterases, a target of pharmacology and toxicology, Biomed. Pap. 155 (2011) 219–223.

[56] R.J. van Marum, Update on the use of memantine in Alzheimer's disease, Neuropsychiatr. Dis. Treat. 5 (2009) 237–47.

[57] W. Greenlee, J. Clader, T. Asberom, S. McCombie, J. Ford, H. Guzik, J. Kozlowski, S. Li, C. Liu, D. Lowe, S. Vice, H. Zhao, G. Zhou, W. Billard, H. Binch, R. Crosby, R. Duffy, J. Lachowicz, V. Coffin, R. Watkins, V. Ruperto, C. Strader, L. Taylor, K. Cox, Muscarinic agonists and antagonists in the treatment of Alzheimer's disease, Farmaco. 56 (2001) 247–50.

[58] A. Fisher, Cholinergic treatments with emphasis on M1 muscarinic agonists as potential disease-modifying agents for Alzheimer's disease, Neurotherapeutics. 5 (2008) 433–42.

[59] A. Lleo, Current therapeutic options for Alzheimers disease, Curr. Genomics. 8 (2007) 550–558.

[60] N.H. Greig, T. Utsuki, Q. Yu, X. Zhu, H.W. Holloway, T. Perry, B. Lee, D.K. Ingram, D.K. Lahiri, A new therapeutic target in Alzheimer's disease treatment: attention to butyrylcholinesterase, Curr. Med. Res. Opin. 17 (2001) 159–165.

[61] S. Darvesh, Butyrylcholinesterase as a diagnostic and therapeutic target for Alzheimer's disease, Curr. Alzheimer Res. 13 (2016) 1173–1177.

[62] D.J. Lehmann, C. Johnston, A.D. Smith, Status of acetylcholinesterase and butyrylcholinesterase in Alzheimer's disease and type 2 diabetes mellitus, Hum. Mol. Genet. 6 (1997) 1933–6.

[63] A.V. Raygani, M. Zahrai, A. Soltanzadeh, M. Doosti, E. Javadi, T. Pourmotabbed, Analysis of association between butyrylcholinesterase K variant and apolipoprotein E genotypes in Alzheimer's disease, Neurosci. Lett. 371 (2004) 142–146.

[64] G. Mushtaq, N.H. Greig, J.A. Khan, M.A. Kamal, K. Fahd, P.O. Box, K. Saudi, Status of acetylcholinesterase and butyrylcholinesterase in Alzheimer ' s disease and type 2 diabetes mellitus, CNS Neurol. Disord. - Drug Targets. (2014) 1432–1439.

[65] V. Andrisano, M. Naldi, A. De Simone, M. Bartolini, A patent review of butyrylcholinesterase inhibitors and reactivators 2010–2017, Expert Opin. Ther. Pat. 28 (2018) 455–465.

[66] R.M. Lane, S.G. Potkin, A. Enz, Targeting acetylcholinesterase and butyrylcholinesterase in dementia, Int. J. Neuropsychopharmacol. 9 (2006) 101–124.

[67] S. Das, S. Basu, Multi-targeting strategies for Alzheimer's disease therapeutics: pros and cons, Curr. Top. Med. Chem. 17 (2017) 3017–3061.

[68] G.T. Grossberg, K.R. Edwards, Q. Zhao, Rationale for combination therapy with galantamine and memantine in Alzheimer's disease, J. Clin. Pharmacol. 46 (2006) 17S–26S.

[69] E. Simoni, M. Bartolini, I.F. Abu, A. Blockley, C. Gotti, G. Bottegoni, R. Caporaso, C. Bergamini, V. Andrisano, A. Cavalli, I.R. Mellor, A. Minarini, M. Rosini, Multitarget drug design strategy in Alzheimer's disease: focus on cholinergic transmission and amyloid-β aggregation, Future Med. Chem. 9 (2017) 953–963.

[70] Lorna Piazzi, Angela Rampa, Alessandra Bisi, Silvia Gobbi, Federica Belluti, Andrea Cavalli, Manuela Bartolini, Vincenza Andrisano, V. Piero, M. Recanatini, 3-(4-{[Benzyl(methyl)amino]methyl}phenyl)-6,7-dimethoxy-2H-2-chromenone (AP2238) inhibits both acetylcholinesterase and acetylcholinesterase-induced β-amyloid aggregation: a dual function lead for alzheimer's disease therapy, J. Med. Chem. 46 (2003) 2279–2282.

[71] C. Meltzer, M.D., G. Smith, S.T. DeKosky, B.G. Pollock, C.A. Mathis, R.Y. Moore, D.J. Kupfer, C.F. Reynolds, Serotonin in aging, late-life depression, and Alzheimer's disease: the emerging role of functional imaging, Neuropsychopharmacology. 18 (1998) 407–430.

[72] C.G. Gottfries, Neurochemical aspects on aging and diseases with cognitive impairment, J. Neurosci. Res. 27 (1990) 541–547.

[73] M. Rosini, E. Simoni, R. Caporaso, A. Minarini, Multitarget strategies in Alzheimer's disease: benefits and challenges on the road to therapeutics, Future Med. Chem. 8 (2016) 697–711.

[74] L. Ismaili, A. Romero, M. do Carmo Carreiras, J. Marco-Contelles, Multitarget-directed antioxidants as therapeutic agents: putting the focus on the oxidative stress, in: M. Decker (Ed.), Des. Hybrid Mol. Drug Dev., First, John Fedor, Cambridge, United States, 2017: pp. 5–46.

[75] D.H. Small, Dysregulation of calcium homeostasis in Alzheimer's disease, Neurochem. Res. 34 (2009) 1824–1829.

[76] B. Sameem, M. Saeedi, M. Mahdavi, A. Shafiee, A review on tacrine-based scaffolds as multi-target drugs (MTDLs) for Alzheimer's disease, Eur. J. Med. Chem. 128 (2017) 332–345.

[77] L. Jalili-Baleh, E. Babaei, S. Abdpour, S. Nasir Abbas Bukhari, A. Foroumadi, A. Ramazani, M. Sharifzadeh, M. Abdollahi, M. Khoobi, A review on flavonoid-based scaffolds as multi-target-directed ligands (MTDLs) for Alzheimer's disease, Eur. J. Med. Chem. 152 (2018) 570–589.

[78] G.L. Ellman, K.D. Courtney, V. Andres, R.M. Featherstone, A new and rapid colorimetric determination of acetylcholinesterase activity, Biochem. Pharmacol. 7 (1961) 88–95.

Chapter 7

Combination of human acetylcholinesterase and serum albumin sensing surfaces as highly informative analytical tool for inhibitor screening

Edoardo Fabini, **Anna Tramarin***, Manuela Bartolini. Journal of Pharmaceutical and Biomedical Analysis (2018), 155: 177-184. Doi 10.1016/j.jpba.2018.03.060.* [1].

Abstract

In the continuous research for potential drug lead candidates, the availability of highly informative screening methodologies may constitute a decisive element in the selection of best-in-class compounds. In the present study, a surface plasmon resonance (SPR)-based assay was developed and employed to investigate interactions between *human recombinant* AChE (*h*AChE) and four known ligands: galantamine, tacrine, donepezil and edrophonium. To this aim, a sensor chip was functionalized with *h*AChE using mild immobilization conditions to best preserve enzyme integrity. Binding affinities and, for the first time, kinetic rate constants for all drug–*h*AChE complexes formation/disruption were determined. Inhibitors were classified in two groups: slow-reversible and fast-reversible binders according to respective target residence time. Combining data obtained on drug–target residence time with data obtained on serum albumin binding levels, a good correlation with potency, plasma protein binding *in vivo*, and administration regimen was found. The outcomes of this work demonstrated that the developed SPR-based assay is suitable for the screening, the binding affinity ranking and the kinetic evaluation of *h*AChE inhibitors. The method proposed ensures a simpler and cost-effective assay to quantify kinetic rate constants for inhibitor–*h*AChE interaction as compared with other proposed and published methods. Eventually, the determination of residence time in combination with preliminary ADME studies might constitute a better tool to predict *in vivo* behaviour, a key information for the research of new potential drug candidates.

*These authors contributed equally to the work

7.1 Introduction

Acetylcholinesterase (AChE) is the most abundant cholinesterase in the human body. Via fast hydrolysis of the neurotransmitter acetylcholine (ACh), it plays a crucial role in terminating cholinergic neurotransmission both in the central and in the peripheral nervous system [2]. Since ACh is directly involved in cognitive processes, alteration of cholinergic system is encountered as upstream or downstream hallmark in many neurodegenerative disorders, including Alzheimer's disease (AD), a progressive age-related pathology characterized by a progressive memory loss which parallels a decrease of the central cholinergic tone, neuronal death and deposition of aggregated proteins inside and outside neurons [3]. Thus, according to the cholinergic hypothesis inhibition of centrally active AChE has been studied as the first avenue to contrast cognitive impairment [4].

AChE inhibitors (AChEI) constitute the largest class of marketed drugs approved for AD treatment and are one of the largest neurological drug class in terms of overall retail spending in several West Countries [5]. Although current marketed drugs mainly exert a symptomatic effect [6], numerous new inhibitors, which combine primary anti-cholinesterase activity with a secondary pharmacological activity (inhibition of amyloid peptide aggregation) are under investigation to find effective disease-modifying agents [7]. Besides application in AD, peripherally active AChEI are used to increase neuromuscular transmission in the treatment of *myasthenia gravis*. Quaternary-ammonium derivatives such as pyridostigmine and neostigmine are orally administered to ameliorate muscular weakness while edrophonium, a short acting AChEI, is used as diagnostic tool [8].

In vitro drug efficacy is classically quantified in terms of equilibrium dissociation constant (K_D) and half-maximal inhibitory concentration (IC_{50}); parameters usually determined in closed systems with invariant concentrations of both ligand and target. However, in living organisms, the target is exposed to continuous fluctuation of ligand concentration, and pharmacological effects are rather dependent on the stability of complexes that the drug forms with primary and secondary targets along with its metabolic stability and serum protein binding [9,10]. In this scenario, characterization of binding mechanisms and determination of kinetic parameters are key elements. Especially, quantification of dissociation rate constant (k_{off}) for drug–target complexes allows to estimate residence time ($\tau = 1/k_{off}$), which has recently emerged as critical feature of many best-in-class compounds [11]. τ has been proposed as a better means to correlate *in vitro* affinities to *in vivo* activities with respect to classical approach [9]. Therefore, accessing kinetic information on drug binding events at initial stages of the drug discovery process is gaining increasing interest among medicinal chemists [12].

Among methods used for kinetic evaluations, surface plasmon resonance (SPR) biosensing has now assumed a central role. Fast, high-throughput and highly-informative assays can be developed to monitor interaction between unlabeled interactants in *real-time* [13]. When SPR biosensing assays are properly designed and trained operators are on the task, technology can be used at many stages of the drug discovery route, from fragment-based screening campaigns to hit-to-lead optimization [14,15].

Considering the huge amount of research conducted in the AD field, kinetic studies on inhibitor–AChE interaction are quite scarce and overlooked. Limited examples presented in the literature employ AChE from mouse [16] or *Torpedo Californica* [17] because of the high cost of the human recombinant isoform; however, species-related differences in bindings are well known and such studies are of limited applicability. Moreover, other proposed methods exploit web tools and mathematical treatment of enzymes kinetic to obtain indirect quantification of molecular binding events [18].

In the present study, *human recombinant* AChE was for the first time tethered to a commercially-available sensing surface and the SPR-based assay was exploited to measure kinetic rate constants of binding events with the marketed reversible AD drugs donepezil, galantamine and tacrine. Former two are rapidly reversible drugs approved by the U.S. Food and Drug Administration (FDA) and the European Medicines Agency (EMA); while the latter was the first AChEI approved for AD treatment now withdrawn from the market [19–21]. To enlarge the screening window edrophonium, a peripherally active competitive AChEI characterized by an inhibitory potency in the micromolar range and fragment-like molecular weight (166 g/mol) was also considered. Compounds were selected to span inhibitory potencies over three orders of magnitude and differ in their mode of action (competitive and mixed type inhibitors) to ensure a case-insensitive evaluation system. Binding affinities, determined by SPR approach, were compared with IC_{50} values determined by classical in solution assay (Ellman's assay) [22]. Additionally, taking advantage of a fast and previously validated screening methodology, SPR platform was employed to estimate binding affinity toward human serum albumin (HSA) for the selected inhibitors. HSA constitutes approximately 50 % of total serum protein content and markedly influences the pharmacokinetic (PK) profile of a compound entering human body [23]. The small time consumed to asses this parameter might be rewarding in the further stages of the drug development process, where poor PK still constitutes an important attrition factor [23–26]

The method proposed here has the advantage of accessing kinetic parameters of AChEI–AChE interactions quickly and easily with respect to other proposed strategies. Moreover, the screening methods can be implemented at early stages of drug discovery where, traditionally, only inhibition

potency is determined. Outcomes from this study aim to constitute a proof of concept of the high information content achieved when target-based and HSA-based SPR-biosensing assays are combined.

7.2 Experimental section

7.2.1 Materials

Human recombinant acetylcholinesterase (*h*AChE) (EC 3.1.1.7) lyophilized powder, fatty-acid free human serum albumin (HSA) A3782 lyophilized powder, S-acetylthiocholine iodide (ACTh), 5,5'-dithio-bis(2-nitrobenzoic acid) (DTNB; Ellman's reagent), tacrine hydrochloride, donepezil hydrochloride, edrophonium chloride, (S)-warfarin and Triton X-100 were purchased from Sigma-Aldrich (Milan, Italy). Galantamine hydrobromide was obtained from Tocris Cookson (UK). Research-grade CM5 sensor chip, *N*-ethyl-*N*-(3-dimethylaminopropyl)-carbodiimide (EDC) and *N*-hydroxysuccinimide (NHS) were purchased from GE Healthcare Bio-Sciences (Uppsala, Sweden). N-2-hydroxyethylpiperazine-N′-2-ethanesulfonic acid (HEPES), ethylenediaminetetraacetic acid (EDTA), sodium chloride, potassium dihydrogenphosphate, dipotassium hydrogenphosphate trihydrate, polyoxyethylenesorbitan monolaurate (p-20), Tris(hydroxymethyl)aminomethane (TRIS), sodium acetate were also purchased from Sigma-Aldrich (Milan, Italy). Deionized water was obtained by Milli-Q system (Millipore, Milford, MA, USA). All solutions were filtered with 0.22 μm membrane filters (Millipore, Milford, MA, USA) before use.

7.2.2 Buffer preparation

For enzymatic activity assay, potassium phosphate buffer (0.1M, pH 8.0)—PB was employed. Running buffer used for *h*AChE immobilization had the following composition: HEPES (0.01M) NaCl (0.15 M) EDTA (0.003 M) (pH 7.4)—HBS. Running buffer used to study inhibitor–*h*AChE interactions had the following composition: KH_2PO_4 (0.1M) K_2HPO_4 (0.1M) with the addition of p-20 0.025% (v/v) (pH 8.0)—PB-T. For HSA immobilization and inhibitors binding analysis the following buffer was employed: Na_2HPO_4 (3.2 mM) KH_2PO_4 (0.5 mM) KCl (1.3 mM) NaCl (135 mM) with 0.05% (v/v) p-20 (pH 7.4)—PBS-T.

7.2.3 Sample preparation

*h*AChE stock solution was prepared dissolving *h*AChE lyophilized powder in PB (pH 8.0; 0.1 M) with the addition of Triton X-100 1% (v/v). To test *h*AChE activity and the inhibition capacity of the selected compounds, the stock solution was further diluted in PB (pH 8.0; 0.1 M) containing 0.1% (v/v) Triton X-100. For SPR immobilization, *h*AChE stock solution was diluted in phosphate buffer (pH 5.0; 0.1 M) containing 0.33% (v/v) Triton X-100. Stock solutions of edrophonium (6 mM), tacrine (4 mM), galantamine (3 mM) and donepezil (3 mM) were prepared in bidistilled water. (S)-warfarin was dissolved in PBS-T in order to obtain a stock solution of 600 μM.

7.2.4 In solution enzymatic activity assay

Enzymatic assays were carried out on a Jasco V-530 double beam spectrophotometer equipped with a HAAKE DC30 thermostating system (Thermo Haake, Germany) and data were processed with GraphPad Prism 4.03 software (GraphPad Software Inc.).

Enzymatic activity in the absence and in the presence of inhibitor were spectrophotometrically assessed using the Ellman's method [22]. Assay solution (1 mL) consisted in: PB (pH 8.0; 0.1 M), 0.02 unit/mL *h*AChE, 550 μM substrate (ATCh) and 340 μM DTNB. Solutions were incubated at 37°C for 20 min before the addition of the substrate. Hydrolysis rate was quantified by measuring changes in the absorbance at 412 nm for 3 min at 37°C.

In the case of inhibition studies, five increasing concentrations of tested inhibitor were assayed (n=3) to obtain percent inhibition in the range of 20-80%. Blank solutions containing all components except *h*AChE were prepared in parallel to account for the non-enzymatic hydrolysis of the substrate. IC_{50} values for selected inhibitors were determined by plotting the percentage of inhibition as function of the decimal log of the tested inhibitor concentration.

7.2.5 Surface plasmon resonance-based analyses

SPR analyses were performed using Biacore™ X100 system (GE Healthcare Bio-Sciences, Uppsala, Sweden) equipped with an in-line degasser and thermostated at 25 °C. SPR data reduction and processing were performed with Biacore™ X100 2.0 evaluation software or Scrubber2 BioLogitech® 2008 software.

7.2.5.1 hAChE immobilization and binding analysis

For preparation of *h*AChE-functionalized surface, enzyme stock solution was diluted to 53.3 units/mL in potassium phosphate buffer (0.1 M) at various pH values (pH range 4.0–6.0) and percentage of Triton X-100 (0.33–1% v/v). Each sample was injected at 10 μL/min for 30 s, and electrostatic pre-concentration at the surface was evaluated. *h*AChE sample diluted in potassium phosphate buffer (pH 5.0; 0.1 M) containing 0.33% (v/v) Triton X-100 was immobilized through amine-coupling procedure, employing HBS as running buffer [27]. Briefly, sensor surface was activated with a 7-min injection (10 μL/min) of EDC (0.4 M)-NHS (0.1 M) (1:1 v/v) mixture and enzyme was injected until an adequate immobilization level of 7000 Response Units (RU) was obtained. Then, quenching of residual active esters on the surface was performed by overnight flowing of TRIS buffer saline: TRIS (0.05 M)-NaCl (0.1 M) (pH 8.0). A reference channel was prepared employing the same protocol apart from enzyme injection. Apparent surface binding

capacity after immobilization process was estimated employing donepezil as test compound according to Eq. (9) (see Section 7.2.5.3).

Binding studies were carried out in multi-cycle kinetic (MCK) mode employing 75 µL/min as flow rate. Injections of running buffer were interspersed among inhibitor injections and used as 'blank' for double-referencing purposes [28]. Inhibitor–*h*AChE interactions were monitored using PB-T (pH 8.0; 0.1 M) as running buffer. Stock solutions of the selected drugs were directly diluted in running buffer to obtain a series of dilutions centered around the reported K_i values [29]. In details, edrophonium 60.0-0.6 µM; donepezil 600-3 nM; galantamine 30.0-0.3 µM; tacrine 8.0 µM-0.1 µM. For edrophonium and donepezil contact time and dissociation time were set at 60 s and 180 s, respectively. For galantamine and tacrine a 60s-association and a 120s-dissociation steps were set. Each interaction was analyzed at least in duplicate.

7.2.5.2 HSA surface preparation and binding analysis

HSA-functionalized surface was prepared according to previously published protocols [26,30–32]. Briefly, HSA was diluted at 30 µg/mL in sodium acetate buffer (0.01 M; pH 5.0) and was immobilized onto CM5 sensor surface exploiting amine-coupling chemistry and employing PBS-T as running buffer. At the end of the immobilization protocol, the functionalized surface was allowed to stabilize overnight. After stabilization, an immobilization level of 7000 RU was obtained.

(S)-warfarin was used as reference compound in order to test surface functionality. (S)-warfarin stock solution was prepared directly in running buffer and injected in a three-fold dilution series from 30 to 0.4 µM. Inhibitor-HSA interaction was monitored in PBS-T, injecting each compound in a three-fold dilution series (from 100 µM to 1.2 µM). Binding studies for drug-HSA complexes were carried out setting association and dissociation time to 45 s, with a flow rate of 75 µL/min.

7.2.5.3 Data evaluation

Apparent surface binding capacity after immobilization was estimated according Eq. (9):

$$R_{max} = MW_{analyte} / MW_{ligand} * RU_{immobilized} * stoichiometry \quad (9)$$

Each set of sensorgrams was processed according to the same procedure. SPR responses obtained in the active channel were corrected for the response obtained in the reference channel and subsequently subtracted of the responses from blanks in order to obtain double-referenced sensorgrams [28]. Corrected responses recorded at steady-state were plotted against the concentration injected and non-linear regression analysis was used to extrapolate the equilibrium dissociation constant (K_D). For inhibitor–*h*AChE interaction, a model accounting for one binding site (i=1), defined by Eq. (10) was employed:

$$R_{eq} = \sum_i \frac{R_{max}(C / K_{Di})}{1 + C / K_{Di}} \quad (10)$$

where c (M) is the inhibitor concentration, R_{eq} (RU) is the response at the steady-state and R_{max} (RU) is the maximal response.

For inhibitor–HSA interactions Eq. (10) was also employed, posing i=2. Inclusion of a secondary binding site accounts for the unspecific binding to HSA likely happening at the high inhibitor concentration employed for the study. Primary K_D extrapolated by this approach was then converted into percentage of drug bound to HSA according to the procedure reported in [31].

For kinetic analysis, sensorgrams were globally fitted to a theoretic model describing a simple, reversible 1:1 binding event (Eq. (11)). Association (k_{on}) and dissociation (k_{off}) rate constants for inhibitor–*h*AChE reaction were extrapolated according to the integrated rate Eq. (12):

$$[A] + [B] \underset{k_{off}}{\overset{k_{on}}{\rightleftharpoons}} [AB] \quad (11)$$

$$[AB] = [AB]_{eq}\,(1 - e^{-(kon[B] + koff)t}) \quad (12)$$

where k_{on} is expressed in $M^{-1}s^{-1}$ and k_{off} is expressed in s^{-1}.

According to 1:1 binding model, the K_D value is equal to the ratio between *off*- and *on*-rate constants, as shown in Eq. (13).

$$K_D = k_{off}/k_{on} \quad (13)$$

On the basis of the applied theoretical model, target residence time (τ), expressed in s, is defined as the inverse of dissociation rate constant [12] as described in Eq. (14):

$$\tau = 1/k_{off} \quad (14)$$

7.3 Results and discussion

7.3.1 Optimization of immobilization and SPR analysis conditions

Amine-coupling can be considered as the first choice for ligand immobilization when protein–small molecules interactions want to be investigated by SPR sensing approach. Stable and high-density surfaces can be generated, and reliable data can be produced even for low molecular weight analytes. However, it is crucial that ligand binding properties are unaltered upon anchorage to dextran matrix. Coupling condition, which envisage acidic, low-ionic-strength solutions, might result too harsh when an intrinsically unstable enzyme like *h*AChE is engaged. Thus, for this study a series of tailor-made immobilization conditions were explored. Each coupling solution was evaluated both for its pre-concentration efficiency through pH-scouting procedure and for its residual enzymatic activity after incubation in each coupling buffer. This latter step is essential to verify whether *h*AChE retains most of its catalytic activity upon exposure to the coupling condition, thus being immobilized in its active form.

Supplementing coupling solution with a non-ionic detergent might reduce reaction efficiency but resulted essential to maintain enzyme stability. Indeed, dilution in phosphate buffer without Triton X-100 determined a significant and fast loss of enzyme activity over short time (data not shown). P-20, a common non-ionic detergent routinely supplemented in SPR running buffer, resulted less efficient than Triton X-100 in stabilizing *h*AChE (p-20 supplemented solution lost 90% of activity within an hour). Based on these results addition of Triton X-100 to AChE solutions was considered essential to maintain enzyme functionality and consequently produce a functional sensing surface.

Concerning pHs, AChE optimum working and storage pH is 7.4–8 or above, depending on the enzyme source; pH values lower than 6.5 seem to reduce not only enzyme activity but also enzyme stability [33]. Nonetheless, covalent immobilization at pH 5.0 of *h*AChE monolithic supports for enzymatic studies was previously achieved with good results [34]. Hence, *h*AChE stock solution was diluted either in 10 mM sodium acetate buffer or in phosphate buffer (0.1 M) at various pH values (pH range 4.0–6.0).

Each sample was injected at 10 μL/min for 30 s and electrostatic pre-concentration at the surface was evaluated. To assess the activity loss upon dilution in the immobilization buffer, *h*AChE solutions used for the pH scouting procedure were further diluted in the activity assay buffer (PB pH 8.0; 0.1 M) and residual activity was evaluated by Ellman's assay [22] . Buffer type resulted to affect enzyme activity with PB performing slightly better than acetate buffer at the same pH value (15% difference in activity). When *h*AChE was dissolved in PB (pH 5.0; 0.1 M) supplemented with 0.33 % (v/v) Triton X-100, highest residual activity was observed and the enzyme could be

efficiently pre-concentrated. Consequently, this condition was chosen to carry out the immobilization procedure on SPR platform.

*h*AChE stock solution (1716 U/mL) was diluted into the former buffer (53.3 U/mL) and 25 units of active enzyme were injected over the activated surface until an immobilization level of 7000 RUs was achieved. Then, deactivation was attained switching running buffer to TBS. Primary amine of TRIS (0.05 M) provided a milder means to quench residual active esters with respect to classical injection of ethanolamine (pH 8.0; 1 M). After an overnight stabilization in TBS, 5500 RUs, corresponding to a surface density of 5.0 ng/mm^2 [27], were stably coupled to the surface (minimal baseline drift was observed, i.e., <0.3 RU/min). Surface binding capacity was estimated to be approximately 20 % of theoretical R_{max} Eq. (9). Despite this might seem a low value, expected R_{max} after amine-coupling is usually around 50 % of theoretical. Due to the random orientation of ligand on the surface, binding site accessibility might be hampered when covalent bond formation occurs in their immediate proximity [27]. Moreover, apparent activity showed by our sensing surface is comparable to data presented in the literature where AChE from other species was tethered to dextran matrices [17,35] or others solid supports [29,34].

7.3.2 Determination of thermodynamic and kinetic parameters of inhibitor–hAChE interaction

Having established *h*AChE could endure coupling condition, a series of well characterized *h*AChE inhibitors (Fig. 26) were employed to test binding performances of the immobilized enzyme.

Selected compounds are all drugs used either in AD treatment or *myasthenia gravis* diagnosis for which bioavailability data and administration regimens are available, so that our results can be compared to well-established parameters.

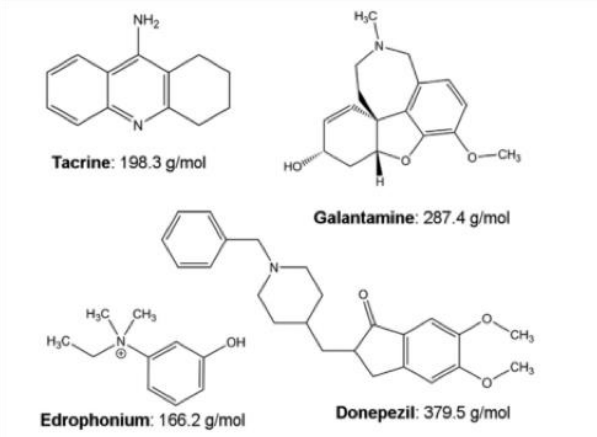

Figure 26| Structure of the selected *h*AChE inhibitors. Molecular weights are reported under the corresponding compound.

Concerning the mechanism of action, tacrine and donepezil are mixed-mode competitors, i.e., they are reported to bind both the *h*AChE catalytic site and the peripheral anionic binding site (at high concentration) while galantamine and edrophonium are substrate-competitive inhibitor. Edrophonium is also characterized by a low molecular weight (166 g/mol). Overall, molecular weights range from 166 g/mol to 379 g/mol and inhibitory potencies span over four orders of magnitude.

To assess whether the *h*AChE sensing surface was suitable to discriminate among the different inhibitors, stock solutions were diluted in running buffer and presented to the *h*AChE-functionalized surface. Resulting sensorgrams were discernible from background noise for all employed concentrations and useful data could always be retrieved (Fig. 27). Binding affinities were compared with inhibitory potencies (IC_{50} values) determined by a classical in solution assay [22] and employing the same *h*AChE used for *h*AChE immobilization and inhibitor solutions used for SPR interaction analysis.

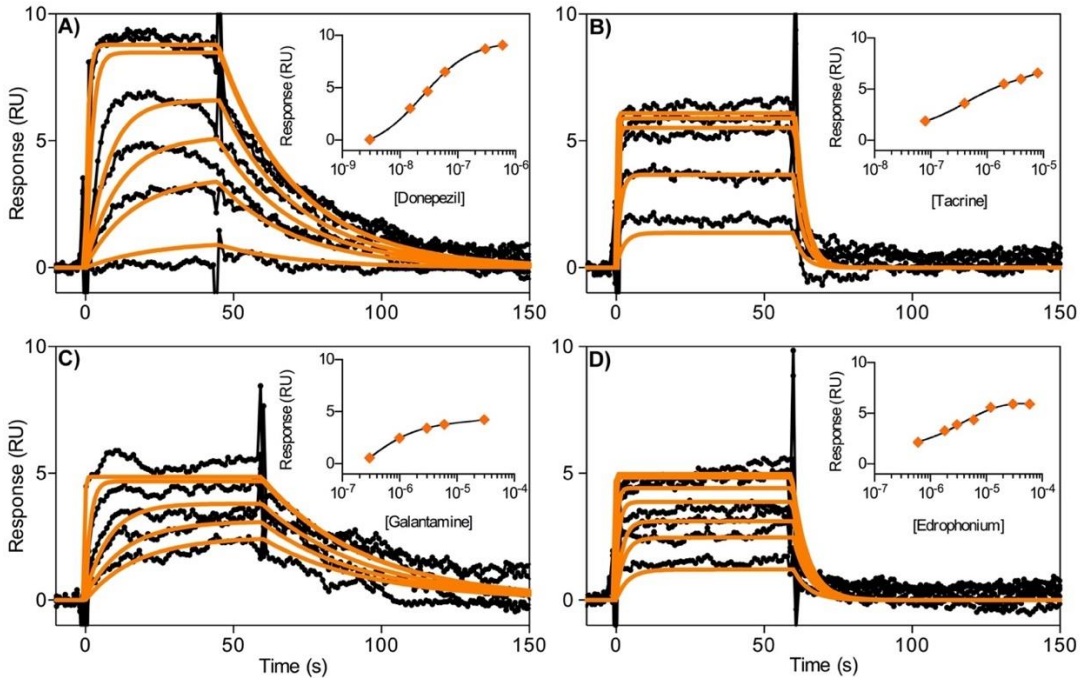

Figure 27| Affinity and kinetic studies of the four selected inhibitors binding to immobilized *h*AChE chip surface. Double-referenced sensorgrams (main) and equilibrium responses (inset) of inhibitors–*h*AChE interactions. The injected inhibitor concentrations were: 3.0, 15.0, 30.0, 60.0, 300.0 and 600.0 nM for donepezil (A); 0.1, 0.4, 2.0, 4.0 and 8.0 μM for tacrine (B); 0.3, 1.0, 3.0, 6.0 and 30.0 μM for galantamine (C); 0.6, 1.8, 3.0, 6.0, 12.0, 30.0 and 60.0 μM for edrophonium (D). Kinetic rate constants were extrapolated applying a theoretic reversible 1:1 binding model (light) to experimental data (dark). K_D for each inhibitor–*h*AChE complex, was extrapolated plotting corrected responses (RU) at steady-state against concentration and fitting experimental data to Eq. (10).

The measured inhibition potencies (Table 7) were in good agreement with those reported in the literature as well as with previously determined inhibition constant (*Ki*), which were calculated under the same experimental conditions [29,34].

Table 7| Half-maximal inhibitory concentrations (IC_{50}) determined by in solution assay, equilibrium dissociation constants (K_D), kinetic rate constants (k_{on}, k_{off}), dissociation constants measured *via* kinetic analysis (k_{off}/k_{on}) and residence time (τ) determined by SPR analysis on *h*AChE-inhibitor complexes. The reported values are the mean of at least two independent measurements. Data are reported with corresponding standard deviation (± SD). Inhibition constants (K_i) are also reported for comparison purposes.

Inhibitor	IC_{50} (M)	K_i (M) [a]	K_D (M)	k_{on} ($M^{-1}s^{-1}$)	k_{off} (s^{-1})	k_{off}/k_{on} (M)	τ (s)
Edrophonium	$(7.30\pm0.35)\cdot10^{-6}$	$(1.63\pm0.23)\cdot10^{-6}$	$(2.28\pm1.07)\cdot10^{-6}$	$(1.07\pm0.54)\cdot10^{5}$	$(2.52\pm1.37)\cdot10^{-1}$	$(2.39\pm0.78)\cdot10^{-6}$	3.96
Tacrine	$(4.01\pm0.10)\cdot10^{-7}$	$(1.51\pm0.16)\cdot10^{-7}$	$(3.61\pm2.92)\cdot10^{-7}$	$(1.46\pm0.56)\cdot10^{6}$	$(3.58\pm0.71)\cdot10^{-1}$	$(2.55\pm0.49)\cdot10^{-7}$	2.79
Donepezil	$(2.03\pm0.13)\cdot10^{-8}$	$(2.05\pm0.33)\cdot10^{-8}$	$(4.34\pm2.68)\cdot10^{-8}$	$(1.81\pm0.08)\cdot10^{6}$	$(4.97\pm1.49)\cdot10^{-2}$	$(2.74\pm0.70)\cdot10^{-8}$	20.12
Galantamine	$(2.00\pm0.23)\cdot10^{-6}$	n.d.[b]	$(3.94\pm0.61)\cdot10^{-7}$	$(9.46\pm0.92)\cdot10^{4}$	$(2.48\pm0.53)\cdot10^{-2}$	$(2.61\pm0.30)\cdot10^{-7}$	40.32

[a] Inhibition constants (K_i) reported in literature and calculated using the same experimental conditions [29].
[b] n.d., not determined.

All monitored interactions (Fig. 27) reached steady-state conditions within the chosen injection time and equilibrium dissociation constant (K_D) could be extrapolated. In agreement with the *Ki* values for the enzyme in solution [29] (Table 7), the strongest binder was identified in donepezil, which showed a $K_D = (4.34 \pm 2.68) \cdot 10^{-8}$ M; the weakest binder was identified in edrophonium whose K_D was $(2.28 \pm 1.07) \cdot 10^{-6}$ M. The latter value also agrees with recent published data obtained by in solution isothermal titration calorimetry (ITC) studies (edrophonium $K_D = 1.4 \pm 0.4$ μM), strongly suggesting immobilization did not hamper *h*AChE binding activity [36].

Concerning reactions profiles, complexes of edrophonium–*h*AChE and tacrine–*h*AChE both showed rapid on-/off-rates resulting in squared-shaped sensorgrams, while complexes of galantamine–*h*AChE and donepezil–*h*AChE displayed significantly slower dissociation events. Sensorgrams quality allowed applying a global kinetic fitting procedure to each data set. All monitored interactions were analyzed employing a simple, reversible, 1:1 binding model (Eq. (10)) that gave in return reasonable numerical values. Association and dissociation rate constants values for edrophonium and tacrine (Table 7) were in good agreement with those reported in literature and

achieved by stopped-flow fluorescence titration in which both compounds showed rapid kinetics [37]. The slight differences in k_{on} and affinity values with respect to those obtained by fluorescence titration might be ascribed to the different enzyme origin (mouse vs human).

Because of the limited number of tested compounds and different chemical structures structure/kinetic relationships cannot be derived. The lower *off*-rates displayed by galantamine and donepezil (slower dissociation) may be partially ascribed to the high stability and thermodynamically favorite conformations resulting from their binding to hAChE, as recently rationalized by molecular dynamic studies [38,39].

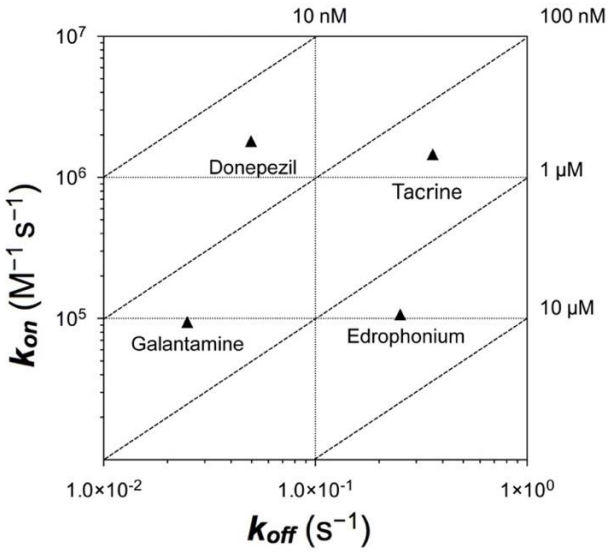

Figure 28| Kinetic chart for tested inhibitors. Plot of association (k_{on}) rate constants as function of dissociation rate constants (k_{off}) of *h*AChE inhibitors. Dotted lines (iso-affinity line) refer to K_D values calculated from kinetic analysis (k_{off}/k_{on}).

Dissecting K_D values in their individual *on-/off*-rate constants provides further insight into the different inhibitor–AChE interactions (Fig. 28). For instance, galantamine and tacrine show rather similar thermodynamic K_D and they lay on extremely close iso-affinity lines; however, the stability of the two inhibitor–*h*AChE complexes diverges, with respective k_{off} values differing more than one order of magnitude. This is not surprising, since chemical entities with similar affinities for the target molecule *in vitro* can show large difference in both k_{on} and k_{off} values. Such differences might reflect differences in binding modes, thereby also differences in their *in vivo* efficacy. Resolving kinetic rate constants make possible to differentiate otherwise undistinguishable compounds providing an additional layer of discrimination when chemical series are tested. Moreover, desired therapeutic effect (short or long action) might be better correlated to fast or slow interaction profiles, so that a good balance between therapeutic and adverse effects can be achieved [9].

The possibility of relating kinetic aspects (K_D=k_{off}/k_{on}) with experimental thermodynamic parameters, i.e. K_D calculated from the total Gibbs free-energy change (ΔG) ($K_D = e^{\Delta G/RT} = e^{(\Delta H - T\Delta S)/RT}$) [40], provides a deeper characterization of biomolecular equilibria. However, the amount of AChE required for *in vitro* thermodynamic studies, among which ITC is the most commonly used approach [41], is not compatible with the extremely high cost of recombinant hAChE. As consequence, experimental thermodynamic data available from literature have been obtained using less expensive non-human AChE isoforms, such as AChE from *Electric eel* or *Torpedo Californica*. Specifically, thermodynamic parameters for the same set of inhibitors object of this study were assessed by Draczkowski *et al.* (2016) using ITC and AChE from *Electric eel* [42]. However, as stated by the authors [42], ITC thermodynamic data did not well correlate with the experimental inhibition constants as they were compromised by a low Wiseman factor c [43], which flatted the experimental ΔGs (range from –39.5 to –42.9 kJ/mol), and, consequently, the related K_D values.

7.3.3 Drug–target residence time and early pharmacokinetic estimation

Binding affinities values measured *via* kinetic analysis ($K_D = k_{off}/k_{on}$) were in excellent agreement with affinity constants determined *via* equilibrium studies. Moreover, maximal responses (R_{max}), refractive index corrections (RI) and residual plots inspection all indicates goodness of fit by our kinetic model. Based on these premises, dissociation rate constants were used to calculate residence time. The four drugs showed different τ (Table 7) and could be ranked in two main groups: (i) fast-reversible binders with residence time lower than 5 s, i.e tacrine (2.79 s) and edrophonium (3.96 s) and (ii) slow-reversible binders, i.e. donepezil (20.12 s) and galantamine (40.32 s). As first approximation, all molecules showed quite rapid escape from their respective binding site(s) on *h*AChE. This could be expected when an enzyme that assumes a crucial role as terminator of signal transduction is targeted for inhibition and adverse effects can arise if inhibitory effect prolongs extensively [44,45].

Looking at duration of action for the selected drugs *in vivo*, a good correlation with target residence time was found. Edrophonium action only lasts 1.2–2.3 min after i.v. administration [46] and tacrine, among anti-AD drugs, has the shortest duration of action (administration: 4 times/day), in agreement with the kinetic classification. On the other hand, galantamine (twice per day) and donepezil (once daily), both have a lower frequency of suggested administration to AD patients, in agreement with their longer residence time. However, pharmacologic effect and length of action for administrated drugs arise from the combination of binding kinetic to the primary target and adsorption, distribution, metabolism and excretion (ADME) profile. Binding to serum proteins represents an important aspect in determining ADME profile of a molecule entering human body.

HSA is the most abundant among circulating protein and plays a central role as transporter of many endogenous and exogenous poorly soluble compounds [23].

Thus, as a proof of concept that combination of residence time and HSA binding might represent a better predictive parameter, the propensity of the four selected drugs to interact with immobilized HSA was estimated through SPR technology. Binding to HSA was rapid and reversible (Fig. 29), as expected when transport proteins are involved in complex formation; additionally, interactions exceeded 1:1 stoichiometric ratio and a binding model accounting for two independent binding sites was employed. This is not surprising since the same molecule can occupy multiple binding sites on HSA, namely at low concentrations binding sites with high affinity and low capacity, at higher concentration binding sites with lower affinity but higher capacity [31,32,47]. Primary affinity measured for the different compounds was converted into bound percentage assuming physiological concentration of the protein (680 µM) and 10 µM of compounds.

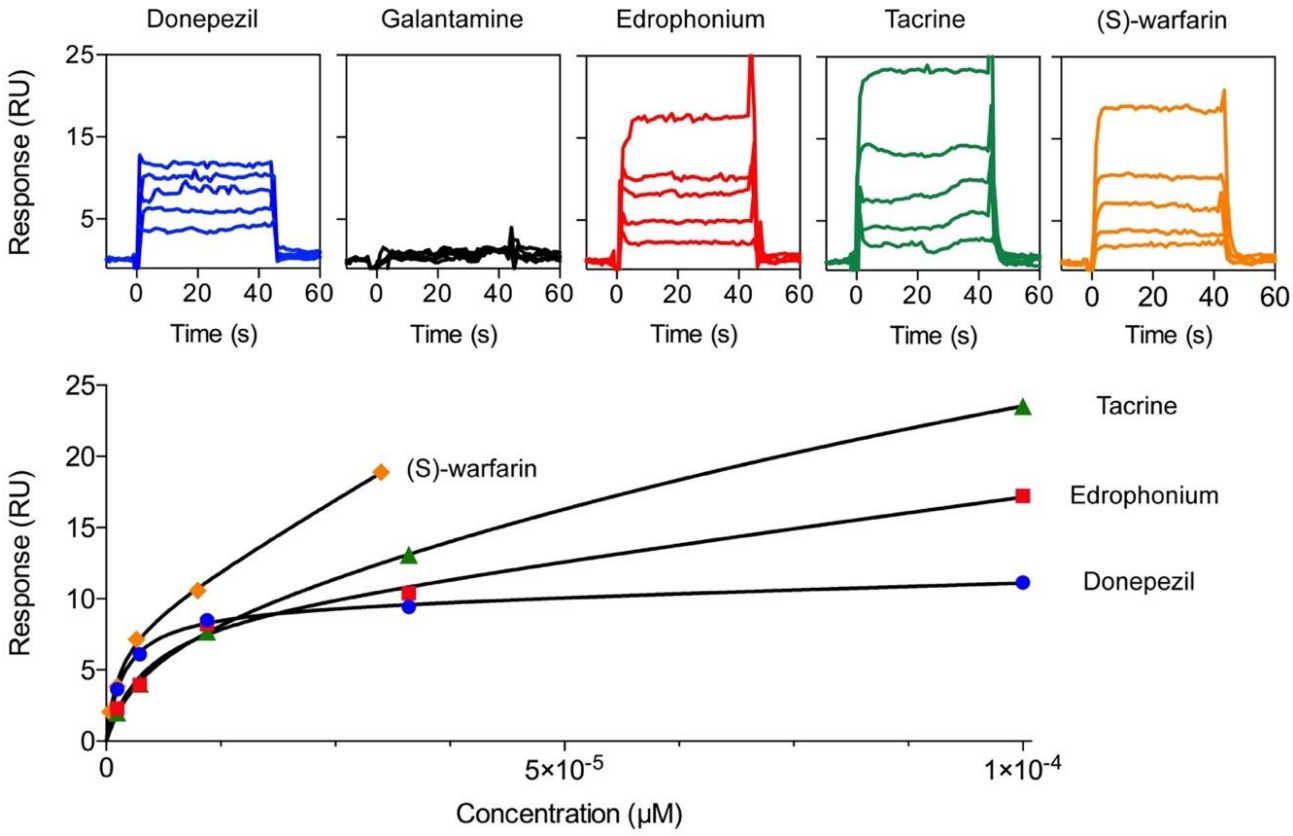

Figure 29| Drugs–human serum albumin (HSA) interaction studies. Double-referenced sensorgrams (upper panel) and equilibrium responses (lower panel) for inhibitor–HSA interactions. All compounds are tested in a three-fold dilution series: (*S*)-warfarin 30 µM to 0.4 µM; inhibitors from 100 µM to 1.2 µM. Corrected responses (RU) at steady-state were fitted to Eq. (10) considering two equivalent binding sites (i =2).

Interestingly, results (Table 8) showed that galantamine did not significantly interact with HSA, while the other inhibitors showed high affinity toward the immobilized plasma protein. Bound percentage for donepezil and galantamine were also comparable to pharmacokinetic data obtained in clinical studies [48]. Galantamine is reported to have ~18 % plasma protein binding percentage and serum half-life of 7h; on the other hand, donepezil has a plasma protein binding percentage of ~96 % and serum half-life of 70 h [48]. Likely, the significant binding of donepezil to HSA, may preserve it from enzymatic and non-enzymatic degradation and excretion enhancing its plasma stability and duration of action. This good correlation further indicates that measuring binding affinity towards immobilized HSA constitutes a good approximation of *in vivo* inhibitor binding to the human serum proteins and may offer a good estimation of its fate after adsorption.

Table 8| Primary equilibrium dissociation constants (K_D) determined for drug–HSA complexes by SPR analysis. Results are listed with corresponding standard error (± SE). Percentage bound values (% bound) to HSA were obtained according to the procedure described in [31].

Drug	K_D (μM)	% Bound
Edrophonium	4.23 ± 2.07	94.4
Tacrine	4.40 ± 1.08	94.2
Donepezil	2.00 ± 0.22	97.2
Galantamine	n.d.[a]	n.d.[a]
(S)-Warfarin	1.40 ± 0.34	98.0

[a] n.d., not determined.

7.4 Conclusions

When enzymes are targeted for inhibition, drug discovery campaigns are usually conducted employing functional assays, where the main focus is on increasing inhibition potency. However, within the same chemical series is not unusual to have compounds with comparable IC_{50} values and same inhibition mode, for which a clear prioritization criterion is hard to identify. In this context, having additional elements to discriminate between chemical entities becomes a clear advantage. Dissociation rate constant (k_{off}), or its reciprocal term residence time (τ) of inhibitor–enzyme complexes, might provide further insight on target-inhibitor interactions, thus aiding the selection process. Moreover, τ is a valid parameter in systems where drug concentration fluctuates over time, as in *in-vivo* settings. At present day there is no simple and cost-effective method to resolve kinetic interactions of *h*AChE inhibitors with their target.

In the present study, an SPR-based biosensing assays has been developed to quantify binding affinities and kinetic rates constant for *h*AChE–inhibitors binding events. The use of a custom coupling solution ensured immobilization of the enzyme in its active form and resulting sensing surface was amenable to measure binding affinities ranging over three orders of magnitude. As test analytes, widely characterized anti-AChE drugs, differing for potencies (*Ki* ranging from 10^{-6} to 10^{-8} M) inhibition mode (competitive or mixed mode) and molecular weight (from 166 to 379 g/mol) were employed. Thermodynamic and kinetic parameters were accurately extrapolated even for edrophonium (fragment-like molecular weight), suggesting the suitability of the method even for fragment-based drug discovery campaigns. Determination of the kinetic rate constants under same experimental conditions for all marketed anti-AChE drugs used in AD constitutes a first of its kind study and provide a better comparison of their kinetic behavior, which allowed their classification into two main classes: slow-dissociating and fast-dissociating reversible inhibitors. Moreover, SPR technology was employed to determine binding level toward immobilized HSA in an easy and fast fashion with the aim of roughly predicting the pharmacokinetic behavior. Combination of data on the primary target with data on HSA found good correlation with drug potency and administration regimens in therapeutic routine.

Application of the proposed method offers a solution to implement inhibition data, traditionally obtained when new *h*AChE inhibitors are tested, with deeper information on the intrinsic drug–target interaction and preliminary pharmacokinetic data. Parameters such as k_{off} and bound percentage to serum proteins can be easily obtained, and favorite chemical scaffolds can be prioritized counting on additional information with respect to what is traditionally considered.

References

[1] E. Fabini, A. Tramarin, M. Bartolini, Combination of human acetylcholinesterase and serum albumin sensing surfaces as highly informative analytical tool for inhibitor screening, J. Pharm. Biomed. Anal. 155 (2018) 177–184.

[2] T. H. Ferreira-Vieira, I. M. Guimaraes, F. R. Silva, F. M. Ribeiro, Alzheimer's disease: targeting the cholinergic system, Curr. Neuropharmacol. 14 (2016) 101–115.

[3] A. Serrano-Pozo, M.P. Frosch, E. Masliah, B.T. Hyman, Neuropathological alterations in Alzheimer disease, Cold Spring Harb. Perspect. Med. 1 (2011) a006189.

[4] A. Contestabile, The history of the cholinergic hypothesis, Behav. Brain Res. 221 (2011) 334–340.

[5] B.E. Leonard, Pharmacotherapy in the treatment of Alzheimer's disease: an update, World Psychiatry. 3 (2004) 84.

[6] M. Pohanka, Cholinesterases, a target of pharmacology and toxicology, Biomed. Pap. 155 (2011) 219–223.

[7] X. Zha, D. Lamba, L. Zhang, Y. Lou, C. Xu, D. Kang, L. Chen, Y. Xu, L. Zhang, A. De Simone, S. Samez, A. Pesaresi, J. Stojan, M.G. Lopez, J. Egea, V. Andrisano, M. Bartolini, Novel tacrine-benzofuran hybrids as potent multitarget-directed ligands for the treatment of alzheimers disease: design, synthesis, biological evaluation, and X-ray crystallography, J. Med. Chem. 59 (2016) 114–131.

[8] A. Jayam Trouth, A. Dabi, N. Solieman, M. Kurukumbi, J. Kalyanam, Myasthenia Gravis: a review, Autoimmune Dis. 2012 (2012) 1–10.

[9] R.A. Copeland, D.L. Pompliano, T.D. Meek, Drug–target residence time and its implications for lead optimization, Nat. Rev. Drug Discov. 5 (2006) 730–739.

[10] R.A. Copeland, Drug–target interaction kinetics: underutilized in drug optimization?, Future Med. Chem. (2016).

[11] L. Xia, W.A.C. Burger, J.P.D. Van Veldhoven, B.J. Kuiper, T.T. Van Duijl, E.B. Lenselink, E. Paasman, L.H. Heitman, A.P. Ijzerman, Structure-affinity relationships and structure-kinetics relationships of pyrido[2,1-f]purine-2,4-dione derivatives as human adenosine A3 receptor antagonists, J. Med. Chem. 60 (2017) 7555–7568.

[12] J.P. Renaud, C.W. Chung, U.H. Danielson, U. Egner, M. Hennig, R.E. Hubbard, H. Nar, Biophysics in drug discovery: impact, challenges and opportunities, Nat. Rev. Drug Discov. 15 (2016) 679–698.

[13] R.L. Rich, D.G. Myszka, Higher-throughput, label-free, real-time molecular interaction analysis, Anal. Biochem. 361 (2007) 1–6.

[14] H. Nguyen, J. Park, S. Kang, M. Kim, Surface plasmon resonance: a versatile technique for biosensor applications, Sensors. 15 (2015) 10481–10510.

[15] W. Huber, F. Mueller, Biomolecular interaction analysis in drug discovery using surface plasmon resonance technology., Curr. Pharm. Des. 12 (2006) 3999–4021.

[16] Z. Radić, P. Taylor, Interaction kinetics of reversible inhibitors and substrates with acetylcholinesterase and its fasciculin 2 complex, J. Biol. Chem. 276 (2001) 4622–4633.

[17] F. Bai, Y. Xu, J. Chen, Q. Liu, J. Gu, X. Wang, J. Ma, H. Li, J.N. Onuchic, H. Jiang, Free energy landscape for the binding process of Huperzine A to acetylcholinesterase, Proc. Natl. Acad. Sci. 110 (2013) 4273–4278.

[18] S. Bevc, J. Konc, J. Stojan, M. Hodošček, M. Penca, M. Praprotnik, D. Janežič, ENZO: a web tool for derivation and evaluation of kinetic models of enzyme catalyzed reactions, PLoS One. 6 (2011) e22265.

[19] M. Bond, G. Rogers, J. Peters, R. Anderson, M. Hoyle, A. Miners, T. Moxham, S. Davis, P. Thokala, A. Wailoo, M. Jeffreys, C. Hyde, The effectiveness and cost-effectiveness of donepezil, galantamine, rivastigmine and memantine for the treatment of Alzheimer's disease (review of Technology Appraisal No. 111): a systematic review and economic model, Health Technol. Assess. (Rockv). 16 (2012).

[20] Y. Ago, K. Koda, K. Takuma, T. Matsuda, Pharmacological aspects of the acetylcholinesterase inhibitor Galantamine, J. Pharmacol. Sci. 116 (2011) 6–17.

[21] M.B. Colovic, D.Z. Krstic, T.D. Lazarevic-Pasti, A.M. Bondzic, V.M. Vasic, Acetylcholinesterase inhibitors: pharmacology and toxicology, Curr. Neuropharmacol. 11 (2013) 315–335.

[22] G.L. Ellman, K.D. Courtney, V. Andres, R.M. Featherstone, A new and rapid colorimetric determination of

acetylcholinesterase activity, Biochem. Pharmacol. 7 (1961) 88–95.

[23] T. Peters Jr., All about albumin, First ed., Academic Press, London, 1996.

[24] T. Bohnert, L.-S. Gan, Plasma protein binding: from discovery to development, J. Pharm. Sci. 102 (2013) 2953–94.

[25] M.J. Waring, J. Arrowsmith, A.R. Leach, P.D. Leeson, S. Mandrell, R.M. Owen, G. Pairaudeau, W.D. Pennie, S.D. Pickett, J. Wang, O. Wallace, A. Weir, An analysis of the attrition of drug candidates from four major pharmaceutical companies, Nat. Rev. Drug Discov. 14 (2015) 475–486.

[26] E. Fabini, U.H. Danielson, Monitoring drug–serum protein interactions for early ADME prediction through Surface Plasmon Resonance technology, J. Pharm. Biomed. Anal. 144 (2017) 188–194.

[27] S. Löfås, A. Mcwhirter, The art of immobilization for SPR sensors, in: Surf. Plasmon Reson. Based Sensors, Springer, Berlin, Heidelberg, 2006: pp. 117–151.

[28] D.G. Myszka, Improving biosensor analysis, J. Mol. Recognit. 12 (1999) 279–284.

[29] M. Bartolini, V. Cavrini, V. Andrisano, Characterization of reversible and pseudo-irreversible acetylcholinesterase inhibitors by means of an immobilized enzyme reactor, J. Chromatogr. A. 1144 (2007) 102–110.

[30] Å. Frostell-Karlsson, A. Remaeus, H. Roos, K. Andersson, P. Borg, M. Hämäläinen, R. Karlsson, Biosensor analysis of the interaction between immobilized human serum albumin and drug compounds for prediction of human serum albumin binding levels, J. Med. Chem. 43 (2000) 1986–1992.

[31] R.L. Rich, Y.S.N. Day, T.A. Morton, D.G. Myszka, High-Resolution and high-throughput protocols for measuring drug/human serum albumin interactions using BIACORE, Anal. Biochem. 296 (2001) 197–207.

[32] E. Fabini, G.M.L. Fiori, D. Tedesco, N.P. Lopes, C. Bertucci, Surface plasmon resonance and circular dichroism characterization of cucurbitacins binding to serum albumins for early pharmacokinetic profiling, J. Pharm. Biomed. Anal. 122 (2016) 166–172.

[33] Y. Cho, T.-S. Ko, S.-H. Cha, D.-E. Sok, Properties of acetylcholinesterase reconstituted in liposomes of a different charge*, Neurochem. Res. 20 (1995) 681–687.

[34] M. Bartolini, V. Cavrini, V. Andrisano, Monolithic micro-immobilized-enzyme reactor with human recombinant acetylcholinesterase for on-line inhibition studies, J. Chromatogr. A. 1031 (2004) 27–34.

[35] E. Milkani, C.R. Lambert, W.G. McGimpsey, Direct detection of acetylcholinesterase inhibitor binding with an enzyme-based surface plasmon resonance sensor, Anal. Biochem. 408 (2011) 212–219.

[36] T. Rosenberry, X. Brazzolotto, I. Macdonald, M. Wandhammer, M. Trovaslet-Leroy, S. Darvesh, F. Nachon, Comparison of the binding of reversible inhibitors to human butyrylcholinesterase and acetylcholinesterase: a crystallographic, kinetic and calorimetric study, Molecules. 22 (2017) 2098.

[37] Z. Radi, P. Taylor, Interaction Kinetics of reversible inhibitors and substrates with acetylcholinesterase and its fasciculin 2 complex*, (2000).

[38] M.R. Ali, M. Sadoqi, S.G. Møller, A. Boutajangout, M. Mezei, Assessing the binding of cholinesterase inhibitors by docking and molecular dynamics studies, J. Mol. Graph. Model. 76 (2017) 36–42.

[39] M.B. Khan, B.K. Palaka, T.D. Sapam, N. Subbarao, D.R. Ampasala, Screening and analysis of acetyl-cholinesterase (AChE) inhibitors in the context of Alzheimer's disease, Bioinformation. 14 (2018) 414–428.

[40] J.M. Berg, J.L. Tymoczko, L. Stryer, Free energy is a useful thermodynamic function for understanding enzymes, in: Biochemistry, Five Ed., 2002.

[41] L. Mazzei, S. Ciurli, B. Zambelli, Isothermal titration calorimetry to characterize enzymatic reactions, Methods Enzymol. 567 (2016) 215–236.

[42] P. Draczkowski, A. Tomaszuk, P. Halczuk, M. Strzemski, D. Matosiuk, K. Jozwiak, Determination of affinity and efficacy of acetylcholinesterase inhibitors using isothermal titration calorimetry, Biochim. Biophys. Acta - Gen. Subj. 1860 (2016) 967–974.

[43] W.B. Turnbull, A.H. Daranas, On the Value of c : Can low affinity systems be studied by isothermal titration calorimetry?, J. Am. Chem. Soc. 125 (2003) 14859–14866.

[44] J. Patocka, K. Kuca, D. Jun, Acetylcholinesterase and butyrylcholinesterase-important enzymes of human body, Acta Medica (Hradec Kral. 47 (2004) 215–28.

[45] H. Dvir, I. Silman, M. Harel, T.L. Rosenberry, J.L. Sussman, Acetylcholinesterase: from 3D structure to

function, Chem. Biol. Interact. 187 (2010) 10–22.

[46] R.S. Matteo, W.L. Young, E. Ornstein, A.E. Schwartz, P.A. Silverberg, J. Diaz, Pharmacokinetics and pharmacodynamics of edrophonium in elderly surgical patients, Anesth. Analg. 71 (1990) 334–9.

[47] J. Ghuman, P.A. Zunszain, I. Petitpas, A.A. Bhattacharya, M. Otagiri, S. Curry, Structural basis of the drug-binding specificity of human serum albumin, J. Mol. Biol. 353 (2005) 38–52.

[48] C.W. Goh, C.C. Aw, J.H. Lee, C.P. Chen, E.R. Browne, Pharmacokinetic and pharmacodynamic properties of cholinesterase inhibitors donepezil, tacrine, and galantamine in aged and young lister hooded rats, Drug Metab. Dispos. 39 (2011) 402–411.

Chapter 8

Multi-target-directed ligands for AD treatment: inhibitory potency evaluation of donepezil-lipoic acid hybrids

This chapter is adapted from:

Bruna S. Terra, Pedro H.C. da Silva, ***Anna Tramarin****, Lucas L. Franco, Elaine F.F. da Cunha, Fernando Macedo Junior, Teodorico C. Ramalho, Manuela Bartolini, Maria Laura Bolognesi, Ângelo de Fátima. Two novel donepezil-lipoic acid hybrids: synthesis, anticholinesterase and antioxidant activities and theoretical studies. Journal of Brazilian Chemical Society (2018), 29: 738-747. Doi 10.21577/0103-5053.20170196.* [1].

Abstract

Alzheimer disease (AD) is a complex disease related to multiple pathogenic mechanisms. A strategy to develop effective drugs is based on the so-called multi-target-directed ligands (MTDL) by using hybrid compounds. So, in the present study, we analyzed two hybrids, containing the indanone-piperidine moiety of donepezil, a drug approved for the treatment of AD, and the lipoic acid scaffold, an antioxidant compound endowed with neuroprotective effects. The latter hybrid displayed moderate inhibitory activity against human AChE and greater activity against human BuChE. The selectivity for BuChE was further rationalized by theoretical study. Importantly, studies carried out by other groups involved in the project showed that the second hybrid had a good antioxidant activity, exhibiting better ability in scavenging 2,2-diphenyl-1-picrylhydrazyl (DPPH) radicals than lipoic acid.

8.1 Introduction

In the continuous research of more efficient drugs for treating Alzheimer disease (AD), the so-called multi-target-directed ligands (MTDLs) approach represents an intriguing strategy [2]. This method builds on the development of a single drug that can simultaneously interact with different targets. The advantages of this polypharmacological strategy, when compared with the administration of a combination of multiple drugs, are the reduction of the risk of drug-drug interactions and a simplification of the pharmacokinetic and pharmacodynamic studies. Moreover, the success rate of the treatment of a complex disease of the elderly, as AD, should be higher [3]. In this context, MTDLs design approach may offer advantages in drug discovery due to multiple targets involved in AD etiology. Near the formation of amyloid plaques, neurofibrillary tangles and the decrease of cholinergic tone and ACh levels, an extensive oxidative stress has been observed which is a result of an altered balance of formation of reactive oxygen species (ROS) *versus* scavenging activity [4,5]. The production of ROS is also related to calcium homeostasis; the misbalance of calcium influx affects the mitochondrial enzymes and ROS production is a normal part of the electron transport chain. However, excessive levels of these species damage proteins, lipids and nucleic acids [6].

Donepezil, a palliative drug approved in 1996, is indicated for the treatment of mild and moderate forms of AD [7]. Its structure represents an attractive starting point for the rational design of new MTDLs that can inhibit acetyl-(AChE) and butyryl-(BuChE) cholinesterases and, at the same time, interact with other targets involved in AD onset and progression [8]. Many prototypes for new drugs based on the hybridization strategy have been developed starting from donepezil fragments, i.e. indanone-piperidine moiety or piperidine-benzyl fragment [9]. Furthermore, donepezil hybrids with tacrine [10,11], diaminobenzyl group, ferulic acid [12], coumarin [13] among others have been prepared. Hybrids containing the piperidine-benzyl moiety of donepezil and lipoic acid (LA) (Fig. 30) were described by several groups [14,15]. The hybrids showed activity against cholinesterase (ChE) enzymes, antagonism toward σ1 receptors, β-secretase inhibition and antioxidant activity.

LA is a natural disulfide compound present in almost all foods from animal and vegetable sources. LA and its reduced form, dihydrolipoic acid (DHLA) (Fig. 30), play an important role in pathological conditions characterized by oxidative stress such as: (*i*) scavenger of ROS, (*ii*) capacity to increase the level of reduced glutathione and other antioxidant enzymes, (*iii*) downregulation of the inflammatory processes, (*iv*) scavenging of lipid peroxidation products, (*v*) redox active transition metal chelation, (*vi*) increase of ACh production by activation of choline acetyltransferase [16,17]. On the basis of such activities, LA can exert beneficial effects in AD, possibly stabilizing cognitive functions [18]. Thus, LA is a good prototype to design new hybrids to combat AD, and

previously developed LA hybrids maintained the antioxidant activity and showed other beneficial activities such as inhibition of AChE and BuChE as well as neuroprotective and anti-inflammatory activity [19,20].

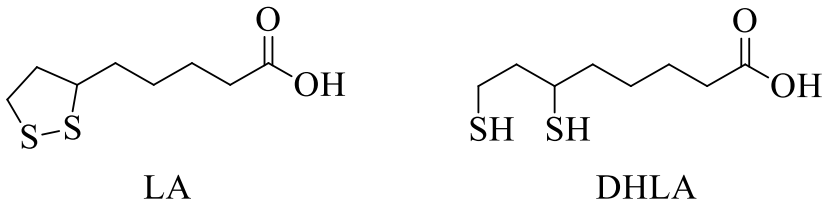

Figure 30| Chemical structures of lipoic acid (LA) and of dihydrolipoic acid (DHLA).

In 2005, Rosini *et al.* [18] reported the synthesis of lipocrine, an LA-tacrine hybrid, which further inspired the development of other hybrids featuring an LA fragment connected with N^1-ethyl-N^1-(2-methoxy-benzyl)-hexane-1,6-diamine moiety or with rivastigmine. Although there are works involving the hybridization of the benzyl-piperidine moiety of donepezil with LA, to our knowledge, there is no report on the hybridization of the indanone-piperidine moiety with LA.

In this context, two hybrids containing the indanone-piperidine moiety of donepezil and the LA scaffold were designed and synthesized by the research group of Ângelo de Fátima with the aim of achieving new MTDLs for the treatment of AD [1]. The newly synthesized hybrids were investigated by us in terms of anticholinesterases activity towards both human AChE (hAChE) and BuChE (hBuChE), using classic in solution approach [21]. The purpose of inhibition studies was the quantification of hybrids inhibition potency as well as the assessment of retained inhibition capacity of these compounds when the pharmacophore of donepezil was combined with LA.

8.2 Experimental section

8.2.1 Materials

Human recombinant acetylcholinesterase (*h*AChE) (EC 3.1.1.7) lyophilized powder, butyrylcholinesterase (E.C. 3.1.1.8) from human serum (hBuChE), S-acetylthiocholine iodide (ACTh), butyrylthiocholine iodide (BTCh), respectively). 5,5'-dithio-bis(2-nitrobenzoic acid) (DTNB; Ellman's reagent), donepezil hydrochloride, dipotassium hydrogenphosphate trihydrate, potassium dihydrogenphosphate and Triton X-100 were purchased from Sigma-Aldrich (Milan, Italy). HPLC grade methanol (MeOH) was supplied by Honeywell (Milan, Italy). Plasma from human prepared from pooled human blood was purchased from Sigma-Aldrich (Milan, Italy).

Deionized water was obtained by Milli-Q system (Millipore, Milford, MA, USA). All solutions were filtered with 0.22 μm membrane filters (Millipore, Milford, MA, USA) before use.

All compounds (Fig. 31) (compound 1 and 2) and lipoic acid were synthesized by Bruna Terra under the supervision of Prof. Ângelo de Fátima and were characterized by ^{1}H NMR, ^{13}C NMR, IR and ESI-MS [1].

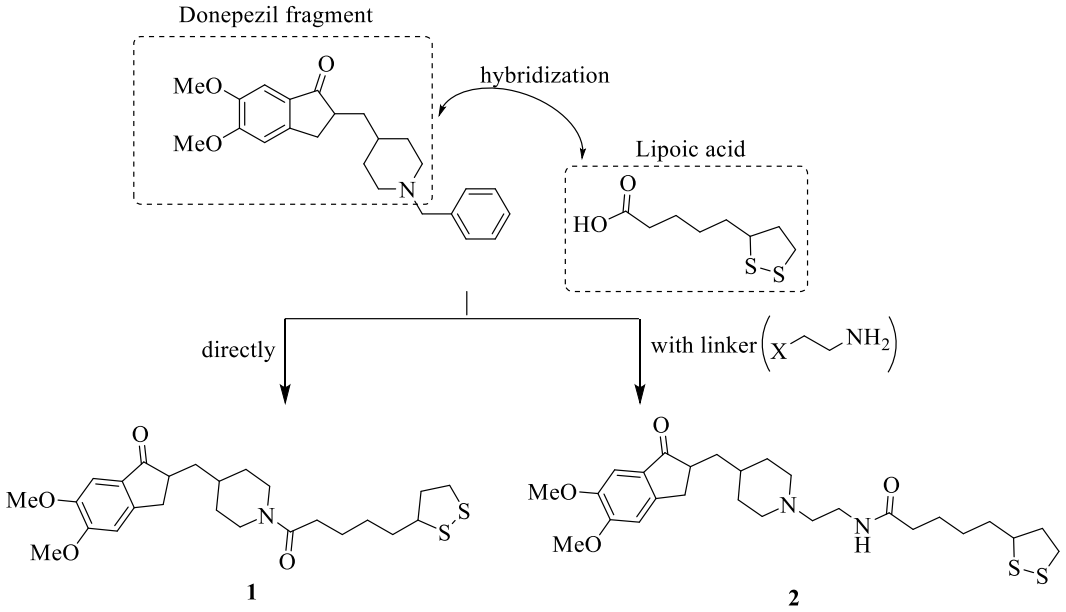

Figure 31| Chemical structures of hybrids 1 and 2. Schematic design strategy for the synthesis of compound 1 and 2 performed by Terra *et al.*

8.2.2 Determination of inhibitory effect on AChE and BuChE activity

The capacity of hybrids and donepezil to inhibit AChE activity was assessed using the Ellman's method [21]. Initial rate assays were performed at 37 °C with a Jasco V-530 double beam Spectrophotometer by following the rate of increase in the absorbance at 412 nm for 3 min. AChE stock solution was prepared by dissolving hAChE in phosphate buffer (0.1 M; pH = 8.0) containing

Triton X-100 0.1%. Stock solution of BuChE was prepared by dissolving the lyophilized powder in an aqueous solution of gelatine 0.1%. The final assay solution consisted of a phosphate buffer (pH = 8.0; 0.1 M), with the addition of 340 μM DTNB, 0.02 unit/mL of hAChE or hBuChE and 550 μM of substrate ATCh or BTCh, respectively. Stock solutions of hybrid **2** were prepared in methanol and diluted in methanol, while donepezil was solubilized in water and dilutions were prepared in water. Five different concentrations of inhibitor were selected in order to obtain inhibition of the enzymatic activity comprised between 20 and 80%. 50 μL aliquots of increasing concentration of inhibitor were added to the assay solution and pre-incubated for 20 min at 37 °C with the enzyme before the addition of the substrate. Assays were carried out with a blank containing all components except AChE or BuChE in order to account for the non-enzymatic reaction. The reaction rates were compared and the percent inhibition due to the presence of inhibitor was calculated. Each concentration was analyzed in duplicate, and IC_{50} values were determined graphically from log concentration–% inhibition curves (GraphPad Prism 4.03 software, GraphPad Software Inc.).

8.2.3 Evaluation of the formation of LA- and hybrid 2-albumin adducts by LC-MS

The reactivity of synthesized compounds to form mixed disulfides with proteins was tested by assessing the capacity of LA and hybrid **2** to form covalent adducts with albumin, which is the most abundant protein in plasma. 10 mM LA and hybrid **2** stock solutions were prepared in methanol. Aliquots of stock solutions were added to pooled human plasma to reach a final concentration of 180 μM. Plasma with the addition of an equal amount of solvent was used as blank sample. All solutions were incubated for 3 h at 37 °C, under gentle shaking (400 rpm) using a Thermomixer (Eppendorf, Milan, Italy). Afterwards, they were diluted in deionized water (1:100) and analyzed by LC-MS using the analytical method previously developed by Naldi *et al.* [22].

8.3 Results and discussion

To determine the potential interest of the new donepezil-LA hybrids for the treatment of AD, the inhibitory potency toward hAChE and hBuChE was assessed by Ellman's method [21]. Results, expressed as half maximal inhibitory concentration (IC_{50}) values, i.e. the IC_{50} that reduces the cholinesterase activity by 50%, are listed in Table 9. In particular, anti-BuChE activity has recently raised interest because it was shown that with AD progression, BuChE activity in specific brain regions increases while AChE activity is greatly reduced [23]. Conversely to donepezil, which is an AChE selective inhibitor, hybrid **2** showed to be a selective BuChE inhibitor. Hybrid **1** was scarcely soluble in the assay conditions. At the highest tested concentration (50 mM) hybrid **1** did not significantly inhibit ChE enzymes.

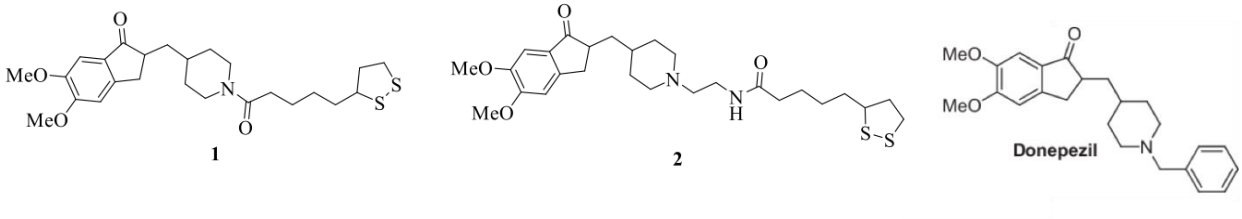

Table 9| Anticholinesterases activity of hybrids **1**, **2** and the reference compound Donepezil

Compound	IC_{50}[a] **hAChE (μM) ±SEM**[b]	IC_{50}[a] **hBuChE (μM) ±SEM**[b]	**BuChE/AChE**
1	n.a.[c]	n.a.[c]	--
2	171 ± 10	62.9 ± 5.4	0.37
Donepezil	0.0203 ± 0.0013	7.13 ±0.19	351

[a] IC_{50}: inhibitory concentration; [b] SEM stands for standard error of the mean; [c] n.a. stands for not active (% inhibition <10%) at the highest concentration achievable (50 μM) in the assay conditions.

In order to prove the rationale of these compounds, their antioxidant activity was tested by other coauthors by means of 2,2-diphenyl-1-picrylhydrazyl (DPPH) antioxidant assay [42]. LA, selected as reference compound, confirmed its weak DPPH radical scavenging activity compared to the corresponding reduced form, i.e. dihydrolipoic acid (DHLA), in agreement with data reported in literature (half maximal effective concentration, EC_{50} >> 100 μM [24], EC_{50} > 500 μM [25,26]). Compound **1** displayed a similarly weak antioxidant profile of LA, exhibiting a scavenging activity lower than 50% at the maximum tested concentration. Conversely, compound **2** showed a concentration-dependent DPPH scavenging activity with an EC_{50} of 300 μM. Notwithstanding the still weak scavenging activity of **2**, since the antioxidant property of LA and related hybrids is

granted by the 1,2-dithiolane moiety, which is maintained in all tested compounds, other studies need to be performed to better understand the observed trend, e.g. by assessing any chemical instability in the assay conditions.

The reactivity of synthesized compounds to form mixed disulfides with proteins was evaluated by assessing the possible formation of covalent adducts between the dithiolane ring of both LA and hybrid **2** with albumin, which was selected as reference protein as the most abundant protein in plasma [22]. LC-MS analysis showed that no structural modification of albumin (no adduct was formed) occurred upon 3h-incubation at 37°C (data not shown) when concentrations equals to the IC_{50} value of **2** were used. These data are in agreement with the high administration dosage suggested for LA (300-600 mg) and the absence of any record on immunogenicity at the recommended dosages [27,28].

Docking studies on these novel hybrids with both hAChE and hBuChE were also performed by coauthors and provided further insights into their binding mode and their potential binding sites. For complete results and discussion of these sections as well as for hybrids synthesis details, please refer to the original article [1].

8.4 Conclusions

In this work, two donepezil-LA hybrids containing the indanone-piperidine moiety of donepezil, namely compound **1** and compound **2,** were designed and synthesized by the group of Ângelo de Fátima with global yields of 42% and 19%, respectively. Anticholinesterase studies performed by us highlighted that hybrid **2** was a selective BuChE inhibitor even if less potent than donepezil. Moreover, integration of these results with antioxidant activity and docking studies carried out by the other research groups involved in the project provided further insights into the behavior of these compounds. Indeed, combination of inhibitory studies with molecular modeling investigation highlighted hybrids binding mode and their binding site on ChE. In particular, the lower activity observed was ascribed to the loss of the interaction with Trp86A, an amino acid of the AChE catalytic site, when the benzyl moiety of donepezil was replaced by LA. Moreover, the selectivity of **2** toward hBuChE may be explained by the larger gorge of this enzyme, which can better accommodate hybrid **2**. Finally, and quite interestingly, hybrid **2** showed better scavenging ability toward DPPH radicals than LA. The combined anti-ChE and antioxidant properties exhibited by the hybrid **2** confirmed its potential as anti-AD agent also suggesting further studies on donepezil-LA hybrids.

References

[1] B.S. Terra, P.H.C. Da Silva, A. Tramarin, L.L. Franco, E.F.F. Da Cunha, F. Macedo, T.C. Ramalho, M. Bartolini, M.L. Bolognesi, Â. De Fátima, Two novel donepezil-lipoic acid hybrids: synthesis, anticholinesterase and antioxidant activities and theoretical studies, J. Braz. Chem. Soc. 29 (2018) 738–747.

[2] A. Cavalli, M.L. Bolognesi, A. Mìnarini, M. Rosini, V. Tumiatti, M. Recanatini, C. Melchiorre, Multi-target-directed ligands to combat neurodegenerative diseases, J. Med. Chem. 51 (2008) 347–372.

[3] M.L. Bolognesi, Polypharmacology in a single drug: multitarget drugs, Curr. Med. Chem. 20 (2013) 1639–45.

[4] D. Praticò, Peripheral biomarkers of oxidative damage in Alzheimer's disease: the road ahead, Neurobiol. Aging. 26 (2005) 581–3.

[5] C. Behl, B. Moosmann, Antioxidant neuroprotection in Alzheimer's disease as preventive and therapeutic approach, Free Radic. Biol. Med. 33 (2002) 182–91.

[6] G.E. Gibson, Interactions of oxidative stress with cellular calcium dynamics and glucose metabolism in Alzheimer's disease, Free Radic. Biol. Med. 32 (2002) 1061–70.

[7] L.H. Opie, Donepezil for severe Alzheimer's disease, Lancet. 368 (2006) 361–362.

[8] L. Ismaili, B. Refouvelet, M. Benchekroun, S. Brogi, M. Brindisi, S. Gemma, G. Campiani, S. Filipic, D. Agbaba, G. Esteban, M. Unzeta, K. Nikolic, S. Butini, J. Marco-Contelles, Multitarget compounds bearing tacrine- and donepezil-like structural and functional motifs for the potential treatment of Alzheimer's disease, Prog. Neurobiol. 151 (2017) 4–34.

[9] M.C. Rodrigues Simões, F.P. Dias Viegas, M.S. Moreira, M. de Freitas Silva, M.M. Riquiel, P.M. da Rosa, M.R. Castelli, M.H. dos Santos, M.G. Soares, C. Viegas, Donepezil: an important prototype to the design of new drug candidates for Alzheimer's disease, Mini Rev. Med. Chem. 14 (2014) 2–19.

[10] P. Camps, X. Formosa, C. Galdeano, T. Gómez, D. Muñoz-Torrero, M. Scarpellini, E. Viayna, A. Badia, M.V. Clos, A. Camins, M. Pallàs, M. Bartolini, F. Mancini, V. Andrisano, J. Estelrich, M. Lizondo, A. Bidon-Chanal, F.J. Luque, Novel donepezil-based inhibitors of acetyl- and butyrylcholinesterase and acetylcholinesterase-induced beta-amyloid aggregation, J. Med. Chem. 51 (2008) 3588–98.

[11] D. Alonso, I. Dorronsoro, L. Rubio, P. Muñoz, E. García-Palomero, M. Del Monte, A. Bidon-Chanal, M. Orozco, F.J. Luque, A. Castro, M. Medina, A. Martínez, Donepezil–tacrine hybrid related derivatives as new dual binding site inhibitors of AChE, Bioorg. Med. Chem. 13 (2005) 6588–6597.

[12] Y. Zhu, K. Xiao, L. Ma, B. Xiong, Y. Fu, H. Yu, W. Wang, X. Wang, D. Hu, H. Peng, J. Li, Q. Gong, Q. Chai, X. Tang, H. Zhang, J. Li, J. Shen, Design, synthesis and biological evaluation of novel dual inhibitors of acetylcholinesterase and β-secretase, Bioorg. Med. Chem. 17 (2009) 1600–1613.

[13] M. Catto, L. Pisani, F. Leonetti, O. Nicolotti, P. Pesce, A. Stefanachi, S. Cellamare, A. Carotti, Design, synthesis and biological evaluation of coumarin alkylamines as potent and selective dual binding site inhibitors of acetylcholinesterase, Bioorg. Med. Chem. 21 (2013) 146–52.

[14] O. Prezzavento, E. Arena, C. Parenti, L. Pasquinucci, G. Aricò, G.M. Scoto, S. Grancara, A. Toninello, S. Ronsisvalle, Design and synthesis of new bifunctional sigma-1 selective ligands with antioxidant activity, J. Med. Chem. 56 (2013) 2447–2455.

[15] M. Estrada, C. Pérez, E. Soriano, E. Laurini, M. Romano, S. Pricl, J.A. Morales-García, A. Pérez-Castillo, M.I. Rodríguez-Franco, New neurogenic lipoic-based hybrids as innovative Alzheimer's drugs with σ-1 agonism and β-secretase inhibition, Future Med. Chem. 8 (2016) 1191–1207.

[16] L. Holmquist, G. Stuchbury, K. Berbaum, S. Muscat, S. Young, K. Hager, J. Engel, G. Münch, Lipoic acid as a novel treatment for Alzheimer's disease and related dementias, Pharmacol. Ther. 113 (2007) 154–164.

[17] A.I. Durrani, H. Schwartz, M. Nagl, G. Sontag, Determination of free α-lipoic acid in foodstuffs by HPLC coupled with CEAD and ESI-MS, Food Chem. 120 (2010) 1143–1148.

[18] M. Rosini, E. Simoni, M. Bartolini, A. Tarozzi, R. Matera, A. Milelli, P. Hrelia, V. Andrisano, M.L. Bolognesi, C. Melchiorre, Exploiting the lipoic acid structure in the search for novel multitarget ligands against Alzheimer's disease, Eur. J. Med. Chem. 46 (2011) 5435–42.

[19] M. Koufaki, A. Detsi, C. Kiziridi, Multifunctional lipoic acid conjugates, Curr. Med. Chem. 16 (2009) 4728–42.

[20] M.L. Bolognesi, A. Minarini, V. Tumiatti, C. Melchiorre, Lipoic acid, a lead structure for multi-target-directed

drugs for neurodegeneration, Mini Rev. Med. Chem. 6 (2006) 1269–74.

[21] G.L. Ellman, K.D. Courtney, V. Andres, R.M. Featherstone, A new and rapid colorimetric determination of acetylcholinesterase activity, Biochem. Pharmacol. 7 (1961) 88–95.

[22] M. Naldi, F.A. Giannone, M. Baldassarre, M. Domenicali, P. Caraceni, M. Bernardi, C. Bertucci, A fast and validated mass spectrometry method for the evaluation of human serum albumin structural modifications in the clinical field, Eur. J. Mass Spectrom. 19 (2013) 491–496.

[23] N.H. Greig, T. Utsuki, Q. Yu, X. Zhu, H.W. Holloway, T. Perry, B. Lee, D.K. Ingram, D.K. Lahiri, A new therapeutic target in Alzheimer's disease treatment: attention to butyrylcholinesterase, Curr. Med. Res. Opin. 17 (2001) 159–165.

[24] M.L. Bolognesi, C. Bergamini, R. Fato, J. Oiry, J.-J. Vasseur, M. Smietana, Synthesis of new lipoic acid conjugates and evaluation of their free radical scavenging and neuroprotective activities, Chem. Biol. Drug Des. 83 (2014) 688–696.

[25] S.R.P. Madawala, R.E. Andersson, J.A. Jastrebova, M. Almeida, P.C. Dutta, Novel conjugates of 1,3-diacylglycerol and lipoic acid: synthesis, DPPH assay, and RP-LC-MS-APCI analysis, J. Lipids. 2011 (2011) 419809.

[26] G. Melagraki, A. Afantitis, O. Igglessi-Markopoulou, A. Detsi, M. Koufaki, C. Kontogiorgis, D.J. Hadjipavlou-Litina, Synthesis and evaluation of the antioxidant and anti-inflammatory activity of novel coumarin-3-aminoamides and their alpha-lipoic acid adducts, Eur. J. Med. Chem. 44 (2009) 3020–3026.

[27] T.S. Foster, Efficacy and safety of α-Lipoic acid supplementation in the treatment of symptomatic diabetic neuropathy, Diabetes Educ. 33 (2007) 111–117.

[28] D.R. Cremer, R. Rabeler, A. Roberts, B. Lynch, Safety evaluation of α-lipoic acid (ALA), Regul. Toxicol. Pharmacol. 46 (2006) 29–41.

Chapter 9

Multi-target-directed ligands for AD treatment: inhibitory potency evaluation of tacrine-dihydropyrimidine hybrids

This chapter is adapted from:

Mourad Chioua, Eleonora Buzzi, Ignatio Moraleda, Isabel Iriepa, Maciej Maj, Artur Wnorowski, Catia Giovannini, ***Anna Tramarin****, Federica Portali, Lhassane Ismaili, Pilar Lóperz-Alvarado, Maria Laura Bolognesi, Krzysztof Jóźviak, J. Carlos Menéndez, José Marco-Contelles, Manuela Bartolini. Tacripyrimidines, the first tacrine-dihydropyrimidine hybrids, as multi-target-directed ligands for Alzheimer's disease. European Journal of Medicinal Chemistry (2018), 155: 839-846. Doi 10.1016/j.ejmech.2018.06.044.* [1].

Abstract

Notwithstanding combination of cholinesterase (ChE) inhibition and calcium channel blockade within a multitarget therapeutic approach is envisaged as potentially beneficial to confront Alzheimer's disease (AD), this strategy has been scarcely investigated. To explore this promising line, a series of 5-amino-4-aryl-3,4,6,7,8,9-hexahydropyrimido[4,5-b]quinoline-2(1*H*)-thiones (tacripyrimidines) were designed by juxtaposition of tacrine, a ChE inhibitor (ChEI), and 3,4-dihydropyrimidin-2(1*H*)-thiones, as efficient calcium channel blockers (CCBs). In agreement with their design, all tacripyrimidines, except the unsubstituted parent compound and its *p*-methoxy-derivative, acted as moderate to potent CCBs with activities generally similar or higher than the reference CCB drug nimodipine and were modest-to-good ChE inhibitors. Most interestingly, the 3'-methoxy-derivative emerged as the first well balanced ChEI/CCB inhibitor, acting as low micromolar hChE inhibitor (3.05 μM and 3.19 μM on hAChE and hBuChE, respectively) and moderate CCB (30.4 % at 1 μM) with no significant hepatotoxicity toward HepG2 cells and good predicted oral absorption and blood brain barrier permeability.

9.1 Introduction

Alzheimer's disease (AD) is a devastating, age-related neurodegenerative disorder [2] which has become a major and rising public health concern because of the high costs related to the management of the increasing number of AD patients, who have no effective treatment for cure. Clinical failure has been partially ascribed to the complexity of AD pathology, which features a multifaceted interplay of several factors, whose exact role is not yet fully understood [3]. This observation has laid down the basis for the current interest in the so-called Multitarget Directed Ligands (MTDLs), a heterogeneous class of compounds that are designed to simultaneously address more than one pathological event [4,5]. Based on this strategy, a number of MTDLs have been developed by modification of commercial drugs and active scaffolds [4-12]. Among those, tacrine-based multitarget derivatives have been shown to be able to hit several key targets involved in AD and exert multiple beneficial activities both *in vitro* and *in vivo*. Indeed, the high ligand efficiency has made tacrine scaffold an ideal starting point for designing and achieving highly active MTDLs [9-11].

Based on these considerations, some years ago José Marco-Contelles *et al.* designed a class of MTDs called tacripyrines (**I** Fig. 32) by juxtaposition of tacrine and nimodipine, as reference molecules endowed with anticholinesterase and calcium antagonism profile, respectively, for the treatment of AD [13,14]. The most interesting tacripyrine, i.e., (±)-*p*-methoxytacripyrine (Fig. 32), showed high selectivity toward AChE, moderate inhibition of calcium intake after potassium stimulation in SHSY5 cells, weak inhibition of the pro-aggregating action of hAChE on Aβ peptide, and moderate inhibition of Aβ self-aggregation (34.9 %) [14,15]. Interest on calcium channel blockers (CCBs) is based on the fact that calcium levels regulate neuronal plasticity underlying learning and memory and neuronal survival. Dysregulation of the intracellular calcium homeostasis in AD is thought to play a role in neuron degeneration and death [16,17]. Consequently, blocking the entrance of Ca^{2+} through L-type voltage-gated calcium channels is considered a valuable strategy to prevent neuronal damage in AD [18,19]. Furthermore, CCBs have been shown to improve cerebrovascular perfusion and attenuate amyloid-β-induced neuronal decline and neurotoxicity, improve cell survival in the presence of Aβ *in vitro*, and exert neuroprotective effects in animal models [20-22]. These beneficial effects have been confirmed in clinical trials for the CCBs nimodipine and nilvadipine, which have reached phase III (ClinicalTrials.gov identifier NCT02017340).

With these premises in mind and in the attempt of balancing the anticholinesterase and Ca-antagonism activities by increasing CCB activity, MTDs tacripyrimidines (**II**, Figure 32) were designed by Contelles and coworkers by focusing again on tacrine scaffold as a template for

cholinesterase (ChE) inhibition and on the well-known capacity of 3,4-dihydropyrimidin-2(1*H*)-thiones (**III**, Figure 32) to act as efficient calcium channel blockers [23,24]. Furthermore, very promisingly, dihydropyirimidine-thiones were recently shown to exert neuroprotective activity toward Aβ-induced toxicity in a yeast model for proteinopathies, likely by attenuating the metal-mediated toxicity of Aβ [25].

In this context, the newly synthesized tacripyrimidines were investigated by us in terms of inhibitory activity toward both human ChE enzymes. Moreover, for the most interesting derivatives the mode of interaction with human AChE (hAChE) was studied by Prof. Isabel Iriepa and coworkers.

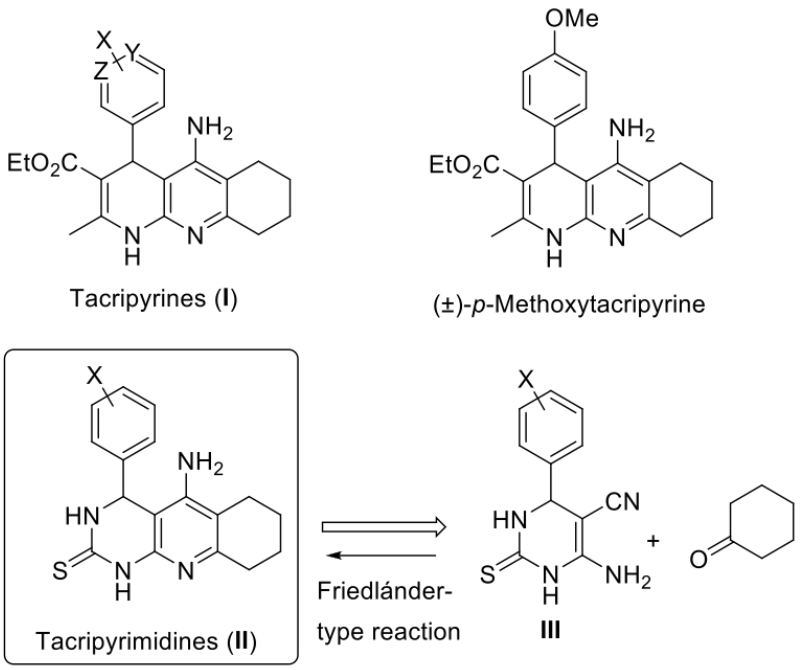

Figure 32| Structure of tacripyrines (I), (±)-p-methoxytacripyrine, and retrosynthetic analysis of the synthesis of tacripyrimidines (II).

9.2 Experimental section

9.2.1 Materials

Human recombinant acetylcholinesterase (*h*AChE) (EC 3.1.1.7) lyophilized powder, butyrylcholinesterase (E.C. 3.1.1.8) from human serum (*h*BuChE), S-acetylthiocholine iodide (ACTh), butyrylthiocholine iodide (BTCh), 5,5'-dithio-bis(2-nitrobenzoic acid) (DTNB; Ellman's reagent), tacrine hydrochloride, dipotassium hydrogenphosphate trihydrate, potassium dihydrogenphosphate and Triton X-100 were purchased from Sigma-Aldrich (Milan, Italy). Deionized water was obtained by Milli-Q system (Millipore, Milford, MA, USA). All solutions were filtered with 0.22 μm membrane filters (Millipore, Milford, MA, USA) before use.

All compounds (Fig. 33) were synthetized by Contelles and coworkers and were characterized by ^{1}H NMR and ^{13}C NMR [1].

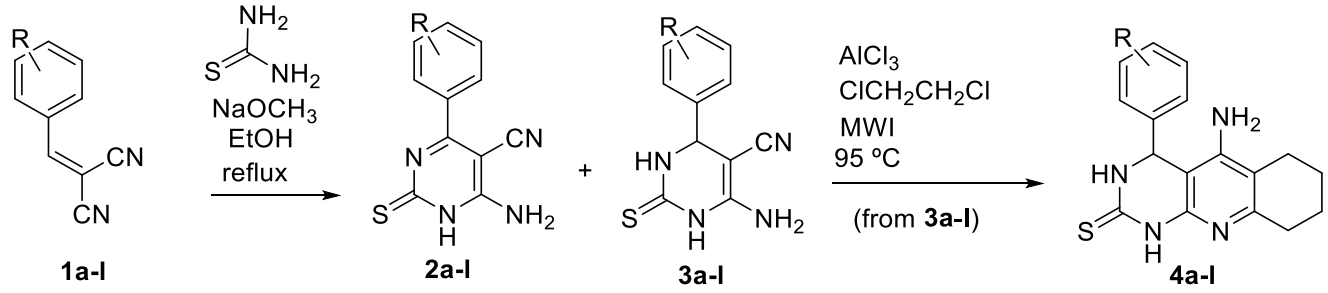

4a (X= H), **4b** (4'-Me), **4c** (3'-Me), **4d** (4'-OMe), **4e** (3'-OMe), **4f** (2'-OMe), **4g** (3',4'-OCH^2O-)
4h (4'-NMe_2), **4i** (4'-F), **4j** (4'-Cl), **4k** (4'-Br), **4l** (4'-NO_2)

Figure 33| Synthesis of tacripyrimidines 4a-l. For synthesis procedure, ^{1}H NMR and ^{13}C NMR please refer to original article [1].

9.2.2 Inhibition of human AChE and BuChE activities

The capacity of tested compounds to inhibit *h*AChE and *h*BuChE activity was assessed using the Ellman's method [26]. Initial rate assays were performed at 37 °C with a Jasco V-530 double beam Spectrophotometer: the rate of increase in the absorbance at 412 nm was followed for 3 min. *h*AChE stock solution was prepared by dissolving human recombinant AChE lyophilized powder in 0.1 M phosphate buffer (pH = 8.0) containing Triton X-100 0.1 %. Stock solution of BuChE from human serum was prepared by dissolving the lyophilized powder in an aqueous solution of gelatine 0.1 %. Stock solutions of inhibitors (1 or 2 mM) were prepared in methanol. Five increasing concentrations of the inhibitor were used, able to give an inhibition of the enzymatic activity in the range of 20-80 %. The assay solution consisted of a 0.1 M phosphate buffer (pH = 8.0), with the addition of 340 mM DTNB, 0.02 unit/mL of *h*AChE or *h*BChE and 550 μM of substrate (ATCh or BTCh, respectively). 50 μL aliquots of increasing concentration of the tested compound were added

to the assay solution and preincubated for 20 min at 37°C with the enzyme, followed by the addition of substrate. Assays were carried out with a blank containing all components except enzymes in order to account for the non-enzymatic reaction. The reaction rates were compared and the percent inhibition due to the presence of tested inhibitor at increasing concentration was calculated. Each concentration was analysed in triplicate, and IC_{50} values were determined graphically from log concentration–inhibition curves (GraphPad Prism 4.03 software, GraphPad Software Inc.). Each IC_{50} value was determined from at least two independent experiments.

9.2.3 Kinetic studies for inhibition of human AChE activity by compounds 4k and 4e

The mode of inhibition of compounds **4k** and **4e** and the corresponded was assessed by building Lineweaver-Burk double reciprocal plots at relatively low concentration of substrate (0.11-0.55 mM) and using the same experimental conditions used to assess hAChE activity see Section 9.2.2). The plots were assessed by a weighted least square analysis that assumed the variance of v to be a constant percentage of v for the entire data set. Data analysis was performed with GraphPad Prism 4.03 software (GraphPad Software Inc.). To confirm the mode of inhibition, Dixon plots were obtained by plotting $1/v$ *versus* inhibitor concentration [27].

K'_i (dissociation constant for the enzyme-substrate-inhibitor complex) value was determined by plotting the apparent $1/v_{max,\,app}$ versus inhibitor concentration [27,28].

9.3 Results and discussion

9.3.1 Inhibition of cholinesterases

With compounds **4a-l** in hand, we first addressed their hChE inhibition capacity, following Ellman's protocol [28]. As shown in Table 10, most of tacripyrimidines **4a-l** are hAChEI with IC_{50} values ranging from 3.05 μM (**4e**) to 31.0 μM (**4i**), with the exception of tacripyrimidine **4k** (hAChE: IC_{50}= 0.0373 μM), the most selective and potent hAChEI within the series. On the basis of the inhibitory potencies, some structure–activity relationship (SAR) could be drawn. Tacripyrimidines bearing strong electron-donor (4'-NMe_2 for **4h**; 2'-OMe for **4f**) or electron-withdrawing (4'-NO_2 for **4l**) substituents, and moderate electron-donor (4'-Me for **4b**) or electron-withdrawing (4'-F for **4i**) substituents, regardless of their location at the aromatic ring, were the weakest hAChEIs. Among tacripyrimidines bearing a methoxy group, the most potent was compound **4e**, followed by **4d** and **4f**, position C3' being clearly preferred to C2' and C4'. This observation is also confirmed by the comparison of compound **4b** (4'-Me) and **4c** (3'-Me). Not surprisingly, the three most potent hAChEIs were the 5-amino-4-(3-bromophenyl)-3,4,6,7,8,9-hexahydropyrimido[4,5-b]quinoline-2(1*H*)-thione (**4k**), bearing a moderate electron-withdrawing substituent (Br) at C'3, followed by compound **4e** (3'-OMe), which was 81.8-fold less potent, and tacripyrimidine **4j** (C'4-Cl). Interestingly, compound **4k** was a 9.4-fold more potent inhibitor than tacrine.

By comparing the inhibition rate of the compounds belonging to the tacripyrimidine series to reference compounds, it can be concluded that **4k**, the most potent AChEI in the tacripyrimidine series, is 10-fold more potent than tacrine in inhibiting hAChE, and it is also about 35 folds more potent than the best tacripyrine (*p*-methoxytacripyrine - p-MT, Table 10).

Concerning inhibition of hBuChE, tacripyrimidines **4a-l** showed significant selectivity for hBuChE, with the exception of compounds **4g**, **4h**, and **4k** (which showed a reverse trend), with IC_{50} values spanning more than four orders of magnitude, i.e., varying from 0.372 μM (**4j**, the most potent hBuChEI within the series) to 154 μM (**4h**). Compound **4e** (3'-OMe) exerted a balanced inhibition of both ChEs, in the micromolar range. Regarding the SAR for BuChE inhibition, almost similar trends were observed. Indeed, the most potent electron-donor substituents (4'NMe_2 in **4h**; 3',4'-OCH_2O- in **4g**, and 2'-OMe in **4f**) afforded the poorest hBuChEIs, C'3 being a preferred position for a better hBuChE inhibition (compare compounds **4b** and **4c** for the Me group), although location at C'4 is also favored (compare compounds **4d-e** for the OMe motif). Compared with tacrine, compound **4j** was a 9.3-fold less potent hBuChEI.

Table 10| IC_{50} (μM) for the inhibition of hAChE and hBuChE by tacripyrimidines **4a-l** and tacrine. Calcium intake blockade induced by tacripyrimidines **4a-l** and nimodipine was tested by coworkers and values are reported for comparison purposes [1].

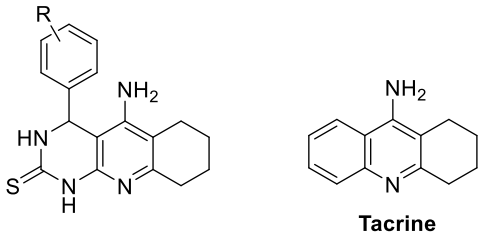

Compound	R	hAChE [a] IC_{50} (μM) ± SEM	hBuChE [a] IC_{50} (μM) ± SEM	calcium intake blockade (%) ± SEM[b]
4a	H	10.8 ± 0.9	5.68 ± 0.38	10.58 ± 1.78[n/s]
4b	4'-Me	23.8 ± 1.4	3.47 ± 0.15	14.69 ± 3.77
4c	3'-Me	10.1 ± 1.1	2.65 ± 0.25	40.01 ± 4.45
4d	4'-OMe	7.64 ± 0.43	1.75 ± 0.14	23.58 ± 2.31
4e	3'-OMe	**3.05 ± 0.28**	**3.19 ± 0.11**	30.40 ± 2.61
4f	2'-OMe	31.2 ± 1.5	11.7 ± 0.6	32.18 ± 2.92
4g	3',4'-OCH_2O-	8.18 ± 0.97	37.5 ± 2.4	36.76 ± 3.57
4h	4'-NMe_2	24.1 ± 3.1	154 ± 23	**59.01 ± 1.69**
4i	4'-F	31.0 ± 1.2	10.0 ± 0.7	23.31 ± 2.96
4j	4'-Cl	5.28 ± 0.19	**0.372 ± 0.021**	38.00 ± 3.36
4k	3'-Br	**0.0373 ± 0.0082**	1.27 ± 0.10	42.23 ± 3.85
4l	3'-NO_2	29.8 ± 1.7	2.68 ± 0.15	**66.79 ± 2.41**
p-MT[b]	-	0.105 ± 0.015	>100	32.75 ± 2.50
Tacrine	-	0.374 ± 0.053	0.0442 ± 0.0017	nd
Nimodipine	-	nd	nd	49.62 ± 1.24

[a] Results are expressed as the mean of at least two experiments in which each datum was obtained in triplicate; [b] p-MT stands for *p*-methoxytacripyrine; data from [14]. SEM stands for standard error of the mean; nd stands for not determined.

It is interesting to note that tacripyrimidines showed a distinctly different behaviour concerning BuChE inhibition in comparison with the previously developed tacripyridines, which were selective AChE inhibitors with no significant activity toward human BuChE [14]. Increasing evidence has shown that inhibition of CNS BuChE activity may be beneficial for the treatment of moderate to severe forms of AD as highlighted by the increasing interest on BuChE as a therapeutic target in AD drug discovery [29] and by the design of BuChE-selective inhibitors [30,31]. In fact, progressive elucidation of the role of BuChE in AD brain has highlighted that, with the progression of the disease, the role played by AChE in the hydrolysis of the neurotransmitter acetylcholine (ACh) decreases. Conversely, BuChE levels and activity in certain regions of AD brain have been

shown to increase [29]. Therefore, selective BuChE inhibitors could be more effective in patients with moderate to severe forms of this disease, although this tentative conclusion has not yet been clinically verified. Indeed, to date, no large-scale clinical trials of selective BuChE inhibitors have been performed in patients with AD. Studies on mild to moderate AD patients, that is the population of patients enrolled in most clinical trials on cholinesterase inhibitors, is unlikely to be able to highlight the benefits of selective BuChE inhibition. In the light of these observations, the *p*-chloro tacripyrimidine **4j**, which was a 14.2-fold more potent hBuChE inhibitor, is worth further investigation. As a perfectly balanced micromolar ChE inhibitor, 3'-methoxy-tacripyrimidine **4e** is also worth to be considered.

9.3.2 Binding mode evaluation for the most promising AChE inhibitors by in solution assay

To achieve a deeper understanding of the mode of interaction of our derivatives, tacripyrimidines **4e** and **4k,** the two most potent hAChE inhibitors, were further investigated. Lineweaver-Burk plots for both compounds showed increasing slopes (lower v_{max}) but unaltered intercept (unvaried K_m value) with increasing inhibitor concentration, indicating a non-competitive type of inhibition (Fig. 34). This type of inhibition was further confirmed by data reprocessing according to the Dixon method (1/*v vs* [I]). The K'_i constant, i.e., the dissociation constant of the enzyme-substrate-inhibitor complex, has been calculated and found to be 3.88 ± 0.30 μM for **4e** and 0.147 ± 0.011 μM for **4k**, respectively. Importantly, the interaction of these compounds with the enzyme's PAS could be advantageous in the light of AChE activity in promoting Aβ aggregation [32].

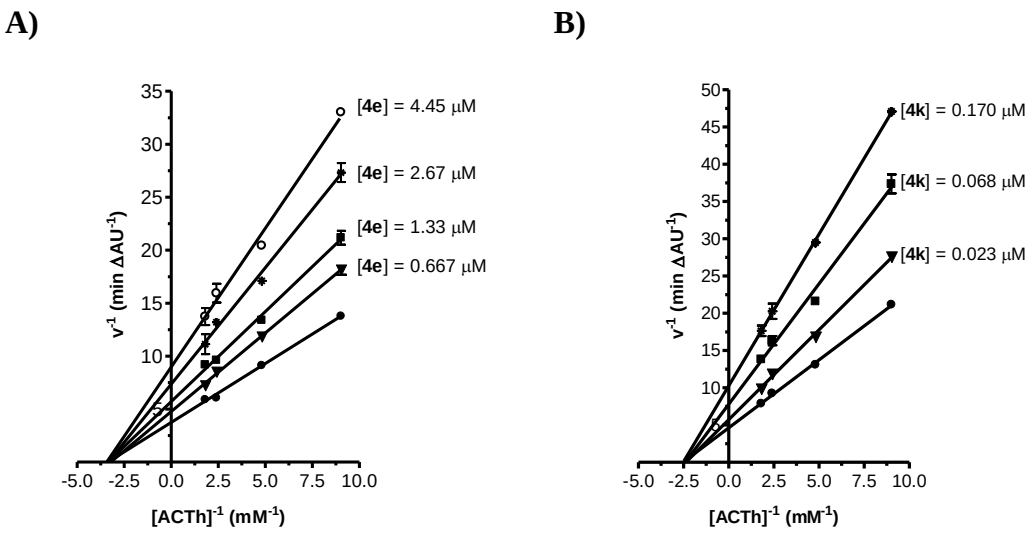

Figure 34| Kinetic study on the mechanism of hAChE inhibition by 4e (A) and 4k (B). Overlaid Lineweaver–Burk reciprocal plots of AChE initial velocity (v) at increasing substrate concentration in the absence and in the presence of inhibitor.

Based on the IC_{50} values and selectivity profile, binding of selected tacripyrimidines **4k** and **4j**, the most potent and selective AChEI and BuChEI, respectively, was investigated by an *in silico* approach (Prof. Iriepa Universidad de Alcalá, Spain) on hAChE and hBuChE. The same analysis was also carried out for tacripyrimidine **4e**, the derivative showing no selectivity.

Concerning **4k**, in agreement with the experimentally confirmed non-competitive mechanism of action of (±)-**4k**, molecular modeling studies indicated that both (*R*)-**4k** and (*S*)-**4k** interact with residues at the PAS and not with those at CAS and highlighted the key interactions involved in the binding (see original article for details). On the other hand, concerning inhibition of hBuChE by **4k**, the best-ranked docking solutions revealed that (i) BuChE can effectively accommodate both enantiomers inside the active site gorge and (ii) both enantiomers have similar binding modes.

In general, the sets of interactions highlighted by docking studies on both ChEs (see full article for a detailed discussion) pointed out that the primary amino group and the halogen atoms are the features which mostly contribute to the inhibitory activities of compounds **4j** and **4k** toward hAChE and hBuChE. The position of the halogen atom also contributes to compound selectivity toward a specific ChE by establishing a network of interactions.

Furthermore, the effectiveness of the MTDLs rational design was verified by investigating the Ca2+ influx induced by K^+-depolarization in SH-SY5Y neuroblastoma cells, previously loaded with the fluorescent dye Fluo-4AM. The study was carried out by the research group of Prof. Jozwiak (Medical University of Lublin, Poland) (Table 10).

In details, Fluo-4-loaded cells were incubated in the presence of tacripyrimidines 4a-l (1 μM) for 10 min and then stimulated with $KCl/CaCl_2$ solution in order to have a final concentration of K^+ and Ca^{2+} of 90 mM and 5 mM, respectively. Fluorescence emission intensity before stimulation and after stimulation was recorded at 535 nm (λ_{exc} = 485 nm). DMSO (0.01%) was used as a vehicle control. Nimodipine was used as a reference inhibitor, causing, at 1 μM, ~50% inhibition of K^+-evoked Ca^{2+} uptake.

All tacripyrimidines, except the unsubstituted derivative **4a**, significantly inhibited Ca^{2+} influx (Table 10) although to different extents. Interestingly, tacripyrimidines **4h** (bearing a dimethylamino substituent at position 4') and **4l** (bearing a nitro-group at position 3') were more potent CCBs than the reference drug nimodipine (59.01% vs 49.62% and 66.79% vs 49.62%, respectively). Furthermore, **4c** and **4k** showed a very good blockade activity (>40% inhibition) which was not significantly different (n.s., $P > 0.05$) from that of nimodipine. Finally, from a statistical point of view, the encountered slightly lower CCB activity of derivatives 4g and 4e was scarcely significantly different to that of nimodipine (*$P > 0.05$).

The calcium channel blockade activity of tacripyrimidines seemed unrelated to the electronic nature of the substituents at the aromatic ring. Indeed, the two most active compounds within this series, i.e., **4h** and **4l**, bore an electron-donor (4'-NMe2) and an electron-withdrawing (3'-NO2) group, respectively. If a homogeneous set of substitution is considered, as in the case of methoxy- or methyl-tacripyrimidines, the 4'-position seems the least favorable one (compare **4b** with **4c** and **4d** with **4e** and **4f**).

For the sake of completeness, it is important to underline that further studies were carried out to assess physico-chemical properties, safety towards hepatoma cells and activity towards amyloid-beta peptide. For full results and their extensive discussions, please refer to the original article [1]. Briefly, the three most interesting tacripyrimidines, namely derivatives **4e**, **4j** and **4k**, were investigated for their antiaggregating activity against $A\beta_{42}$ self-aggregation by Prof. Bartolini. The tested tacripyrimidines exhibited poor inhibitory potency, with a % inhibition of about 10%.

Furthermore, because of the hepatotoxicity displayed by tacrine in human body, all tacrine-based hybrids were assayed on human hepatoma cells (HepG2) to assess their safety. This study was performed by Dr. Giovannini (S.Orsola-Malpighi Hospital, CRBA, Bologna, Italy) using tacrine as positive control. Compounds were assayed in the concentration range 10-300 µM. Cell viability at 24 h was determined by quantifying ATP as an indicator of metabolically active cells, using a luminescence-based assay (CellTiter-Glo® Assay, Promega). Among tacripyrimidines, only derivatives **4b** (4'-Me derivative) and **4j** (4'-Cl) showed higher hepatic cell toxicity than tacrine, while most tacripyrimidines were found to be similarly or slightly less toxic than tacrine. Quite promisingly, **4e** emerged as the safest tacripyrimidine, with no toxic effect on HepG2 cells even at the highest tested concentration. Although to a lower extent, **4l** also turned out to be safer than tacrine with a reduction of only 17% of the cell viability at the highest dose (300 µM).

Finally, *in-silico* calculation of ADME parameters, carried out by Prof. Iriepa and coworkers, allowed assessing the ability of these compounds to be absorbed after oral administration, to cross the BBB and reach the central nervous system (CNS).

9.4 Conclusions

The development of new drug candidates for an effective treatment of AD is a challenging task for medicinal chemists, and also a research area with a potentially tremendous impact in society. In this scenario, the contribution of the academic research to the definition of an effective therapeutic intervention is destined to increase as a consequence of the recent cut of AD focused research programs by some pharmaceutical companies. Having this in mind, new 5-amino-4-aryl-3,4,6,7,8,9-hexahydropyrimido[4,5-b]quinoline-2(1*H*)-thione MTDLs able to modulate both cholinesterase activity and calcium influx mediated by voltage-dependent calcium channels have been studied. Indeed, *in vitro* inhibition studies performed by us, combined with *in silico* studies, showed that activity toward the two selected targets is modulated by the substituent attached to the aromatic ring at position C4. Derivatives bearing halogens (Br, Cl) at C3' and/or C4' position showed the highest inhibitory potencies toward hChEs. Moreover, combination of CCB studies performed by coauthors showed that the introduction of a dimethylamino group at position 4' or a nitro group at position 3' afforded the best calcium channel blockers, with potencies higher than that of the reference CCB drug nimodipine.

Considering the overall biological profile of tacripyrimidines, including predicted ADME parameters and hepatotoxicity, tacripyrimidine **4e** emerged as the first well balanced inhibitor of ChEs and calcium channel, endowed with no significant hepatotoxicity toward HepG2 cells and excellent predicted oral absorption and BBB permeability [1].

Not less importantly, in the light of the role of BuChE as prevalent ACh degradating enzyme in moderate-to-advanced forms of AD and considering the potential role of BuChE in the etiology and progression of AD, the 3'-nitro-tacripyrimidine **4l,** which acts as moderately selective micromolar hBuChE inhibitor (AChE/BuChE = 10, $IC_{50(\mathrm{BuChE})}$ = 2.68 μM) and potent CCB with a significantly higher activity than nimodipine, can also be considered as a promising candidate for further development.

References

[1] M. Chioua, E. Buzzi, I. Moraleda, I. Iriepa, M. Maj, A. Wnorowski, C. Giovannini, A. Tramarin, F. Portali, L. Ismaili, P. López-Alvarado, M.L. Bolognesi, K. Jóźwiak, J.C. Menéndez, J. Marco-Contelles, M. Bartolini, Tacripyrimidines, the first tacrine-dihydropyrimidine hybrids, as multi-target-directed ligands for Alzheimer's disease, Eur. J. Med. Chem. 155 (2018) 839–846.

[2] M. Goedert, M.G. Spillantini, A century of Alzheimer's disease, Science, 314 (2006) 777-781.

[3] J. Cummings, G. Lee, T. Mortsdorf, A. Ritter, K. Zhong, Alzheimer's disease drug development pipeline: 2017, Alzheimers Dement (NY), 3 (2017) 367-384.

[4] A. Cavalli, M.L. Bolognesi, A. Minarini, M. Rosini, V. Tumiatti, M. Recanatini, C. Melchiorre, Multi-target-directed ligands to combat neurodegenerative diseases, J Med Chem 51 (2008) 347–372.

[5] M. Rosini, E. Simoni, R. Caporaso, A. Minarini, Multitarget strategies in Alzheimer's disease: benefits and challenges on the road to therapeutics, Future Med Chem, 8 (2016) 697-711.

[6] F. Prati, A. Cavalli, M.L. Bolognesi,Navigating the chemical space of multitarget-directed ligands: from hybrids to fragments in alzheimer's disease, Molecules, 21 (201**6**) 466.

[7] R. León, A.G. García, J. Marco-Contelles, Recent advances in the multitarget-directed ligands approach for the treatment of Alzheimer's disease, Med Res Rev, 33 (2013) 139-189.

[8] M. Unzeta, G. Esteban, I. Bolea, W.A. Fogel, R.R. Ramsay, M.B. Youdim, K.F. Tipton, J. Marco-Contelles, Multi-target directed donepezil-like ligands for alzheimer's disease, Front Neurosci, 10 (2016) 205.

[9] B. Sameem, M. Saeedi, M. Mahdavi, A. Shafiee, A review on tacrine-based scaffolds as multi-target drugs (MTDLs) for Alzheimer's disease, Eur J Med Chem, 128 (2017) 332-345.

[10] H. Lin, Q. Li, K. Gu, J. Zhu, X. Jiang, Y. Chen, H. Sun, Therapeutic agents in Alzheimer's disease through a multi-target directed ligands strategy:recent progress based on tacrine core, Curr Top Med Chem, 17 (2017) 3000-3016.

[11] L. Ismaili, B. Refouvelet, M. Benchekroun, S. Brogi, M. Brindisi, S. Gemma, G. Campiani, S. Filipic, D. Agbaba, G. Esteban, M. Unzeta, K. Nikolic, S. Butini, J. Marco-Contelles, Multitarget compounds bearing tacrine- and donepezil-like structural and functional motifs for the potential treatment of Alzheimer's disease, Prog Neurobiol, 151 (2017) 4.34.

[12] N. Guzior, A. Wieckowska, D. Panek, B. Malawska, Recent development of multifunctional agents as potential drug candidates for the treatment of Alzheimer's disease, Curr Med Chem, 22 (2015) 373-404.

[13] J. Marco-Contelles, R. León, C. de Los Ríos, A. Guglietta, J. Terencio, M.G. López, A.G. García, M. Villarroya,Novel multipotent tacrine-dihydropyridine hybrids with improved acetylcholinesterase inhibitory and neuroprotective activities as potential drugs for the treatment of Alzheimer's disease, J Med Chem, 49 (2006) 7607-7610.

[14] J. Marco-Contelles, R. León, C. de los Ríos, A. Samadi, M. Bartolini, V. Andrisano, O. Huertas, X. Barril, F.J. Luque, M.I. Rodríguez-Franco, B. López, M.G. López, A.G. García, M. C. Carreiras, M. Villarroya, Tacripyrines, the first tacrine-dihydropyridine hybrids, as multitarget-directed ligands for the treatment of Alzheimer's disease, J Med Chem, 52 (2009) 2724-2732.

[15] M. Bartolini, M. Pistolozzi, V. Andrisano, J. Egea, M.G. López, I. Iriepa, I. Moraleda, E. Gálvez, J. Marco-Contelles, A. Samadi, Chemical and pharmacological studies on enantiomerically pure p-methoxytacripyrines, promising multi-target-directed ligands for the treatment of Alzheimer's disease, ChemMedChem, 6 (2011) 1990-1997.

[16] M.F. Cano-Abad,M. Villarroya, A.G. García, N.H. Gabilan, M.G. López,Calcium entry through L-type calcium channels causes mitochondrial disruption and chromaffin cell death, J Biol Chem, 276 (2001) 39695-39704.

[17] G. Zundorf, G. Reiser, Calcium dysregulation and homeostasis of neural calcium in the molecular mechanisms of neurodegenerative diseases provide multiple targets for neuroprotection, Antioxid Redox Signal, 14 (2011) 1275-1288.

[18] M. Sobrado, M.G. López, F. Carceller, A.G. García, J.M. Roda, Combined nimodipine and citicoline reduce infarct size, attenuate apoptosis and increase bcl-2 expression after focal cerebral ischemia, Neuroscience, 118 (2003) 107-113.

[19] V. Nimmrich, A. Eckert, Calcium channel blockers and dementia, Br J Pharmacol, 169 (2013) 1203-1210.

[20] W. Zhao, J. Wang, L. Ho, K. Ono, D.B. Teplow, G.M. Pasinetti, Identification of antihypertensive drugs which

inhibit amyloid-beta protein oligomerization, J Alzheimers Dis, 16 (2009) 49-57.

[21] T.S. Anekonda, J.F. Quinn, C. Harris, K. Frahler, T.L. Wadsworth, R.L. Woltjer, L-type voltage-gated calcium channel blockade with isradipine as a therapeutic strategy for Alzheimer's disease, Neurobiol Dis, 41 (2011) 62-70.

[22] K. Iwasaki, N. Egashira, Y. Takagaki, Y. Yoshimitsu, I. Hatip-Al-Khatib, K. Mishima, M. Fujiwara,Nilvadipine prevents the impairment of spatial memory induced by cerebral ischemia combined with beta-amyloid in rats,Biol Pharm Bull, 30 (2007) 698-701.

[23] K.Atwal, B.N. Swanson, S.E. Unger, D.M. Floyd, S. Moreland, A. Hedberg, B.C. O'Reilly, Dihydropyrimidine calcium channel blockers.3.3-Carbamoyl-4-aryl-1,2,3,4-tetrahydro-6-methyl-5-pyrimidinecarboxylic acid esters as orally effective antihypertensive agents, J Med Chem, 34 (1991) 806-811.

[24] I.S. Zorkun, S. Sarac, S. Celebi, K. Erol, Synthesis of 4-aryl-3,4-dihydropyrimidin-2(1H)-thione derivatives as potential calcium channel blockers, Bioorg Med Chem, 14 (2006) 8582-8589.

[25] D. Tardiff, L.E. Brown, X. Yan, R. Trilles, N.T. Jui, M.I. Barrasa, K.A. Caldwell, G.A. Caldwell, S.E. Schaus, S. Lindquist, Dihydropyrimidine-thiones and clioquinol synergize to target beta-amyloid cellular pathologies through a metal-dependent mechanism, ACS Chem Neurosci, 8 (2017) 2039-2055.

[26] G.L. Ellman, K.D. Courtney, V. Andres, Jr., R.M. Feather-Stone, A new and rapid colorimetric determination of acetylcholinesterase activity, Biochemical pharmacology, 7 (1961) 88-95.

[27] M. Dixon, The determination of enzyme inhibitor constants, Biochem J, 55 (1953) 170-171.

[28] R.B. Silverman, The organic chemistry of enzyme-catalyzed reactions, Academic Press, San Diego, 2000.

[29] A. Nordberg, C. Ballard, R. Bullock, T. Darreh-Shori, M. Somogyi, A review of butyrylcholinesterase as a therapeutic target in the treatment of Alzheimer's disease, Prim Care Companion CNS Disord, 15 (2013) PCC.12r01412.

[30] S.N. Dighe, G.S. Deora, E. De la Mora, F. Nachon, S. Chan, M.O. Parat, X. Brazzolotto, B.P. Ross, Discovery and structure-activity relationships of a highly selective butyrylcholinesterase inhibitor by structure-based virtual screening, J Med Chem, 59 (2016) 7683-7689.

[31] B. Brus, U. Kosak, S. Turk, A. Pislar, N. Coquelle, J. Kos, J. Stojan, J.P. Colletier, S. Gobec, Discovery, biological evaluation, and crystal structure of a novel nanomolar selective butyrylcholinesterase inhibitor, J Med Chem, 57 (2014) 8167-8179.

[32] M. Bartolini, C. Bertucci, V. Cavrini, V. Andrisano,beta-Amyloid aggregation induced by human acetylcholinesterase: inhibition studies, Biochem Pharmacol, 65 (2003) 407-416.

Conclusions and future perspectives

Studying molecular biorecognition phenomena is pivotal to rationally interpret the complex network of communications which regulates physiological and pathological events. To be effective, this investigation requires advanced methodologies and analytical strategies to profile the binding partners and detail the structural features involved in such interaction. Several analytical techniques have been developed and applied over the years to clarify different aspects of the biorecognition processes and, depending on the analytical issue to be addressed, the most suitable (and available) strategy has been adopted. In this context, combination of different analytical techniques including circular dichroism spectroscopy (CD), surface plasmon resonance (SPR) and high-performance liquid chromatography coupled with mass spectrometry (HPLC-ESI-MSMS), among others, can facilitate the understanding of complex systems and multifaced biorecognition phenomena. Based on these considerations such approach has been pursued to investigate two targets of pharmaceutical interest, namely human serum albumin (HSA) and human cholinesterases (ChEs).

In particular, interest on HSA structural modifications and their involvement in affecting HSA binding properties arose from the importance of altered forms of HSA as circulating biomarkers as well as prognostic factors and possible mediator of pathological events such as activation of the human receptor for advanced glycation end products (RAGE) upon advanced glycation in hyperglycemic conditions.

Due to the strict connection between HSA binding properties and protein integrity, the assessment of HSA binding capacity is of relevance in clinical research as well as in the early stages of drug discovery. In the first work proposed, CD spectroscopy proved to be a trustworthy technique when the drug–HSA interactions are investigated, especially when possible competitors need to be considered. The proposed method enabled to clarify the role of N-acetyltryptophan and sodium octanoate in the impairment of HSA binding capacity when they are added as stabilizers in pharmaceutical formulations containing HSA (*i*-HSA). In particular, site-II ICD markers showed to be efficient tools in the evaluation of the effect of stabilizers on *i*-HSA binding properties and the CD-based assay enabled monitoring effective stabilizers clearance and recovery of binding properties within the development of more efficient removal strategies.

Affinity chromatography, MS and SPR, instead, resulted highly informative to investigate biorecognition phenomena when used in combination. In particular, this multimethodological strategy was employed to obtain further insights into the interaction of glycated HSA (HSAgly) and the extracellular region (VC1) of RAGE. This modified form of circulating HSA, formed at higher amount in pathological conditions such as diabetes, may trigger inflammation and sustain chronic complications through RAGE activation. For this reason, the characterization of such interaction represents an emerging aspect to be elucidated. The herein proposed strategy enabled the

quantification of HSAgly-VC1 complex affinity and allowed to draw some preliminary hypotheses on the HSA region involved in the binding. Indeed, the majority of HSA peptides, identified by combining affinity chromatography and MS, revealed a possible involvement of subdomain IA (63 % of peptides being retained onto the VC1 affinity column), as well as residue K525 as key glycated residue in the interaction with the receptor. In analytical terms, the outcomes of this study showed that combination of all these techniques may be a useful strategy to shed light on complex interacting ligands.

In drug discovery, targeting ChEs has constituted and still constitutes an important strategy for Alzheimer's disease (AD) treatment, especially in the light of new strategies based on multi-target compounds. In this context, classical in solution assays can be paralleled to new highly informative approaches, providing important elements for aiding the selection of favorite chemical scaffolds. Herein, in solution assays were performed for the evaluation of biological activity and the binding mode of new hybrid inhibitors, i.e. donepezil and tacrine hybrids, designed on the basis of the so-called multi-target-directed ligand (MTDL) strategy. Data achieved enabled to elucidate some structure-activity relationships for ChEs inhibition and, in combination with *in vitro* and *in silico* studies carried out by other groups involved in the projects, allowed to identify some promising new MTDLs which could be further developed. In particular, most interesting results were achieved with the so-called tacripyrimidine derivatives which combine anticholinesterase activity with CCB properties. Furthermore, since a better prioritization of new chemical entities may reduce attrition rate in the drug discovery process, a human acetylcholinesterase (hAChE)-based SPR platform was developed. The SPR-based assay was employed to define kinetic rates constants and thermodynamic parameters for the inhibitors–*h*AChE binding events. Indeed, the definition of residence time and kinetic parameters by SPR technology besides the assessment of potency and inhibition profile might result useful powerful strategy in the early drug discovery phase.

As conclusive remark, all analytical strategies summarized in this dissertation share the common purpose to elucidate biorecognition events and/or uncover alterations of such mechanisms which may result in pathological events. The final goal is to provide pivotal information which can help understanding pathophysiological mechanisms and facilitate the development of new and more effective drugs.

Non sei partito per conoscerti meglio,
o conoscere meglio i tuoi amici.
Volevi disconoscerti, se mai. Dimenticare il tuo nome
e restare nudo con la fatica e la gioia.
Vicino a qualcuno di cui potevi fidarti
e alle cose essenziali che conoscevi da sempre.
(Nessuno lo saprà. E. Brizzi)

Alla Prof.ssa Bartolini e al Prof. Bertucci

Perché la loro supervisione, il loro supporto e i consigli mai mancati mi hanno permesso di imparare e di crescere ‘‘puntando sempre un po’ più in là’’.

A Edo, Thomas, Daniele e Marina

Perché l’aver trovato amici con cui lavorare e condividere questo percorso ha colorato e reso piene di bei ricordi persino le più lunghe giornate in laboratorio.

A Samuele

Perché qualunque sia il futuro, è stato la mia costante e la mia squadra in tutte le fasi che mi hanno portato fino a qui.